

Laying the Groundwork for a Tantalum Dearomatization Agent

Adam Christopher Milan Nichols-Nielander
Roanoke, VA

B.S. Chemistry, University of Virginia, 2009

A Thesis presented to the Graduate Faculty
of the University of Virginia in Candidacy for the Degree of
Master of Science

Department of Chemistry

University of Virginia
August, 2010



Adam Nichols-Nielander

Frank Richardson

Laying the Groundwork for a Tantalum Dearomatization Agent

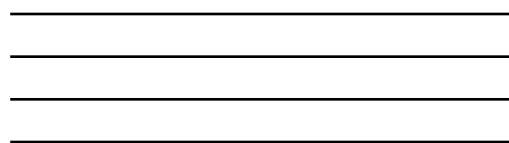
Adam Christopher Milan Nichols-Nielander
Roanoke, VA

B.S. Chemistry, University of Virginia, 2009

A Thesis presented to the Graduate Faculty
of the University of Virginia in Candidacy for the Degree of
Master of Science

Department of Chemistry

University of Virginia
August, 2010



Abstract

Chapter 1 provides a brief description of the synthesis of the π -basic dearomatization agents $\{\text{Os}(\text{NH}_3)_5\}$, $\{\text{TpRe}(\text{CO})\text{L}\}$ ($\text{L}=\text{tBuNC}$, PMe_3 , py , MeIm , and NH_3) and $\{\text{TpW}(\text{NO})(\text{PMe}_3)\}$. It also submits a theoretical explanation for the phenomenon of dearomatization via π back bonding. The basic principles for the synthesis of a dearomatization agent that have been derived from these past syntheses are discussed in the context of the characteristics that we hoped to design into a new tantalum based dearomatizing metal fragment.

Chapter 2 provides a literature review of low valent tantalum chemistry in order to elucidate the synthetic tools that were available for the synthesis of new low valent tantalum species. It also describes multiple pathways that were envisioned for the synthesis of a tantalum dearomatization agent based on these tools. Pathways initially based on high valent tantalum chemistry are also discussed. Chapter 2 also reports the attempts that were made to use the high valent TaCl_5 as starting materials for the synthesis of low valent tantalum species. The difficulties and eventual abandonment of this pathway are noted. The synthesis of $[\text{Et}_4\text{N}][\text{Ta}(\text{CO})_6]^-$ is discussed and the failure of $[\text{Ta}(\text{CO})_6]^-$ to have its ligand set modified by thermal substitution is reported.

Chapter 3 focuses on the modification of $[\text{Ta}(\text{CO})_6]^-$. Chapter 3a describes the photolytic substitution of carbonyl ligands on $[\text{Ta}(\text{CO})_6]^-$. $[\text{Et}_4\text{N}][\text{Ta}(\text{CO})_5(\text{PPh}_3)]$, $[\text{Et}_4\text{N}][\text{Ta}(\text{CO})_5(\text{PMe}_3)]$, and $[\text{Et}_4\text{N}][\text{Ta}(\text{CO})_5(4\text{-DMAP})]$ were synthesized. Electrochemical and infrared data is reported for these species. The substitutional lability of the 4-DMAP ligand of $[\text{Et}_4\text{N}][\text{Ta}(\text{CO})_5(4\text{-DMAP})]$ was explored. Efforts to synthesize

[Et₄N][Ta(CO)₅(η²-benzene)], [Et₄N][Ta(CO)₅(η²-naphthalene)], and [Et₄N][Ta(CO)₅(η²-cyclopentene)] using photolytic conditions failed. Attempts to synthesize [Et₄N][Ta(CO)₄(bipy)], [Et₄N][Ta(CO)₄(tBipy)], and [Et₄N][Ta(CO)₄(η²-naphthalene)] are discussed.

Chapter 3b describes the chemistry of [Ta(CO)₆]⁻ after 2e⁻ oxidation. The synthesis of TaTp(CO)₄, [TaTpm(CO)₄]I, TaTp(CO)₃PMe₃, and [TaTpm(CO)₃PMe₃]I are discussed. These represent the first mononuclear tantalum complexes to include Tp and Tpm. Attempted reductions, nitrosylations, and photolyses with these compounds are discussed.

Table of Contents

Abstract	ii
Table of Contents	iv
List of Tables, Figures, and Schemes	vi
List of Abbreviations	ix
Acknowledgements	xi
Chapter 1: Introduction to Dearomatization and π-Basic Dearomatization Agents	
1.1 Introduction	2
1.2 π-basic Metal Coordination	2
1.3 Dearomatization via Metal Back Donation	5
1.4 Rhenium and Tungsten Dearomatization Agents	10
1.5 Planning for Tantalum	13
1.6 Conclusion	17
1.7 References	18
Chapter 2: Tantalum Chemistry	
2.1 Introduction	21
2.2 High Valent Tantalum Chemistry	22
2.3 Tetraethylammonium hexacarbonyltantalate	27
2.4 Electrochemical Predictions	33
2.5 Chemistry of $[\text{Et}_4\text{N}][\text{Ta}(\text{CO})_6]$	35
2.6 Plan of Action	39
2.7 Conclusion	43

2.8 Experimental	44
2.9 References	49
Chapter 3	
Part A: Ligand Substitution Via Photolysis	
3a.1 Introduction	54
3a.2 Direct Substitution	55
3a.3 Substitution of Carbonyls for Monodentate σ donors	59
3a.4 Substitution of 4-DMAP	63
3a.5 Substitution of Carbonyls of Polydentate σ donors	64
3a.6 Conclusion	72
Part B: Ligand Substitution Via Oxidation	
3b.1 Introduction	73
3b.2 Electrochemistry and Computational Clues	76
3b.3 Addition of Tp and Tpm	78
3b.4 Removal of a CO	82
3b.5 Conclusion	87
3ab.1 Experimental	88
3ab.2 References	99
Conclusion	103
Appendix	105/A-1

List of Tables, Figures, and Schemes

List of Figures

Figure 1.1: Depiction of π back bonding into a benzene ring.	5
Figure 1.2: Molecular Orbital Diagram depicting metal-to-benzene π back bonding.	6
Figure 1.3: Proposed tantalum dearomatization agent with a dihapto-coordinated benzene and a Tp ligand.	16
Figure 2.1: Previously synthesized tantalum species with coordinated aromatics.	22
Figure 2.2: Crystal structure and drawing of Ta(V) trimer.	26
Figure 2.3: Yield of each synthesis reported in Table 2.2 .	30
Figure 2.4: Depiction of 100 mL Schlenk flask.	47
Figure 3a.1: Molecular Orbital diagram of electron promotion.	54
Figure 3a.2: Crystal structure of $[\text{Et}_4\text{N}][\text{Ta}(\text{CO})_5\text{PPh}_3]$ (2).	63
Figure 3a.3: X-ray structure of $[\text{Et}_4\text{N}][\text{Ta}(\text{CO})_4(\text{bipy})]$.	68
Figure 3a.4: Explanation for why complexation of an aromatic ligand to a metal fragment was not observed using photolysis.	71
Figure 3b.1: Angle measured in C-H bond angle measurement.	77
Figure 3b.2: Crystal structure of $\text{TaTp}(\text{CO})_4$ (4).	79
Figure 3b.3: Schematic representation of $\text{TaCp}(\text{CO})_4$.	80
Figure 3b.4: Crystal structure of $[\text{TaTp}(\text{CO})_4]\text{I}$ (5).	81
Figure 3ab.1: Depiction of compound 4 .	91
Figure 3ab.2: Depiction of compound 5 .	92

Figure 3ab.3: Depiction of compound 6. 93

Figure 3ab.4: Depiction of compound 7. 97

List of Schemes

Scheme 1.1: Aromatic compounds successfully bound by the $\{\text{Os}(\text{NH}_3)_5\}^{2+}$ metal fragment. 3

Scheme 1.2: Ratio of phenol tautomers for the free and $\{\text{Os}(\text{NH}_3)_5\}^{2+}$ bound phenol 4

Scheme 1.3: $[\text{Os}]^{2+}$ bound phenol species undergoes electrophilic attack in the presence of maleic anhydride. 5

Scheme 1.4: The reduction of aromatic and non-aromatic species. 9

Scheme 1.5: Synthesis of a tungsten based dearomatization agent. 13

Scheme 2.1: Attempted Tp-Ta(V) syntheses. 23

Scheme 2.2: Attempted reductions and substitutions with TaCl_5 . 25

Scheme 2.3: Low pressure and high pressure synthesis of $[\text{Ta}(\text{CO})_6]^-$ 28

Scheme 2.4: Mono- and Disubstituted $[\text{Ta}(\text{CO})_6]^-$ derivatives. 37

Scheme 2.5: Compounds accessible from oxidation of $[\text{Ta}(\text{CO})_6]^-$. 38

Scheme 2.6: Plan for the synthesis of a tantalum dearomatization agent. 40

Scheme 2.7: Substitutions attempted with $[\text{Ta}(\text{CO})_6]^-$. 42

Scheme 3a.1: Photochemical reactions of **1** and C-C double bond containing π acids. 56

Scheme 3a.2: Illustration of metal binding to disrupt dearomatization and allow for conjugation of the methoxy moiety into the remaining diene of anisole. 58

Scheme 3a.3: Photolysis with monodentate σ donors. 60

Scheme 3a.4: Photochemical reactions attempted with polydentate ligands. 65

Scheme 3b.1: Synthesis of (trimpsi)Ta(CO) ₂ (NO).	74
Scheme 3b.2: Ta(trimpsi)(CO) ₂ (NO) oxidation scheme.	75
Scheme 3b.3: Photolysis reactions attempted with TaTp(CO) ₄ and predicted products.	83
Scheme 3b.4: Proposed synthesis to dicarbonyl nitrosyl d ⁶ complexes from 6 and 7 .	86
List of Tables	
Table 2.1: Price of metal starting materials from Strem Chemical Inc.	23
Table 2.2: Table describing the attempted syntheses of [Et ₄ N][Ta(CO) ₆]	29
Table 2.3: Comparison of IR and CV signatures of Ta(CO) ₆ ⁻ and TpW(PMe ₃)(NO)(CO).	35
Table 3a.1: Table reporting electrochemical and infrared data collected after irradiation of 1 with the listed ligand.	70
Table 3b.1: Calculations hypothetical η ² -coordinated benzene complexes of tantalum.	76

List of Abbreviations

ampy	2-aminopyridine
bipy	2,2'-bipyridyl
CFL	Compact Fluorescent Lightbulb
Cp	Cyclopentadienyl
CV	Cyclic Voltammetry
DMAP	Dimethylaminopyridine
DME	1,2 Dimethoxyethane
dmen	N,N'-dimethylethylenediamine
dppe	1,2-bis(diphenylphosphino)ethane
en	Ethylenediamine
Et	Ethyl
ⁱ Pr	Isopropyl
IR	Infrared Spectroscopy
KTp	Potassium Hydridotris(pyrazolyl)borate
MeCN	Acetonitrile
MeIm	Methyl Imidazole
NMR	Nuclear Magnetic Resonance
OTf	Triflate (CF ₃ SO ₃ ⁻)
PPh ₃	Triphenyl phosphine
Silox	(tBu ₃)SiO ⁻
tBipy	4,4' tertbutyl-2,2'-Bipyridyl

terpy	2,2':6',2''-terpyridine
TFA	Trifluoroacetate
THF	Tetrahydrofuran
tmen	N,N,N',N'-tetramethylethylenediamine
Tp	Hydridotris(pyrazolyl)borate
Tp*	Hydridotris(3,5-dimethylpyrazolyl)methane
Tpm	Hydridotris(pyrazolyl)methane
Trimpsi	tBuSi(CH ₂ PMe ₂) ₃

Acknowledgements

Of all of the sections of this thesis, this part has concerned me the most. The Harman lab has a long tradition of strong acknowledgements sections in theses, and I have spent the better part of my nearly five years of lab time worrying over how I would live up to the genius of acknowledgments legends like Peter Graham and Kevin Welch. I expected to be able to put more effort into this section than any other, but the authoring of this thesis has taken a lot more out of me than I anticipated, and thus this section has been written with the little energy I have remaining. At any rate, my time has come and for better or worse I submit this acknowledgements to the annals of Harman lab history.

The first person I need to thank is Dean Harman. It was a historic day in the Fall of '06 when Mike got tired of me asking questions and sent me to Dean instead. This cycle would continue on a nearly daily basis for the next four years. So thanks for dealing with my daily knock on the door, even when I often couldn't explain why I was there. I now am headed to Caltech to form the Harman Lab triforce with Hill Harman and Rachel Klet; hopefully we will represent you well.

I wouldn't be where I am today without the other members of the Harman lab who have led me through this process. Mike Todd was my original mentor and the one who first had to deal with my impetuosity. Thanks for putting up with me while I learned the ropes. Dan Harrison was probably the person in lab I spent the most time harassing though. He was 'my' graduate student after Mike left, and working on pyridine chemistry with him earned me my first paper. He probably would have graduated long ago if it weren't for me breaking up his day into as small of pieces as possible or

disrupting him in the graduate student office, and I always appreciated his exaggerated sense of my capabilities. I also appreciate him walking outside with me when I thought I was going to pass out from excessive carbon monoxide inhalation. And also I'd like to throw in that Dan gave me perhaps my worst grade on any assignment at UVa on an organic lab report. And of course our trips to Guadalajara. I feel our relationship, especially in the last couple months, was a fiery one, something Ralph Allen can attest to. Which brings me to Vic Zottig. The first time I saw Vic was at the last Christmas party in Dean's old house, and I thought he was Dan's brother. In retrospect, I wish I had gone hiking and wine tasting with him more often. His knowledge of organic chemistry will serve the lab well in the future. I'd like to thank Monica Kasbekar for distracting me in our office for three years, and for helping me with problem sets long into the night after spending the day time avoiding said problem sets. She always worked harder than me and I'm sure her new life as an MD in St. Louis will go well. Becky Salomon and I graduated at almost the same time, and without her this thesis probably would have been rejected by the Graduate school a number of times due to poor formatting. Thanks for being the lead TA in 181L, and when I say thanks, I mean I may never forgive you for making me wake up at 7:30 am on a Friday to practice the lab for the next week. Laura Strausberg, thanks for your careful editing eye on this paper. I may never understand the importance of proper grammar, but because you did, this thesis was written in English and not in a secret language only I could understand. To Jared, Sisi, and Nathan, you all will be here long after I am gone and represent the next generation of the Harman lab, take the torch carefully and use the red fire extinguisher if it gets out of control, the

yellow one is for metal fires only. And to Bill, Dalsher, and Diana, you made the summers very enjoyable, good luck in your future endeavors, be they more summers in the Harman lab, completing HRMS and NMR experiments, medical schools, driving recklessly on I-95, or going to graduate school.

I also want to thank my friends for helping me relax over the last five years. If it weren't for them, I would probably have published at least five papers on dearomatized tantalum complexes and may even be up for a Nobel prize or something of the like, but at least I got to play a lot of Starcraft, Halo 3, and Smash Bros. instead. So thanks to Brian, Alex, Alex, Berge, Julien, David and Eddie for help keeping me well rounded. Hopefully 1.21.09 will eventually be recognized as a day of infamy as it rightly should be.

I would be remiss to not thank my family and my girlfriend. Thanks to my mom and dad for sending me to UVa and for being there whenever I needed to call them, as well as funding my life for four years. Good luck to my sister Caroline as she begins her own college experience at South Carolina. Finally, thanks to my girlfriend Jackie for always being loving and supportive and for dealing with my absence during the thesis writing process. You make my life much better.

I also need to thank Dr. Burnett for his help during my undergraduate career Master's degree year. As an undergraduate, he helped me find money to stay over my first summer and this year, he dealt with me every time I needed an exception from the norm to get this degree, which seemed to happen every day. And Bonnie Milligan for allowing me to get this degree despite missing all conceivable deadlines. Finally, I want to make a couple of official acknowledgements. I would like to thank the Harrison

Research Fellowship, as well as the Goldwater Fellowship, NSF, and NDESG committees for funding me as an undergraduate and now as a graduate student. I had a good run at UVa, and I will always miss the people I am leaving. Hopefully I never forget the times I had here because it really was the time of my life. Like my time in the Harman lab, this acknowledgements section is rambling, disorganized, probably full of mistakes, and despite my desire to extend it forever, is over.

Chapter 1:

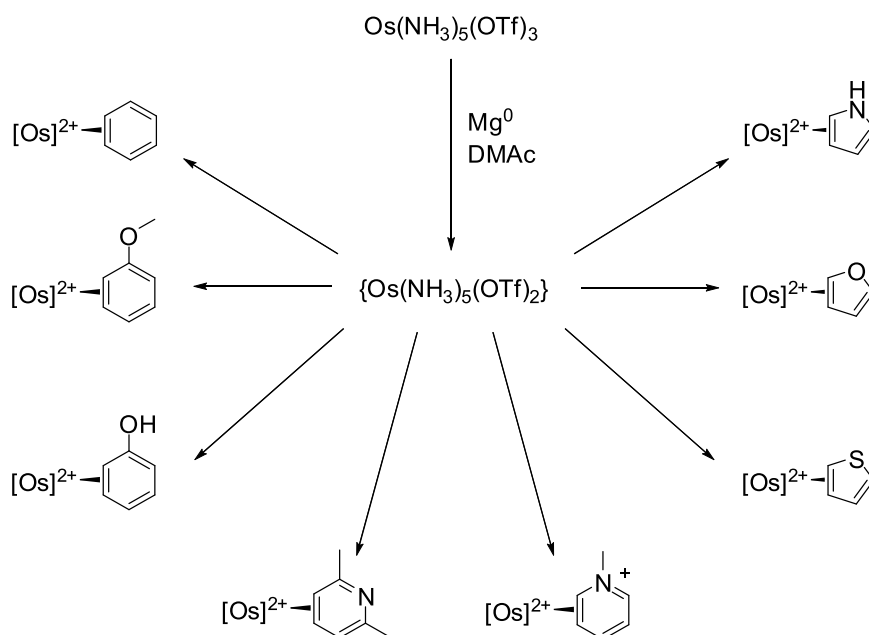
Introduction to Dearomatization and π -Basic
Dearomatization Agents

1.1. Introduction

Due to their inherent stability, aromatic compounds are both abundant in nature and inexpensive to obtain. They also contain carbocyclic or heterocyclic ring systems with multiple sites of unsaturation which serve as points of attachment for functional groups. These ring systems, both saturated and unsaturated, are prevalent in many areas of chemistry, and are quite often found in natural products.¹⁻² This combination of being common, inexpensive, and containing the ring scaffolding ubiquitous in many areas of chemistry makes aromatic compounds tantalizing starting materials for the synthesis of more complex molecules. However, the stability of aromatics complicates their usefulness in synthetic chemistry. In order to utilize the sites of unsaturation in these compounds, the stability that is imparted by the aromaticity must be overcome. While harsh conditions can be used to achieve this, as best illustrated by the Birch reduction, more mild conditions are preferable.¹⁻² One such method for the disruption of aromaticity is the dihapto coordination of an aromatic to a strongly π -basic metal fragment.

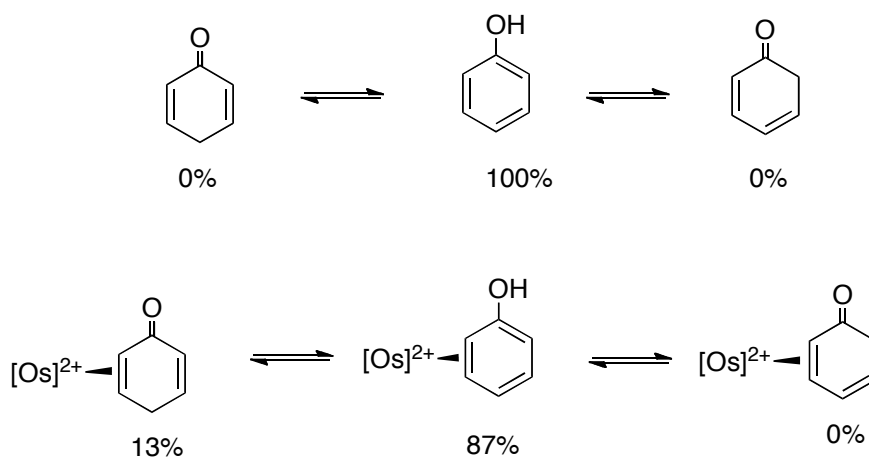
1.2 π -Basic Metal Coordination

The use of π -basic metal systems to activate aromatic systems began in the late 1980's when the $\{\text{Os}(\text{NH}_3)_5\}^{2+}$ metal fragment was elucidated by Harman and Taube.³ Using $[\text{Os}(\text{NH}_3)_5(\text{OTf})][(\text{OTf})_2]$ as a precursor, a number of $18e^-$, d^6 arene and heterocyclic π -bound systems were synthesized (**Scheme 1.1**).



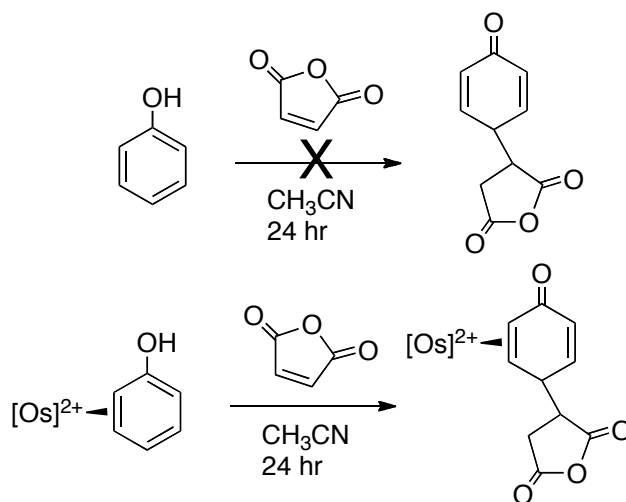
Scheme 1.1: Aromatic compounds successfully bound by the $\{\text{Os}(\text{NH}_3)_5\}^{2+}$ metal fragment.³⁻⁶ $[\text{Os}]^{2+} = \{\text{Os}(\text{NH}_3)_5\}^{2+}$

The characteristics of these complexed aromatic systems suggest that their aromaticity had been disrupted. One such example can be seen in the case of $\text{Os}(\text{NH}_3)_5(\eta^2\text{-phenol})$. In solution, phenol exists exclusively in its aromatic form. However, phenol dihapto coordinated to the $\{\text{Os}(\text{NH}_3)_5\}^{2+}$ metal system shows a 1:5 equilibrium between its aromatic form and the 2,5-cyclohexadien-1-one (**Scheme 1.2**)⁷.



Scheme 1.2: Ratio of phenol tautomers for the free and $\{\text{Os}(\text{NH}_3)_5\}^{2+}$ bound phenol.⁷

It is generally expected that the ketone in a keto-enol equilibrium will be favored, and it is the aromatic stabilization that forces phenol into its enolic form. Thus, the movement of the equilibrium towards the ketone suggests some of the aromatic stabilization has been negated. Moreover, the η^2 bound phenol undergoes electrophilic attack by maleic anhydride under much milder conditions than would have been necessary for the same reaction for the free ligand (**Scheme 1.3**).⁸ Not only does this example demonstrate that dearomatization occurred, but it can be seen that this method allows for the use of mild conditions to derive new compounds from aromatic species.



Scheme 1.3: Unlike the free ligand, $[\text{Os}]^{2+}$ bound phenol species undergoes electrophilic attack in the presence of maleic anhydride.

1.3. Dearomatization via Metal Back Donation

This dearomatization phenomenon can be explained using a qualitative molecular orbital argument. At the most basic level, what is occurring is the donation of electron density from a filled metal d-orbital into an empty antibonding orbital of an aromatic compound (**Figure 1.1**). This acts to remove one of the double bonds from the aromatic ring, leaving a more reactive diene behind.

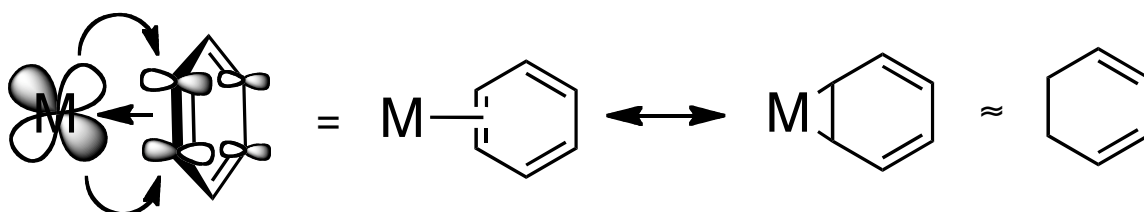


Figure 1.1: Depiction of π back bonding into a benzene ring. Note the arrow from the benzene to the metal, representing the formation of the σ -bond.

It is also illuminating to consider the molecular orbital diagram (**Figure 1.2**)

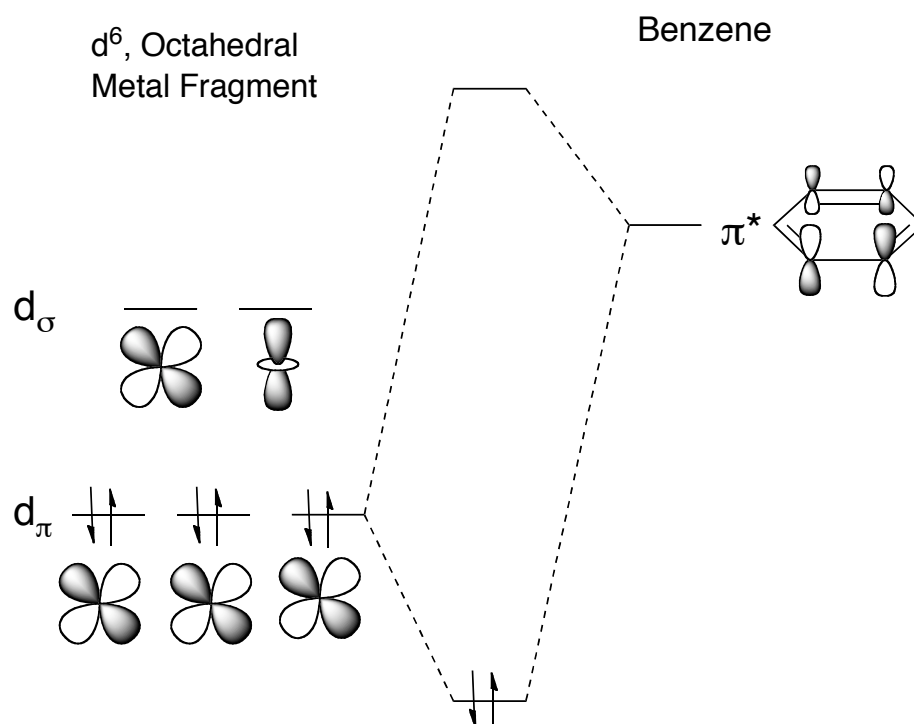


Figure 1.2: Qualitative molecular orbital diagram depicting metal-to-benzene π back bonding.

Using **Figure 1.2** as a guide, one can imagine that by adjusting the energy of the filled d-orbitals, the extent of donation into an aromatic ring can be tuned. This level of donation is directly related to the extent to which dearomatization is observed. That is, the greater the donation, the more dearomatized the ring becomes.

From one perspective, the donation of electron density from the metal to the ring can be thought of as a “partial” reduction of the aromatic ring. It is known that the reduction of a non-aromatic $4n$ e^- species ($n=1,2,3\dots$), such as cyclooctatetraene, to a $4n+2$ e^- species imparts aromaticity on the previously non-aromatic compound (**Scheme 1.4**).¹ Partial aromaticity has been observed in cyclooctatetraene through the

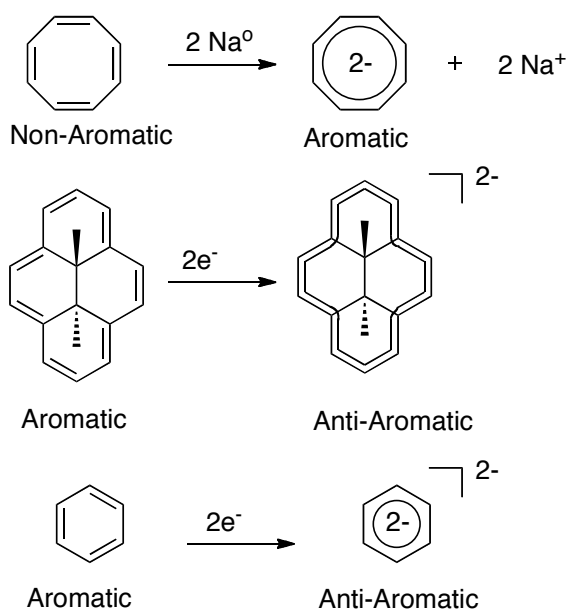
complexation of the π -basic metal fragment $\{(R_2PCH_2CH_2PR_2)Ni\}$ ($R = iPr, tBu$).⁹

Conversely, it is expected that the donation of $2e^-$ to a $4n+2 e^-$ ring would form an antiaromatic or non-aromatic ring. Along these lines, donation from an electron-rich metal to a benzene ring would form a complex that exhibited some of the characteristics of a $4n e^-$ non-aromatic or antiaromatic species. We hypothesize that a dianionic $8e^-$ benzene might be expected to have the following characteristics: loss of planarity, single and double bonds of alternating length, and greatly increased reactivity relative to its $6e^-$ counterpart. The first two characteristics are hypothesized based on the assumption that an $8e^-$ benzene will distort to minimize conjugation and avoid the 'energy cost' associated with antiaromaticity. The increased reactivity should be associated with either a planar antiaromatic or a non-planar non-aromatic system since in both cases aromaticity has been disrupted. We also expect that the benzene dianion will be particularly reactive with electrophiles based on the drive to stabilize the negative charge associated with a dianion. While the metal donation is not so great that it simply loses two electrons to the aromatic ring in a redox fashion to form the benzene dianion, the donation leads to the exhibition of these characteristics to a degree, much in the same way donation by an electron-rich metal fragment into cyclooctatetraene led to exhibition of partial aromaticity.⁹ For example, the benzene ring of $TpW(NO)(PMe_3)(\eta^2\text{-benzene})$ is no longer planar, has varying C-C bond lengths, and is particularly susceptible to electrophilic attack. However, it can be seen that this explanation for dearomatization described above is not a complete description of the altered reactivity we observe for our complexed benzene

systems because it does not include a description the covalent bond(s) that are formed between the metal center and the bound carbons of the benzene ring.

From another perspective, the dearomatization phenomenon can be explained as a result of the reduction of one of the double bonds of the benzene rings using two of the high energy d-orbital electrons depicted in **Figure 1.2**. This reduction forms a metallocyclopropane species, seen in **Figure 1.1**, leaving an isolated cyclohexadiene. Clearly, this explanation has also led us to a dearomatized benzene and also explains why we rarely note reactions at the bound C-C bond. However, this explanation does not easily describe the increased reactivity towards electrophiles that the coordinated ligand experiences; that is, the cyclohexadiene species seen coordinated to the metal fragment is more reactive toward electrophiles than free cyclohexadiene.

The reactivity of the bound ligand is neither that of an isolated diene, nor a reduced aromatic species, but rather somewhere in between. The depiction of these metal complexes using the resonance form seen on the left in **Figure 1.1** describes both the electron donation into the π -system and the isolation of the diene that are noted experimentally.



Scheme 1.4: The reduction of cyclooctatetraene leads to the formation of an aromatic compound. The reduction of the pyrene derivative leads to the formation of an antiaromatic system.¹⁰ The reduction of benzene leads to the theoretical 8e⁻ benzene dianion.

As demonstrated, with five σ -donating amine groups, the osmium metal fragment is electron rich enough to donate electron density into the aromatic system and dearomatize it.³ This osmium system was used for many years to perform unique organic transformations on aromatic compounds.^{4,5,8} However, this system has a number of limitations: the reactions are not catalytic, the starting material OsO₄ is toxic, and stoichiometric quantities of the expensive osmium metal are required.¹¹ Furthermore, the osmium system is sensitive to strong base, is only slightly soluble in many organic solvents, and is not amenable to chromatographic separations. If the use of π -basic metals was going to be an efficient route for organic synthesis, these problems would need to be overcome. Thus, the search for a new π -basic metal system began.

1.4 Rhenium and Tungsten Dearomatization Agents

It was hypothesized that a new π -basic metal fragment could be synthesized even if the identity of the metal in the fragment was changed. Referring back to **Figure 1.2**, it is important to note that the energy of each of the d_{π} orbitals is dependent on the identity of both the metal and its ligands. The energy of the d_{π} orbitals would be expected to shift higher or lower with the addition of more electron donating or withdrawing ligands, respectively, despite the fact that an interaction between the d_{π} and ligand orbitals is not explicitly drawn. Similarly, the energy of those d_{π} orbitals would be affected by changing the identity of the metal center; that is, replacement of the osmium metal with a metal with a lower effective nuclear charge would shift the d_{π} orbital energy up. A balance between these factors should be attainable and dearomatization possible with many different metal fragments. It should be noted at this point, though, that this argument only considers the energy of the π symmetry orbitals, and not the size of the orbitals or their overlap. Nor does it take into account the possible importance of the metal-aromatic ligand σ bond or the importance of the steric environment of a metal system.

It was also hypothesized that electrochemistry, specifically cyclic voltammetry, would be a useful tool in identifying the changes that a metal fragment underwent as its ligand set was adjusted. It was posited that the measured potential of a metal system was directly correlated to the energy of its highest energy d_{π} orbital, and that if a Re metal system could be synthesized with a potential similar to that of the $\text{Os}(\text{NH}_3)_5(\eta^2\text{-benzene})$ (III/II $E_{1/2}=0.16$ V vs. NHE), it would show the same dearomatizing ability.¹²

With this, the synthesis of a rhenium-based dearomatization agent began.

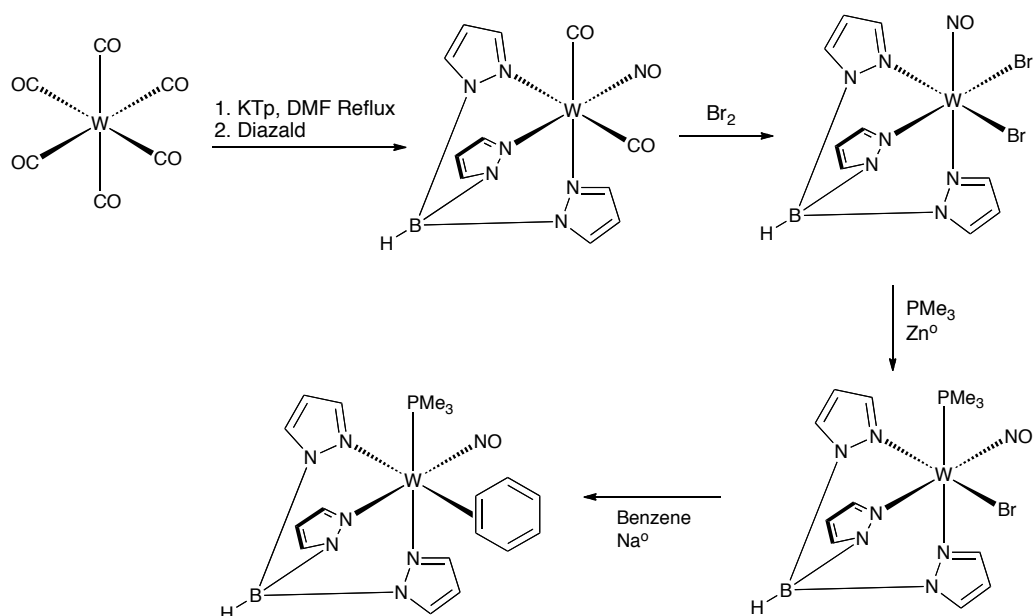
Initially, efforts were directed towards making metal species with ligand sets similar to the $\{\text{Os}(\text{NH}_3)_5\}^{2+}$ system. The early synthesized Re systems included trans- $[\text{ReCl}_2(\text{NH}_3)_4]\text{PF}_6$ and trans- $[\text{ReCl}_2(\text{ampy})_2]\text{PF}_6$. These systems were so electron rich that the Re(I) oxidation state could not be achieved.¹³ Operating under the described hypothesis, polypyridyl ligands were incorporated into the rhenium ligand set. It was hoped that the π acidity associated with the polypyridyls would lower the overall electron density of the rhenium systems. Metal fragments such as $\{\text{Re}(\text{terpy})(\text{PPh}_3)\text{Cl}\}$, $\{\text{Re}(\text{terpy})(\text{PMe}_3)_2\}$, and $\{\text{Re}(\text{tbipy})(\text{ampy})(\text{PPh}_3)\}$ were produced, but still did not coordinate aromatic molecules. A CV study of the dinitrogen complexes of each metal fragment and the $\{\text{Os}(\text{NH}_3)_5\}^{2+}$ fragment showed that the polypyridyl rhenium species were much more reducing.¹¹ In order to better match the reduction potential of the $\{\text{Os}(\text{NH}_3)_5\}^{2+}$ system, a carbonyl ligand was included in the rhenium ligand set. The strong π acidity of the carbonyl was expected to lower the valence orbital energies at the rhenium center in order to better match the osmium system. The incorporation of the carbonyl eventually led to the $\text{TpRe}(\text{CO})(\text{MeIm})(\eta^2\text{-benzene})$ complex. Although there were other related Re metal fragments capable of binding naphthalene, the $\{\text{TpRe}(\text{CO})(\text{MeIm})\}$ fragment was the only one shown to bind and dearomatize benzene. The II/I $E_{1/2}$ of the $\text{TpRe}(\text{CO})(\text{MeIm})(\eta^2\text{-benzene})$ complex was measured to be -0.16 V vs. NHE, supporting the hypothesis that electrochemical matching should be a useful tool in determining the proper ligand set for a dearomatization agent.¹⁴ Furthermore, as evidenced by the ability of the bound benzene to undergo a cycloaddition with N-

methylmaleimide when the benzene ligand of $\text{Os}(\text{NH}_3)_5(\eta^2\text{-benzene})$ would not, the rhenium species was found to be more activating than the osmium system.¹¹ However, like the osmium metal fragment, the rhenium fragments had limitations that encouraged us to search for yet another dearomatization agent. The synthesis of the $\text{TpRe}(\text{CO})(\text{MeIm})(\eta^2\text{-benzene})$ was painstaking, required 26 days to synthesize, and the cost of rhenium was still prohibitive due to the stoichiometric nature of the reactions.

Thus, the search for a tungsten-based π -basic metal fragment began.

A comparison of the d^5/d^6 reduction potentials between the $\text{TpRe}(\text{CO})_3$ and the $\text{TpW}(\text{NO})(\text{CO})_2$ indicated that the $\{\text{TpW}(\text{NO})\}$ metal fragment was 300 mV more reducing than the $\{\text{TpRe}(\text{CO})\}$.¹¹ This data were coupled with knowledge of the potentials for the series $\{\text{TpRe}(\text{CO})(\text{L})\}$ ($\text{L}=\text{NH}_3$, MeIm, py, PMe_3 , tBuNC). The $\text{TpRe}(\text{CO})(\text{PMe}_3)(\eta^2\text{-benzene})$ showed a II/I $E_{1/2}=0.23$ V. Thus, if $\{\text{TpRe}(\text{CO})\}$ was replaced with $\{\text{TpW}(\text{NO})\}$, it was hypothesized that $\{\text{TpW}(\text{NO})(\text{PMe}_3)\}$ would be the proper metal fragment for dearomatization.

Using the following scheme, the $\text{TpW}(\text{NO})(\text{PMe}_3)(\eta^2\text{-benzene})$ was synthesized.



Scheme 1.5: Synthesis of a tungsten based dearomatization agent.¹⁵

Again, it was found that the electrochemistry matched well with the two previous species ($E_{p,a} = -0.13$ V vs. NHE). The $\{\text{TpW}(\text{NO})(\text{PMe}_3)\}$ fragment showed increased activation relative to the Os and Re systems, continuing the trend of more activating metal fragments. Under the same conditions that the $\text{TpRe}(\text{CO})(\text{MeIm})(\eta^2\text{-benzene})$ performed the cycloaddition with N-methylmaleimide, $\text{TpW}(\text{NO})(\text{PMe}_3)(\eta^2\text{-benzene})$ performed the same reaction at a rate four times faster.¹¹

1.5 Planning for Tantalum

With the tungsten system thoroughly characterized, the question arose as to the level of generality of the original hypothesis that the identity of the metal was not important for the synthesis of a dearomatization agent. Also, moving from right to left among the third row metals (Os, Re, W), the synthesis of each new dearomatization also

showed stronger activation of the organic ligands, despite electrochemical measurements indicating that the $\text{TpRe}(\text{CO})(\text{MeIm})(\eta^2\text{-benzene})$ species was the most electron rich. The question arose as to whether the identity of the metal had any impact on the level of activation. The natural forward progression to answer both of these questions was to begin the synthesis of a new tantalum-based metal fragment capable of dearomatizing arenes and heterocycles.

The purpose of the experimental work described herein was to lay the groundwork for a tantalum-based dearomatization agent tantalum. Using years of knowledge collected during the syntheses of dearomatization agents based on three different third row metal systems, a number of tenets were laid down to guide the design of the tantalum dearomatization agent. The first was that the final metal fragment should be a monomeric, d^6 , $18e^-$ system and assuming that one of the ligand sites will be occupied by the organic ligand of interest, the 'dearomatizing metal fragment' will need to be a $16e^-$ species. Having a coordinatively saturated metal is important because the presence of an open coordination site in a theoretical $16e^-$ dearomatization agent invites the possibility of associative substitution. That possibility, along with the strong driving force (rearomatization) associated with loss of a dearomatized organic ligand, would likely make a $16e^-$ species ineffective. The belief in a need for a d^6 system was due in part to previous experiences with Os, Re, and W and part in a belief that a d^4 system would have issues with its geometry. If the d^4 system was octahedral, it would be prone to associative substitution of the coordinated ligand. If the d^4 metal fragment with an aromatic ligand coordinated was expected to be seven-coordinate, steric problems may

prevent species from binding that otherwise would have bound a metal center with the same level of back bonding. The second tenet was that the ligands of the dearomatizing agent would have to be resistant to reaction or dissociation themselves. To protect against dissociation, it was determined that if reasonable or possible, the facially coordinating, tridentate tris(pyrazoyl)borate or tris(pyrazoyl)methane ligands would be employed. These ligands are preferred because we have had extensive experience with synthesis and characterization of Tp complexes in the past. Also, their tridentate nature should prevent loss of the Tp or Tpm ligand by substitution.¹⁶ Furthermore, the use of a facially coordinating tridentate σ donor ligand ensures that the coordination site for the aromatic molecule will be trans to a σ donor. This prevents a π -acidic ligand from preventing the coordination of an aromatic molecule via trans influence.

Of course, it is most important to find the proper balance of metal-centered electron density. Too little electron density will not support the desired metal to π^* back bonding. Too much electron density and oxidative addition may be observed. This was clearly noted in the case of the $\text{TpW}(\text{NO})(\text{PMe}_3)(\eta^2\text{-benzene})$, which exists in equilibrium with the 7-coordinate $\text{TpW}(\text{NO})(\text{PMe}_3)(\text{H})(\text{Ph})$. This suggests that the tungsten metal fragment was nearly too electron rich. It should be noted that Tp and Tpm may play a role in preventing oxidative addition by occupying such a large volume of the ligand sphere. That is, they could be imagined to sterically hinder the metal system such that the 7-coordinate species consistent with oxidative addition is less favored relative to the 6-coordinate dihapto coordinated species.

At this point, only two remaining variable ligands are left if a species that follows the above plan is to be synthesized. With analogy to $\{\text{TpW}(\text{PMe}_3)\text{NO}\}$, the two ligands will both have to be π acids such as CO, NO, PF_3 , or others to compensate for the lower overall effective nuclear charge of tantalum relative to tungsten.

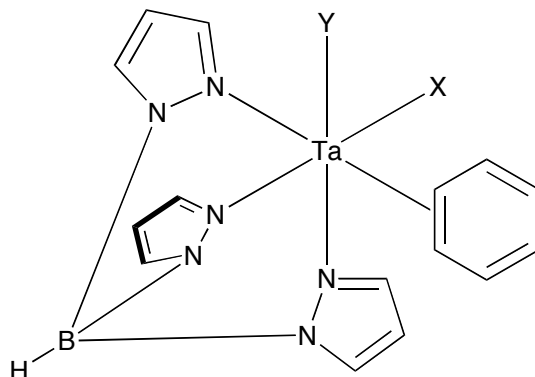


Figure 1.3: Proposed tantalum dearomatization agent with a dihapto-coordinated benzene and a Tp ligand. (X, Y = π acids).

As seen in **Figure 1.3**, this requires that there be a π acid directly interacting with the d_π orbital expected to participate in back bonding. Such a situation appears inevitable and it was hoped that as long as there is no strong π acid trans to the organic ligand, dearomatization will still be possible as long as the electrochemical potentials still correlated well with the other dearomatizing metal fragments. Because of a dearth of Ta(-1) species, there is no direct electrochemical comparison available to make more concrete predictions about the necessary ligand set. Thus, it was planned to synthesize an $16e^-$, d^6 tantalum dearomatizing metal fragment that included either a Tp or Tpm ligand along with π acids to tune the electron density at the metal center.

1.6 Conclusion

If the stabilization inherent to aromatic molecules can be overcome, they have many valuable properties that synthetic chemists could use to their advantage. One way to overcome aromaticity is through dihapto coordination of the aromatic molecule to a strongly π -basic metal fragment. This disruption of aromaticity is believed to be the result of π back donation from the metal to the π^* orbital of the aromatic molecule. The ability to bind an aromatic to a metal fragment and subsequently perform organic chemistry on the bound ligand was initially demonstrated with the $\{\text{Os}(\text{NH}_3)_5\}^{2+}$ metal fragment. It was hypothesized that by adjusting the ligand set, other metals could be used in the same manner. Utilizing electrochemistry to monitor the 'electron-richness' of different metal fragments and electrochemical data to predict species that would have good electrochemical matches to the already known $\{\text{Os}(\text{NH}_3)_5\}^{2+}$, the $\text{TpRe}(\text{CO})(\text{MeIm})(\eta^2\text{-benzene})$ and subsequently the $\text{TpW}(\text{PMe}_3)(\text{NO})(\eta^2\text{-benzene})$ complexes were formed. It was found that as we synthesized dearomatization agents using earlier third row metals, the activating ability of the metals also increase. To continue testing the hypothesis that the identity of the metal center did not preclude a dearomatization agent from being formed and that earlier third row metals provide greater activation of aromatic molecules, we decided to synthesis a tantalum-based dearomatization agent. Based on experience, we determined that a d^6 , $18e^-$, monomeric $\text{Ta}(-1)$ species with a Tp or a Tpm ligand would be useful and that multiple π acids would be necessary to stabilize the otherwise highly electron rich tantalum center.

1.7 References

- 1) Carey, F.A.; Sundberg, R.J.. *Advanced Organic Chemistry Part A: Structure and Mechanisms, Fifth Ed.*; Springer Press: New York, 2007.
- 2) Carey, F.A.; Sundberg, R.J.. *Advanced Organic Chemistry Part B: Reactions and Synthesis, Fifth Ed.*; Springer Press: New York, 2007.
- 3) Harman, W. D.; Taube, H. *J. Am. Chem. Soc.*, **1987**, 109, 1883-1885
- 4) Harman, W. D.; Sekine, Mikiya; Taube, Henry. *J. Am. Chem. Soc.*, **1988**, 110, 5725-5731.
- 5) Cordone, Rossella; Harman, W. Dean; Taube, Henry. *J. Am. Chem. Soc.*, **1989**, 111, 5969-5970.
- 6) Harman, W. Dean. *Chem. Rev.*, **1997**, 97, 1953.
- 7) Kopach, Michael E.; Hipple, William G.; Harman, W. Dean. *J. Am. Chem. Soc.*, **1992**, 114, 1736-1740.
- 8) Kopach, Michael E.; Gonzales, Javier; Harman, W. Dean. *J. Am. Chem. Soc.* **1991**, 113, 8972-8973.
- 9) Bach, Ingrid, Porschke, Klaus-Richard; Proft, Bernd; Goddard, Richard; Kopsike, Carsten; Kruger, Carl; Rufinska, Anna; Seevogel, Klaus. *J. Am. Chem. Soc.* **1997**, 119, 3773-3781.
- 10) Haddon, R. C. *Tetrahedron*, **1972**, 28, 3613-3633.
- 11) Graham, Peter Michael. *Ph. D. Dissertation*; University of Virginia: Charlottesville, 2005.

- 12) Harman, W. Dean; Taube, Henry. *J. Am. Chem. Soc.*, **1988**, 110, 5403-5407.
- 13) Orth, S.D.; Barrera, J.; Sabat, M.; Harman, W. D. *Inorg. Chem.* **1994**, 33, 3026.
- 14) Meiere, Scott. H; Brooks, Benjamin C.; Gunnoe, T. Brent; Sabat, Michal; Harman, W. Dean. *Organometallics* **2001**, 20, 1038-1040.
- 15) Graham, P. M; Meiere, S. H.; Sabat, M.; Harman, W. D. *Organometallics* **2003**, 22, 4363.
- 16) Crabtree, Robert H. *The Organometallic Chemistry of the Transition Metals, Fourth Edition*. John Wiley & Sons: Hoboken, NJ. 2005.

Chapter 2:

Introduction to Tantalum Chemistry

2.1. Introduction

Over the past twenty years, the Harman lab has synthesized a number of π -basic metal fragments. These systems, moving from $\{\text{Os}(\text{NH}_3)_5\}^{2+}$ to $\{\text{TpRe}(\text{CO})(\text{MeIm})\}$ to $\{\text{TpW}(\text{PMe}_3)(\text{NO})\}$, have each proven capable of activating aromatic compounds towards organic transformations that were otherwise inaccessible. This demonstrated that the dearomatization phenomenon was not limited by the central metal atom identity. Moreover, as earlier metals were employed, a pattern of increasing activation was observed (See Chapter 1). With these patterns in mind, we endeavored to synthesize a Group V dearomatization agent. Tantalum was chosen based on previous experience with third row metals and an expectation that it would be the group V metal most capable of back bonding.¹

As discussed in Chapter 1, the intention was to synthesize a d^6 , $16e^-$ tantalum metal fragment that employed either Tp or Tpm ligand along with at least one strong π acid. However, we quickly realized that unlike for the later 3rd row metals previously used, low valent early metal chemistry was not nearly as well explored, particularly in the case of tantalum nitrosyls.² In fact, at the time this project began, only a handful of tantalum nitrosyl compounds had been characterized.² Compounding the problem, a SciFinder search indicated that no tantalum Tpm compounds of any kind had been reported, and only the $\text{TaTp}(\text{Me})_3\text{Cl}$ as well as a Ta(V) Tp^* species had been characterized using Tp.³ Also, no low valent tantalum starting materials were commercially available.⁴

Previous work by Wolczanski and coworkers had elucidated dihapto coordinated arenes to tantalum metal fragments. These species were d^0/d^2 , $10e^-$ species (**Figure 2.1**), and a crystal structure of the $(\text{silox})_3\text{Ta}\{\eta^2\text{-(N,C)-NC}_5\text{H}_5\}$ indicated that the aromaticity had been disrupted.⁵⁻⁷ However, no chemistry was developed for the organic ligands of the described systems.

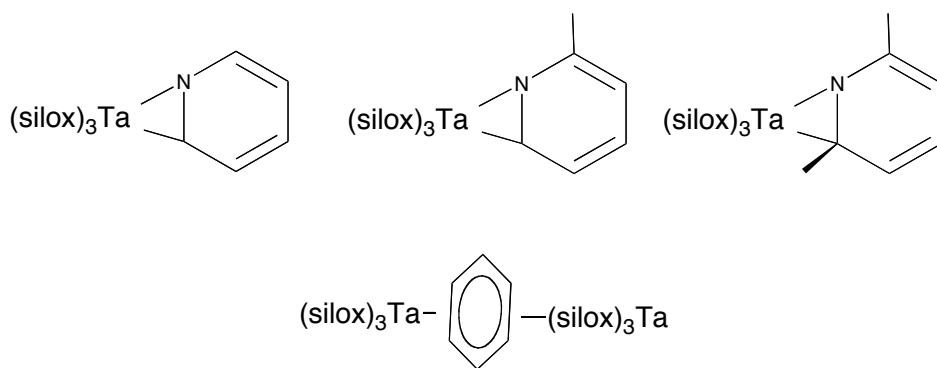


Figure 2.1: Previously synthesized tantalum species with dihapto coordinated aromatics.
5-6

Although it would have been reasonable to use this system and test it for activation of the bound ligand, we felt that with the large differences between the motifs evinced in Chapter 1 and those illustrated by the $\{\text{Ta}(\text{silox})_3\}$ metal fragments, we were more likely to successfully synthesize a metal fragment capable of dearomatization and subsequent organic transformation of the bound aromatic if the metal fragment was designed in line with the tenets laid out in Chapter 1.

2.2 High Valent Tantalum Chemistry

Because there were no commercially available low valent tantalum starting materials, TaCl_5 was selected as the starting material of choice. When compared to the

starting materials of the other third row metals used in dearomatization, the pricing of TaCl₅ fares well, although its cost is so close to that of the W(CO)₆ that little financial advantage can be considered in choosing one over the other (**Table 2.1**).

Compound	OsO ₄	HReO ₄	W(CO) ₆	TaCl ₅
Lot Size	5 x 1g	50 g [†]	100 g	50 g
Cost (\$)	448.00	1,200	312	134.00
Cost(\$/mol metal)	22,776.32	11593.85	1097.93	959.98

Table 2.1: Price of metal starting materials from Strem Chemical Inc. (for largest lot size).

^a Listed as Osmium(VIII) oxide (99.95+%-Os)

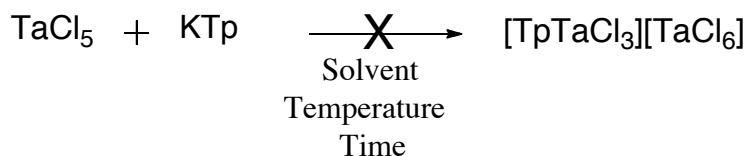
^b Listed as Perrhenic acid, aqueous solution (50-54% Re) (99.99%-Re) PURATREM

^c Listed as Tungsten carbonyl, 99% (<0.3%-Mo)

^d Listed as Tantalum(V) ethoxide (99.99+%-Ta) PURATREM

[†] 50-54% Re aqueous solution

Although it was clear that a reduction would have to take place, initial efforts were directed towards the substitution of chlorides for Tp in hopes of taking advantage of the substitutional lability of the chloride ligands.⁸ The existence of the related [Tp*TaCl₃][TaCl₆] and TaCpCl₄ gave us confidence that the addition of Tp was possible.⁸⁻⁹ Unfortunately, all attempts to use variations on the reaction scheme seen in **Scheme 2.1** resulted in unidentifiable products and intractable mixtures. This is the same result reported by Reger and coworkers.¹⁰

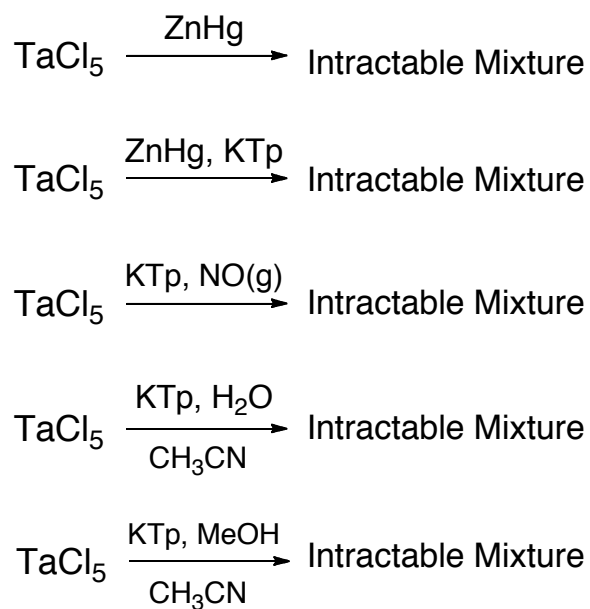


Solvent= DCM, CH₃CN, Toluene
 Temperature= RT, -30° C
 Time= 10 min - 7 days

Scheme 2.1: Attempted Tp-Ta(V) syntheses.

While ^1H NMR showed signals suggestive of a symmetrical set of pyrazoles in a Tp set, there were several distinct patterns that were observed, and often reactions continued to evolve over the course of many days without one distinct major product forming. When CH_2Cl_2 was used, multiple clear ^1H NMR ethyl signals were observed, suggesting that the TaCl_5 was reacting with the solvent. Moreover, replicating the evolution along a single reaction path was difficult.

Other reactions with TaCl_5 were attempted (**Scheme 2.2**). The reduction with $\text{NO}(\text{g})$ was inspired by a successful reduction that was performed in the Harman lab to synthesize the Mo(II) species $\text{TpMo}(\text{NO})(\text{Cl})_2$ species from the Mo(V) species MoCl_5 .¹¹ The reactions in the presence of MeOH and H_2O were performed with the hope that oxo, hydroxy or methoxy groups might add to the tantalum center and act as π bases to stabilize the electron deficient metal center and allow the Tp ligand to complex to tantalum. Again, only intractable mixtures were formed and no identifiable compounds were synthesized from any of these reactions.



Scheme 2.2: Attempted reductions and substitutions with TaCl₅.

The lack of success synthesizing new species from TaCl₅, as well as the fact that TaCl₅ did not have identifiable CV, IR, or NMR signals led us to believe a new direction was needed. Ta(V) chemistry was finally abandoned when the structure of a crystal from a reaction of TaCl₅ and KTP in CH₃CN was solved (**Figure 2.2**).

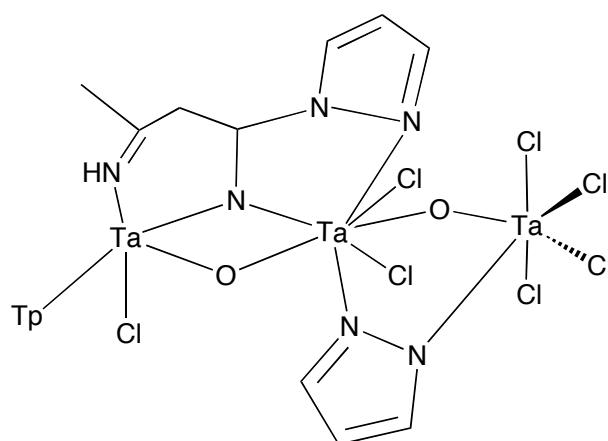
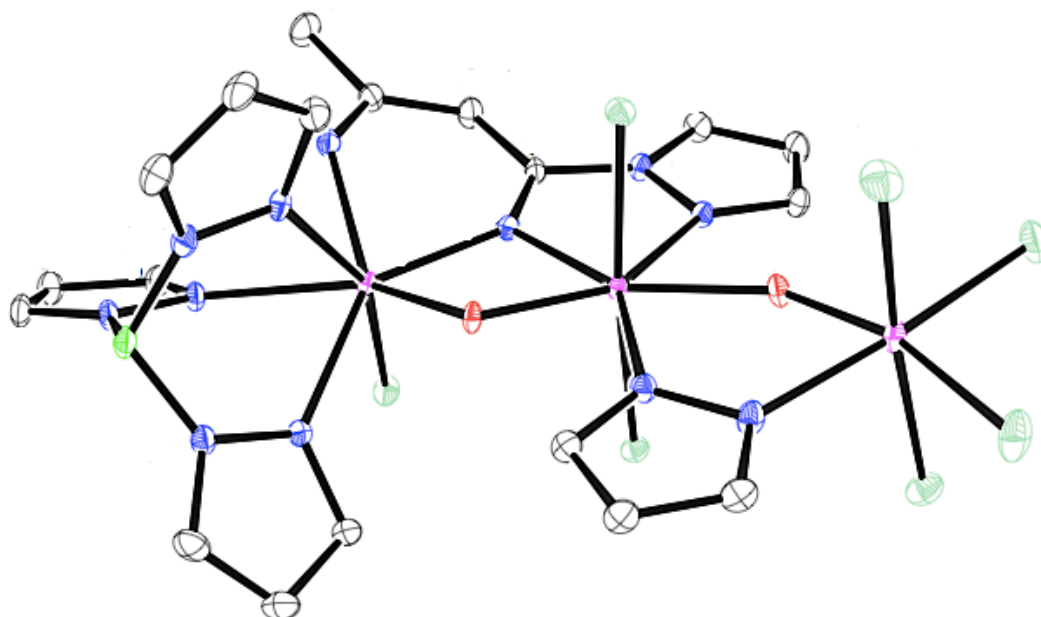


Figure 2.2: Crystal structure and drawing of a Ta(V) trimer.

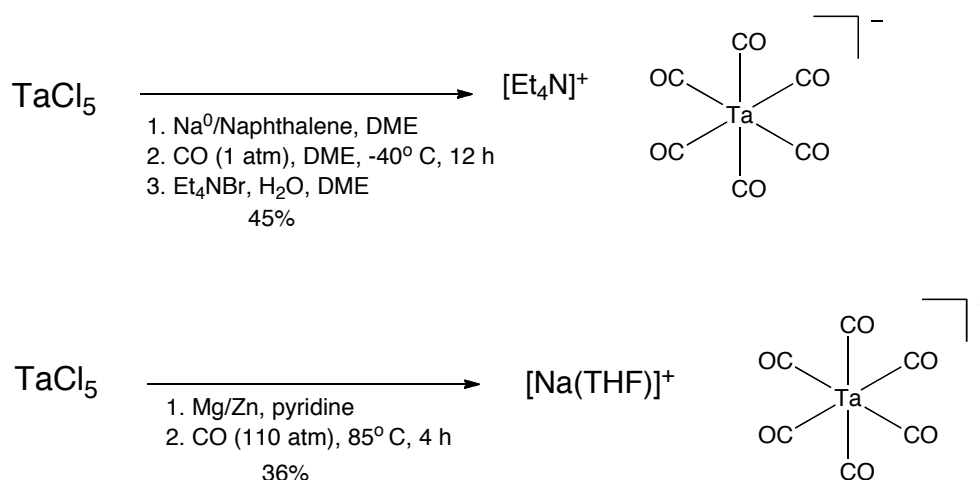
The observed crystal structure showed that TaCl₅ was capable of cleaving the B-N bond of Tp, was reacting with the CH₃CN solvent, and was extremely sensitive to some unknown source of oxygen. Two CH₃CN molecules can be seen incorporated in

the structure. The B-N bond cleavage is consistent with unpublished results from Hubert-Pfalzgraf.¹² These facts suggested that new methods needed to be considered if tantalum(-1) species were going to be synthesized.¹³

2.3 Tetraethylammonium hexacarbonyltantalate

Once the high valent chemistry was abandoned, $[\text{Ta}(\text{CO})_6]^-$ was targeted as a possible starting material. For a number of reasons, $[\text{Et}_4\text{N}][\text{Ta}(\text{CO})_6]$ was attractive. Unlike the d^0 $10e^-$ TaCl_5 , the d^6 , $18e^-$ $[\text{Et}_4\text{N}][\text{Ta}(\text{CO})_6]$ was predicted (and later shown) to be far less reactive. It is also isoelectronic with $\text{W}(\text{CO})_6$, the starting material that had been used for the $\{\text{TpW}(\text{NO})\text{PMe}_3\}$ synthesis, making it much simpler to build analogies between the already elucidated tungsten fragment synthesis and proposed tantalum fragment syntheses. Also unlike the TaCl_5 , $[\text{Et}_4\text{N}][\text{Ta}(\text{CO})_6]$ had easily collectable electrochemical and infrared signatures. This allowed us to utilize these tools in a similar manner to the way that they had been used during the rhenium and tungsten syntheses to quantify changes electron richness and back donating ability as the ligand set was modified.

The first step in utilizing $[\text{Et}_4\text{N}][\text{Ta}(\text{CO})_6]$ was to successfully synthesize it. Unlike $\text{W}(\text{CO})_6$, $[\text{Ta}(\text{CO})_6]^-$ is not commercially available. Two methods have been described in the literature for the synthesis of the $[\text{Ta}(\text{CO})_6]^-$ anion. Calderazzo and coworkers reported a synthesis of $[\text{Na}(\text{THF})][\text{Ta}(\text{CO})_6]$ in 35% yield using zinc and magnesium in pyridine under 110 atm CO pressure.¹⁶ Ellis et al. reported the synthesis of the $[\text{Et}_4\text{N}][\text{Ta}(\text{CO})_6]$ in 45% yield using sodium naphthalenide in DME at atmospheric pressures of CO (**Scheme 2.3**).¹⁷⁻¹⁹



Scheme 2.3: Low pressure and high pressure synthesis of $[\text{Ta}(\text{CO})_6]^-$

Due to the high pressures required for the Calderazzo synthesis, the Ellis procedure was chosen for synthesis of $[\text{Et}_4\text{N}][\text{Ta}(\text{CO})_6]$.¹⁹ The first challenge met in this process was modifying the reported procedure for glovebox use. This was met with some trepidation because other literature sources reported that the 45% yields reported by Ellis were difficult to obtain, even when replicating the procedure using the original Schlenk line techniques. Multiple sources reported 15-20% yields on average.²¹⁻²² **Table 2.2** and **Figure 2.3** below relate the work performed to obtain the $[\text{Et}_4\text{N}][\text{Ta}(\text{CO})_6]$ product.

Reaction Code	Scale (TaCl ₅)	Yield	Atmosphere (X/X) ^a	Time (min) (X/X/X) ^b	Temperature (° C) (X/X) ^c
AN3-088	1.00 g	0.05g , 2%	N ₂ /N ₂ :CO	65/910/170	-45/-45
AN3-096	1.00 g	0.194g, 12.7%	N ₂ /N ₂ :CO	25/1025/45	-50/-50
AN3-112	1.00 g	0.033 g	N ₂ /N ₂ :CO	35/1100/45	-50/-50
AN3-116	1.00 g	0	N ₂ /N ₂ :CO	30/120/55	-50/-50
AN3-122	1.00 g	0.340 g, 26%	N ₂ /N ₂ :CO	25/720/25	-50/-50
AN3-130	1.00 g	0.003 g	N ₂ /N ₂ :CO	30/1200/45	-50/-50
AN3-138	1.00 g	0.187 g , 13%	N ₂ /N ₂ :CO	35/720/65	-48/-48
AN3-142	1.00 g	0 g	N ₂ /N ₂ :CO	30/730/40	-50/-50
AN3-150	1.00 g	0 g	N ₂ /N ₂ :CO	40/665/25	-50/-50
AN3-152	1.00 g	0 g	N ₂ /N ₂ :CO	10/230/0	-50/-50
AN3-154	1.00 g	0.220 g, 16.4%	N ₂ /N ₂ :CO	5/205/145	-45/-45
AN3-156	1.00 g	0.120 g, 9.02%	N ₂ /N ₂ :CO	60/660/140	-45/-45
AN3-158	1.00 g	0.024 g , 1.8%	N ₂ /N ₂ :CO	50/205/150	-50/-50
AN3-164	1.00 g	0 g	N ₂ /N ₂ :CO	70/65/115	-50/-50
AN3-166	1.00 g	0 g	N ₂ /N ₂ :CO	10/920/125	-40/-60
AN3-172	1.00 g	0 g	N ₂ /N ₂ :CO	15/420/800	-60/-60
AN3-176	1.00 g	0 g	N ₂ /N ₂ :CO	30/660/150	-40/-60
AN3-180	1.00 g	0 g	N ₂ /N ₂ :CO	10/1125/10	-60/-60
AN3-182	1.00 g	0 g	N ₂ /N ₂ :CO	10/610/75	-60/-60
AN3-188	1.00 g	0 g	N ₂ /N ₂ :CO	20/690/120	-60/-60
AN3-200	1.00 g	0 g	N ₂ /N ₂ :CO	140/710/180	-40/-60
AN3-204	1.00 g	0.097g, 7.3%	Ar/Ar:CO	25/800/55	-50/-50
AN3-206	1.00 g	0.235, 17.5%	Ar/Ar:CO	5/795/180	-50/-50
AN3-216	1.00 g	0.075, 5.6%	Ar/Ar:CO	50/725/385	-40/-60
AN3-248	1.00 g	0 g	Ar/Ar:CO	50/685/120	-40/-60
AN3-254	1.00 g	0.037 g, 2.76%	Ar/Ar:CO	30/915/120	-50/-50
AN3-262	1.00 g	0.447 g, 34%	Ar/CO	75/765/205	-50/-50
AN3-264	1.00 g	0.437 g, 33%	N ₂ /CO	65/845/240	-50/-50
AN3-274	5.00 g	1.30 g, 19.5%	N ₂ /CO	120/760/210	-37/-37
AN3-276	5.00 g	1.69 g, 25.2%	N ₂ /CO	90/835/140	-37/-37
AN3-278	5.00 g	1.47 g, 22.1%	N ₂ /CO	50/800/110	-37/-37
AN3-280	5.00 g	1.16 g, 17.5%	N ₂ /CO	60/675/70	-38/-38
AN3-282	5.00 g	1.18 g, 17.7%	N ₂ /CO	25/980/25	-33/-33

Table 2.2: Table describing the attempted syntheses of [Et₄N][Ta(CO)₆].

^a Composition of reaction atmosphere (Before CO addition/After CO addition). N₂:CO indicates a ~30:70 mixture of gases.

^b Time allowed for each phase of reaction (Time stirred pre-CO addition/Time stirred post-CO addition/warming time)

^c Temperature at each phase of reaction (Temperature before CO addition/Temperature after CO addition)

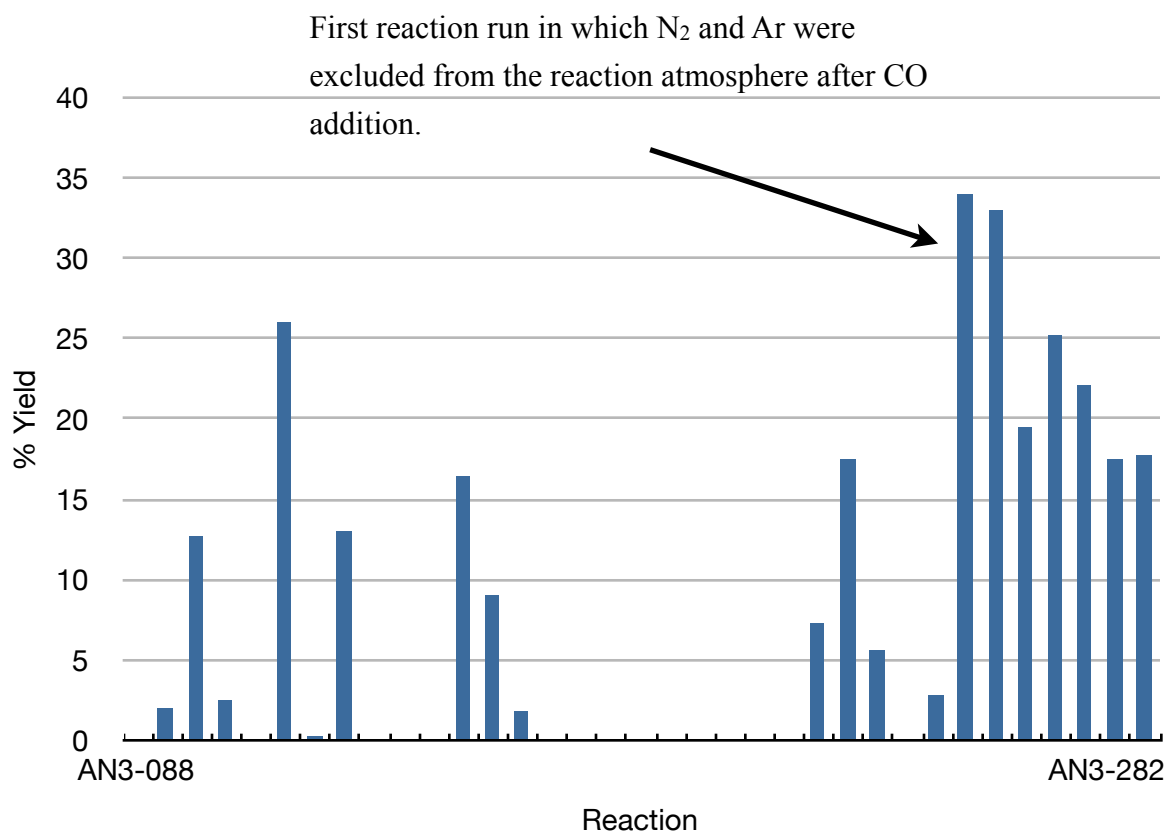
Yield of $[\text{Et}_4\text{N}][\text{Ta}(\text{CO})_6]$ - Syntheses in Chronological Order

Figure 2.3: Yield of each synthesis reported in **Table 2.2**. The x-axis represents the chronology of the reactions performed from left to right.

From the data in **Table 2.2** and **Figure 2.3**, it is apparent that the composition of the reaction atmosphere is extremely important in the synthesis. Early experiments focused on altering the time allotted for each step of the reaction, and as seen most clearly in **Figure 2.3**, occasionally good results could be obtained. However, the results were erratic even when the reaction conditions were nearly identical (e.g., compare reactions AN3-122 and AN3-142), making it difficult to begin the process of synthesis optimization. We concede that **Table 2.2** has few sets of reaction conditions which were

identical, but also argue that the differences noted between reactions that did work well and those that did not were often small enough that they could not explain why sometimes $[\text{Et}_4\text{N}][\text{Ta}(\text{CO})_6]$ was obtained and other times was not obtained. At first, it was believed that the propensity of TaCl_5 to decompose under the N_2 atmosphere of the glovebox was to blame. A procedure for the resublimation of TaCl_5 was developed, but neither using resublimed material nor using commercially resublimed TaCl_5 immediately after it was received resolved the problem. After numerous attempts, it was hypothesized that the problem may have been that an N_2 atmosphere was being used instead of the argon atmosphere used by Ellis.¹⁷ The reaction atmosphere that had been used was a mixture of CO and N_2 which was achieved by the addition of CO through a septum into a reaction flask equipped with a unfilled balloon. CO was added until the total volume was approximately 70% CO . When Ar was employed, the results were initially promising, but eventually showed the same erratic nature as before. However, because all reactions were run in the N_2 atmosphere of the glovebox, N_2 may have gotten into the reaction atmosphere even when only Ar was expected. Often when 0% or very low yields were noted, a red solution would be observed after filtration of the crude reaction solution instead of the expected yellow solution. Serendipitously, it was observed that if this red solution was bubbled with $\text{CO}_{(\text{g})}$ for even 10 minutes, it would convert to a yellow solution. This visual cue led to performing the synthesis in the presence of only CO . In **Figure 2.3**, it can clearly be seen that once this change was made, the yields became much higher and more consistent. Because the $[\text{Ta}(\text{CO})_6]^-$ product is stable under both Ar and N_2 , it was surprising to find that the reaction worked well in the presence of only CO ,

but was essentially ineffective if the composition of CO to Ar or N₂ was ~70:30. One possible explanation is that N₂ reacted with some intermediate formed after CO addition.²³ This could explain why the N₂ seemingly had no effect on the reaction yields when present before CO addition. In order for this hypothesis to be true, some amount of N₂ from the reaction atmosphere must have leaked into the reaction flask even when the reaction was supposed to be under Ar only. It is also possible that without very high partial pressures of CO, the reaction simply cannot form the product quickly enough, and some unstable intermediate in the reaction decomposes prior to forming product. These hypotheses could explain an isolated successful reaction by invoking the occasional reaction in which the CO partial pressure was higher than expected or the partial pressure of N₂ was particularly low. Unfortunately, due to the erratic nature of the reactions prior to the use of a CO reaction atmosphere, little can be drawn from the data in terms of optimal times to be used at each stage of the reaction. One important point to be considered for future optimization of this experiment is that Ellis and coworkers report that from the tris(η^4 -naphthalene)tantalate intermediate, the addition of CO leads to 99% [Ta(CO)₆]⁻ in ten minutes.²³ **Table 2.2** shows that the large scale reactions (5.00 g) were run at higher temperatures than the small scale (1.00 g) reactions. Unfortunately, the cooling equipment readily available was not capable of cooling the larger reaction apparatus to -50° C; we expect that with the proper equipment yields and optimization, yields exceeding the reported maximum of 34% (AN3-262) should be obtainable for the large scale synthesis.

$[\text{Et}_4\text{N}][\text{Ta}(\text{CO})_6]$ showed a number of experimental characteristics worth noting. The ^1H NMR of $[\text{Et}_4\text{N}][\text{Ta}(\text{CO})_6]$ showed, as expected, only peaks for the $[\text{Et}_4\text{N}]^+$ counterion. Of particular interest was the methyl signal of the ethyl moieties. These protons were split into a triplet in which each peak of the triplet gave a 1:1:1 three line pattern. It was assumed that the nitrogen nucleus ($\text{spin}=1$) was the source of the additional coupling instead of the simple triplets one might expect. It was surprising that the the hydrogens in the C-H methyl bond and the nitrogen were coupled, but that the hydrogen of the C-H methylene bond and the nitrogen were not.

2.4 Electrochemical Predictions

Because electrochemistry was so integral to the discovery of dearomatizing metal fragments with rhenium and tungsten, we wanted to direct effort towards making reasonable predictions about the electrochemistry of our target compounds in order to determine the likelihood that they would be successful dearomatizing agents.

There are very few Ta(-1) species reported in the literature, fewer that have reported electrochemical values, and even fewer that have ligand sets that do not contain four or five carbonyls. This made it very difficult to find compounds that were similar to our target compounds to make electrochemical comparisons. One species, Ta(trimpsi)(CO)₂(NO) did have an electrochemical measurement reported ($E_{p,a}=0.01$ V vs. NHE).¹⁴ This is similar to the hypothetical TaTp_m(CO)(NO)(η^2 -benzene) in that both contained the metal fragment {Ta(tridentate ligand)(CO)(NO)}. {TaTp_m(CO)(NO)} was chosen as our hypothetical metal fragment because it matched the characteristics for a dearomatization agent discussed in Chapter 1. When TpW(PMe₃)(NO)(CO) ($E_{p,a}=0.32$ V)

is compared to $\text{TpW}(\text{PMe}_3)(\text{NO})(\eta^2\text{-benzene})$ ($E_{\text{p,a}}=-0.13$ V), it is seen that the exchange of a CO for $\eta^2\text{-benzene}$ leads to a $\Delta E_{\text{p,a}}\approx-0.45$ V. Thus, under the assumption that these changes in electrochemistry are purely additive (and that the $E_{\text{p,a}}$ values accurately reflected E° values), it was predicted that $\text{Ta}(\text{trimpsi})(\text{CO})(\text{NO})(\eta^2\text{-benzene})$ would have an approximate $E^\circ=-0.45$ V. This was somewhat negative of the desired predicted potential ($\sim E^\circ=-0.1$ V). The $E^\circ\approx-0.1$ V was desired because it matched the potential of the rhenium and tungsten metal fragments bound in an η^2 fashion to a benzene ligand. In order to predict how the exchange of a trimpsi ligand for a Tpm ligand would affect the electrochemistry, methods described by Lever were used.²⁴ Lever describes a method of predicting the effect of a change in ligand set on the III/II potential of ruthenium systems by making the assumption of ligand additivity and the use of tables of data on different possible ligands. Using his method, the predicted III/II potentials for $\text{Ru}(\text{CO})_3(\text{Pz})_3^{2+}$ and $\text{Ru}(\text{CO})_3(\text{PMe}_3)_3^{2+}$ were found to be 3.46 V and 3.84 V, respectively. The necessary data to make predictions about tantalum 0/-1 potentials were not offered by Lever. This $\Delta E=-0.38$ was used to make the prediction that $\text{TaTpm}(\text{CO})(\text{NO})(\eta^2\text{-benzene})$ would have an $E^\circ=-0.83$ V. While clearly this prediction was on shaky ground, it provided the idea that one of our target compounds may be too electron rich and that the trimpsi derivative may actually be a better option should the Tp and Tpm fail. Because we believed that the electrochemical prediction may be quite different from the actual potential, the expectation that $\{\text{TaTpm}(\text{CO})(\text{NO})\}$ could be the metal fragment we were searching for was maintained. It should be noted that there are a couple of questionable assumptions in this prediction, such as the assumption that the prediction for replacing a

trimpsti with Tpm on a ruthenium with three carbonyls will be the same as on a tantalum with a carbonyl and a nitrosyl. The assumption that the difference in electrochemistry after the replacement of a CO for an η^2 -benzene in the tungsten system (with one strong π acid) versus replacement of CO for an η^2 -benzene in the tantalum system (with two strong π acids) is also a suspect assumption.

It is interesting to note that when $[\text{Ta}(\text{CO})_6]^-$ is compared to the $\text{TpW}(\text{PMe}_3)(\text{NO})(\text{CO})$ species, $[\text{Ta}(\text{CO})_6]^-$ appears to actually be more electron rich (**Table 2.3**). The fact that if CO is replaced with benzene in the $\text{TpW}(\text{PMe}_3)(\text{NO})(\text{CO})$ species dearomatization is achieved makes this point particularly tantalizing inasmuch as it suggests $\{\text{Ta}(\text{CO})_5\}^-$ may actually be electron rich enough to bind aromatic molecules. This is explored in Chapter 3a.

	$[\text{Et}_4\text{N}][\text{Ta}(\text{CO})_6]$	$\text{TpW}(\text{PMe}_3)(\text{NO})(\text{CO})$
CV (CH_3CN)	$E_{p,a}=0.24 \text{ V}^a$	$E_{p,a}=0.32 \text{ V}^b$
IR (HATR)	1817 cm^{-1}^a	1864 cm^{-1}^c

Table 2.3: Comparison of IR and CV signatures of $[\text{Ta}(\text{CO})_6]^-$ and $\text{TpW}(\text{PMe}_3)(\text{NO})(\text{CO})$.

^a This work

^b See reference 25

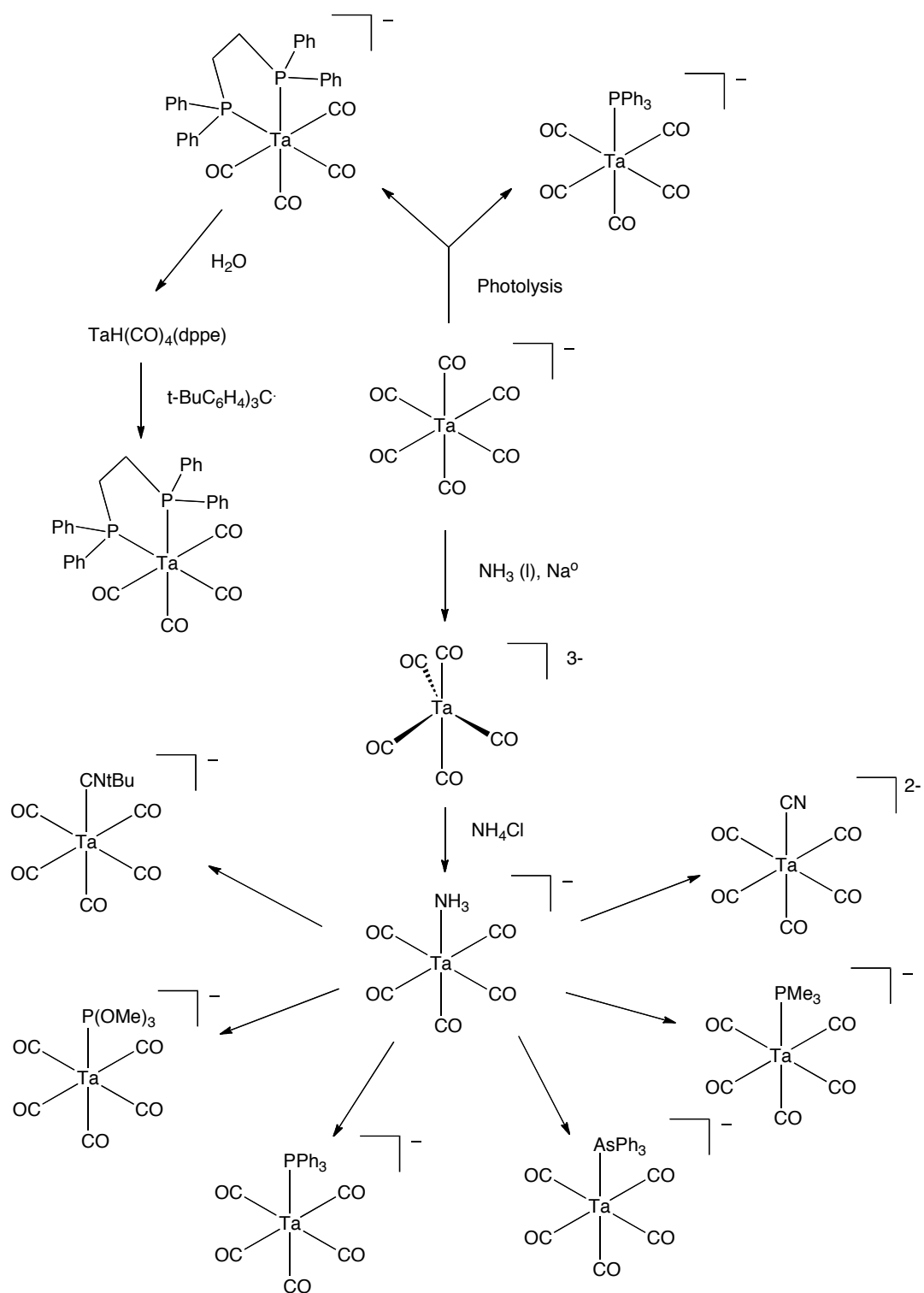
^c Work performed by Peter Graham.

2.5 Chemistry of $[\text{Et}_4\text{N}][\text{Ta}(\text{CO})_6]$

While the chemistry of $[\text{Et}_4\text{N}][\text{Ta}(\text{CO})_6]$ has not been exhaustively explored, a number of basic reactions have been elucidated which were instructive during the construction of an outline for the synthesis of the tantalum dearomatization agent.

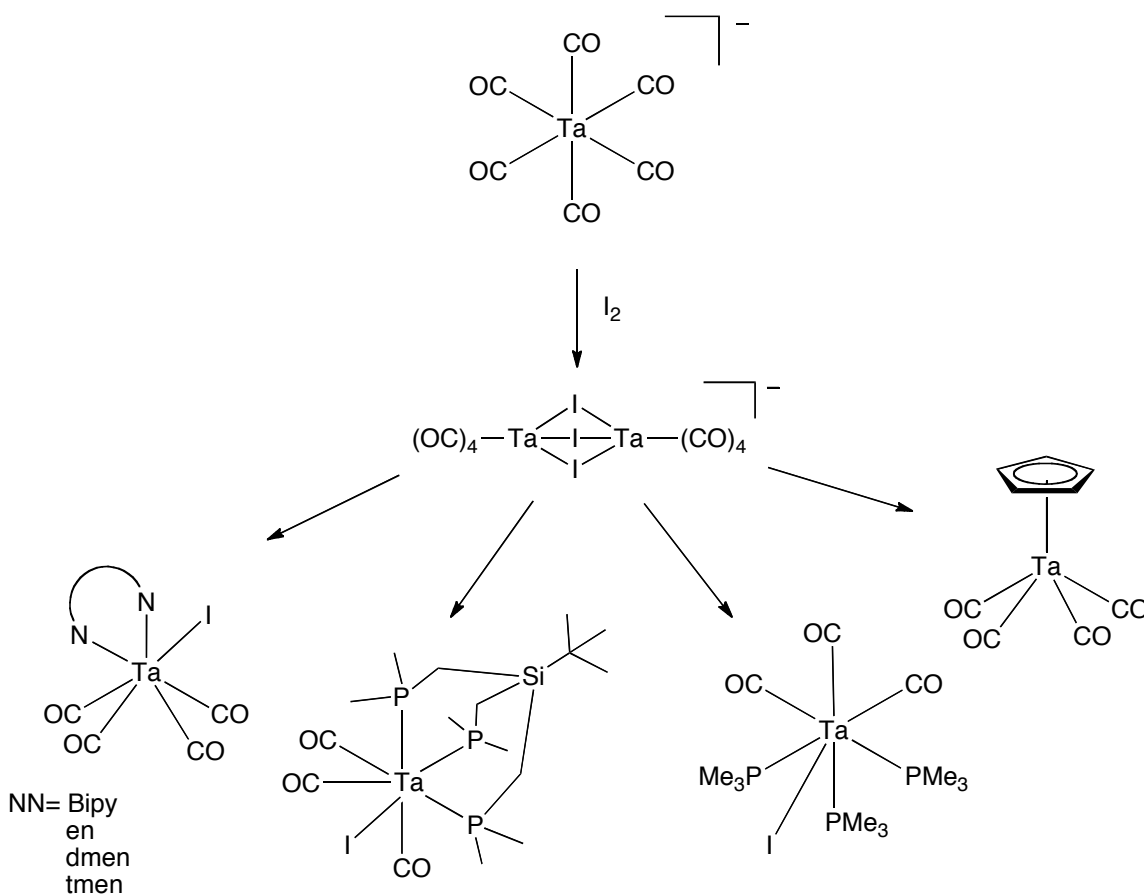
A number of single and double ligand substitutions have been performed by Ellis and coworkers. The syntheses of both $[\text{Et}_4\text{N}][\text{Ta}(\text{CO})_5\text{PPh}_3]$ and $[\text{Et}_4\text{N}][\text{Ta}(\text{CO})_4\text{dppe}]$

were performed via photolysis of the $[\text{Ta}(\text{CO})_6]^-$.²⁶ In a separate work, Ellis reports the reduction of the $[\text{Ta}(\text{CO})_6]^-$ to $[\text{Ta}(\text{CO})_5]^-$.²⁷ Using the highly reduced $[\text{Ta}(\text{CO})_5]^{3-}$, the substitutionally labile $[\text{Ta}(\text{CO})_5\text{NH}_3]^-$ was synthesized and used to make a number of different products (**Scheme 2.4**). Also, the $[\text{Et}_4\text{N}][\text{Ta}(\text{CO})_4\text{dppe}]$ was used in the synthesis of the only known monomeric $17e^-$ Ta species.²¹



Scheme 2.4: Mono- and Disubstituted $[\text{Ta}(\text{CO})_6]^-$ derivatives.

Calderazzo and coworkers also reported a number of ligand substitutions. Unlike those already covered, oxidation of the $[\text{Ta}(\text{CO})_6]^-$ was used to favor the loss of the π -acidic CO. Perhaps most importantly, the formation of a number of easily synthesized, labile, binuclear d^4 Ta species were reported. Of these, the $[\text{Ta}_2(\text{CO})_8\text{I}_3]^-$ species is pictured in **Scheme 2.5**.^{1,28} As shown in **Scheme 2.5**, these binuclear species were valuable reagents in the formation of wide range of carbonyl containing tantalum species.



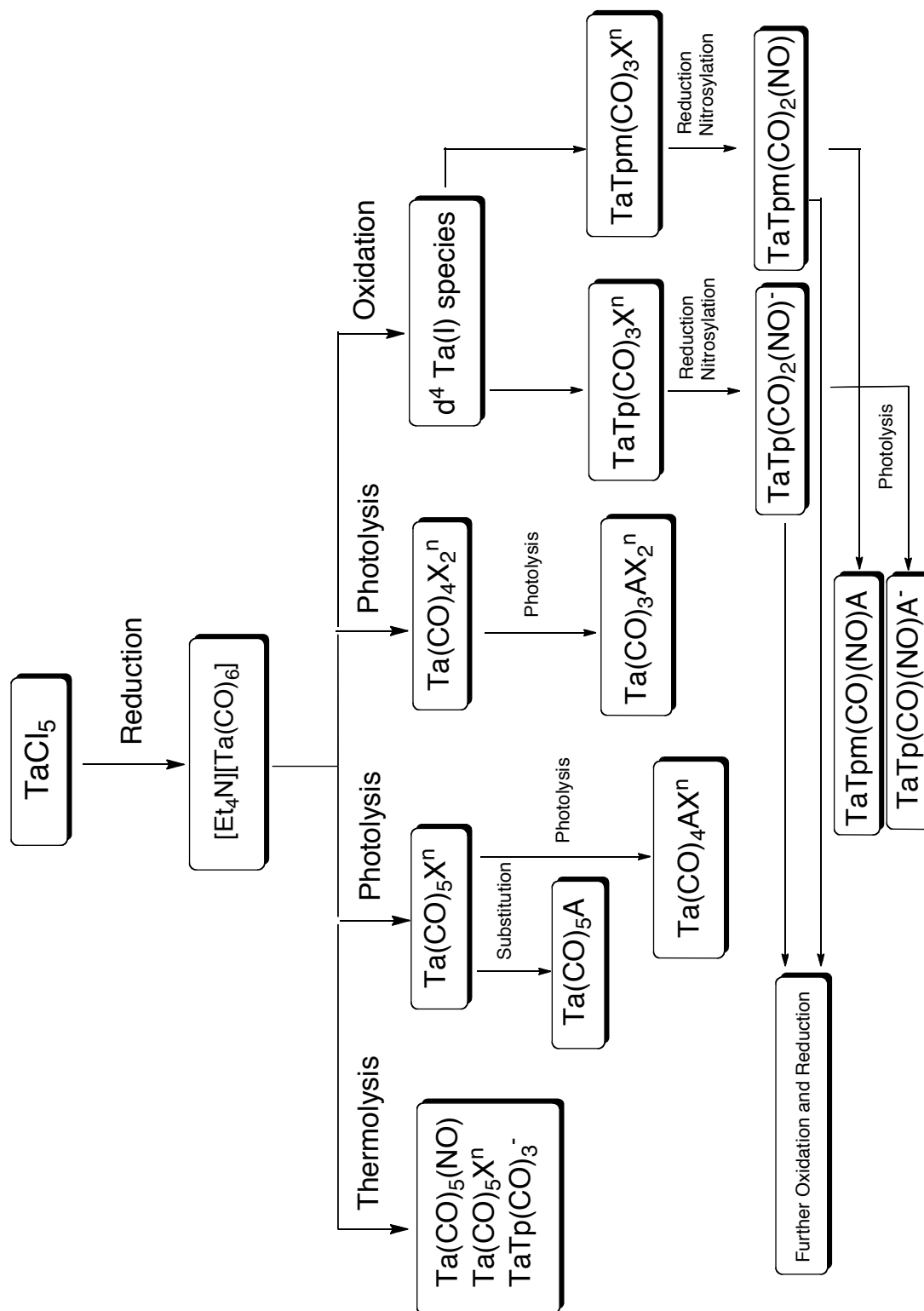
Scheme 2.5: Compounds accessible from oxidation of $[\text{Ta}(\text{CO})_6]^-$.^{1,2,9,28-30}

The reactions in **Scheme 2.4** and **Scheme 2.5** demonstrate a number of important points. Monosubstituted Ta(-1) pentacarbonyls can be accessed, as well as disubstituted

Ta(-1) tetracarbonyls. In the Ta(I) oxidation state, tetracarbonyls species, tricarbonyl species, and dicarbonyl species are accessible.^{1,2,9,28-30} Also, it is possible to reduce these species back to formal Ta(-1) species using the proper conditions, as well as perform nitrosylations as demonstrated by Legzdins and coworkers.²

2.6 Plan of Action

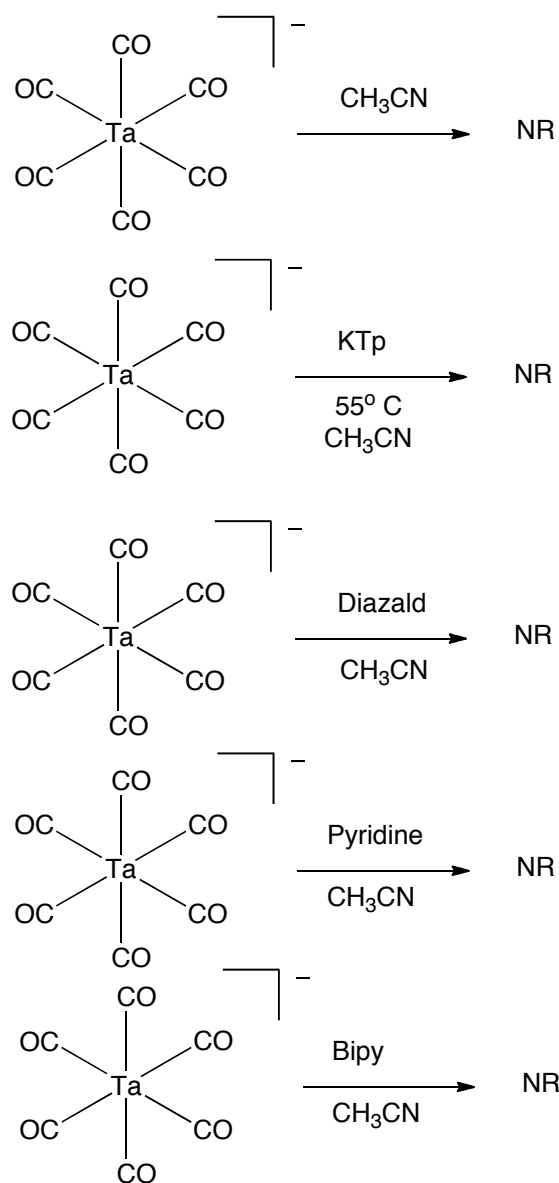
With the $[\text{Et}_4\text{N}][\text{Ta}(\text{CO})_6]$ in hand and the high valent tantalum chemistry abandoned, an outline was formed for the synthesis of the dearomatization agent using the previously described tantalum chemistry as a guide (**Scheme 2.6**).



Scheme 2.6: Plan for the synthesis of a tantalum dearomatization agent. X= σ donor; n = undefined charge; A= aromatic species

The flow chart in **Scheme 2.6** describes the synthesis of a number of new tantalum based compounds which are synthesized using the methods described in section 2.5. Although the right most portion of the flow chart best reflects the ideas considered in Chapter 1 for a dearomatization agent, it seemed foolish to not consider the other paths considering the ease with which they could be executed. From **Scheme 2.6**, TaTp(CO)(NO(η^2 -benzene)) and [TaTp(CO)(NO)(η^2 -benzene)]⁻ in particular were identified as target compounds. Through the use of CV and IR to quantify the ability of the synthesized species to donate electron density, it was hoped that the proper combination of σ donors and π acceptors could be found.

Because of the ease with which they could be executed, the thermal substitution reactions were attempted first. These were also the reactions most analogous to the initial steps of the TpW(PMe₃)(NO)(η^2 -benzene) synthesis (See Chapter 1).



Scheme 2.7: Substitutions attempted with $[\text{Ta}(\text{CO})_6]^-$. No reactions were observed.

It was hoped that the initial substitution could be effected simply by the addition of the desired ligand. In particular, it was conceived that nitrosylation via Diazald would be accessible considering the electron rich nature of the $[\text{Ta}(\text{CO})_6]^-$. However, it was found that the $[\text{Et}_4\text{N}][\text{Ta}(\text{CO})_6]$ was thermally quite stable to substitution, a conclusion

well supported in the literature.^{18,21,26} This conclusion can also be explained by considering the electron rich nature of the $[\text{Ta}(\text{CO})_6]^-$. The strong back bonding into the CO observed via the ν_{CO} would suggest a very stable Ta-CO bond. In the reactions above, even ambient light was carefully excluded. When it was not, it was often noted visually that reactions occurred. The results of these light-driven reactions is the focus of Chapter 3a.

2.7 Conclusion

We have endeavored to synthesize an electron-rich tantalum-based metal fragment capable of disrupting the inherent stability of an aromatic molecule. Because it is easily accessible, a number of reactions were performed using TaCl_5 as a starting material. Unfortunately, TaCl_5 proved to be difficult to control under reasonable reaction conditions, and it was determined that $[\text{Ta}(\text{CO})_6]^-$ was a more useful starting material. Extensive work went into modifying the reported $[\text{Et}_4\text{N}][\text{Ta}(\text{CO})_6]$ synthesis for glovebox use, and 34% yields are currently obtained using the modified procedure. Although chemistry with $[\text{Ta}(\text{CO})_6]^-$ has not been extensively explored, there are a number of basic reactions which were used to generate a plan for the synthesis of a dearomatization agent. Early reactions with $[\text{Ta}(\text{CO})_6]^-$ proved it to be thermally stable to substitution; therefore, other reaction conditions were considered.

2.8 Experimental

General Methods

NMR spectra were obtained on a 300 or 500 MHz spectrometer (Varian INOVA). All chemical shifts are reported in ppm. Proton shifts are referenced to tetramethylsilane (TMS) utilizing residual ^1H signals of the deuterated solvents as an internal standard. Coupling constants (J) are reported in hertz (Hz). Infrared spectra (IR) were recorded on a MIDAC Prospect Series (Model PRS) spectrometer as a glaze on a Horizontal Attenuated Total Reflectance (HATR) accessory (Pike Industries). Electrochemical experiments were performed under a dinitrogen atmosphere using a BAS Epsilon EC-2000 potentiostat. Cyclic voltammetry data was taken at ambient temperature at 100 mV/s (25 °C) in a standard three-electrode cell with a glassy carbon working electrode using tetrabutylammonium hexafluorophosphate (TBAH) as an electrolyte (approx. 0.5 M in an appropriate solvent). All potentials are reported versus NHE (Normal Hydrogen Electrode) using cobaltocenium hexafluorophosphate ($E_{1/2} = -0.78$ V) or ferrocene ($E_{1/2} = +0.55$ V) as an internal standard. The peak-to-peak separation was 100 mV or less for all reversible couples. Unless otherwise noted, all synthetic reactions were performed in a glovebox under a dry nitrogen atmosphere. Anhydrous (99.5%) 1,2 dimethoxyethane was used as received from Sigma-Aldrich. Acetonitrile was dried using an alumina packed still. Drisolve tetrahydrofuran (THF) was used as received. These and other solvents and liquid reagents were thoroughly purged with nitrogen prior to use. Deuterated solvents were used as received from Cambridge Isotopes.

[Et₄N][Ta(CO)₆] (1)

The follow procedures were derived from the procedures reported by Ellis, et. al. in 1983 and 1995.¹⁷⁻¹⁸ They have been modified in size and such that the synthesis may be performed without the use of Schlenk line techniques.

Sodium (ca. 0.400 g, 0.0174 mol) was cut into small pieces (ca. 1 mm³) and added to a solution of 20 mL DME in a 100 mL Schlenk flask (**Figure 15**). A glass-covered magnetic stirbar was added to create a suspension of Na⁰ in DME. Naphthalene (2.18 g, 0.0170 mol) was dissolved in 10 mL DME and added to the suspension in order to prepare a solution of the deep green NaC₁₀H₈. The suspension was sealed from outside atmosphere and allowed to stir at room temperature for 4 hours, after which time it was cooled to -50° C. Cold DME (10 mL, -50° C) was added to a 30 mL test tube with a teflon-covered magnetic stir bar and TaCl₅ (1.00g, 0.00167 mol) was added to the cold DME over a period of 15 minutes. Care was taken to ensure a slow, even addition of TaCl₅ to prevent degradation of the starting material. The cold TaCl₅ solution was then transferred to a cold (-50° C), rapidly stirred slurry of NaC₁₀H₈ in the 100 mL Schlenk flask. Note that solid is often noted prior to the addition of TaCl₅ to NaC₁₀H₈; there can be enough solid to make stirring difficult. Addition of TaCl₅ should cause any solid to disappear quickly. The flask was sealed and the NaC₁₀H₈ solution turned from a deep green to a deep brown or reddish color at this time. After 1 hour of vigorous stirring at -50° C, the N₂ in the reaction flask was flushed out and replaced with CO. This was accomplished by bubbling CO through the reaction mixture for 3 minutes, then sealing the reaction flask. The ⊥ sidearm (See **Figure 2.4**) of the reaction flask was sealed with a

filled CO balloon to increase the amount and pressure of CO in the reaction flask. After 12 hours, the solution was allowed to slowly warm to 0° C over 3.5 hours. The solution was then stirred at room temperature for an additional 30 minutes. The CO filled balloon was removed, exposing the solution to the N₂ atmosphere, and the brownish-red solution was filtered through a 60 mL M fritted glass funnel with a 3 cm celite plug over a 250 mL filter flask. An intense yellow filtrate was collected. The brown solid layer collected was washed with DME until filtering liquid appeared clear. The remaining solid was discarded and the yellow filtrate was evaporated to a total volume of ca. 20 mL. H₂O (ca. 100 mL) was added to the solution, causing massive precipitation of naphthalene. Mixture was filtered through a 150 mL M fritted glass funnel over a 250 mL filter flask to give a yellow filtrate. The naphthalene was washed with 3 x 15mL H₂O. Et₄NBr (0.88 g, 0.0042 mol) was dissolved in 5 mL H₂O. The aqueous Et₄NBr was added to the yellow filtrate, again causing massive precipitation, this time of [Et₄N][Ta(CO)₆]. The product was collected on a 60 mL M fritted glass funnel and stored in a vacuum desiccator overnight. Note that the filtrate of this precipitation should be clear or a very pale yellow. The dried solid still in the 60 mL M fritted glass funnel was dissolved in DME and collected in a 125 mL filter flask. The yellow filtrate was evaporated to ca. 5 mL DME and excess hexanes were added to precipitate [Et₄N][Ta(CO)₆]. The yellow precipitate was collected on a 30 mL M fritted glass funnel. The filtrate was noted to be clear at this point. Often it was noted that a significant amount of solid adhered to the glass filter flask upon precipitation. In these cases, a small amount of DME was added to the flask to dissolve the solid, and the DME solution was transferred to a polypropylene

container, where it was again precipitated with excess hexanes. This precipitate was collected using the same fritted glass funnel. Note: THF can be used during the final precipitation for purification. **1** is soluble in MeCN, THF, DME, CH₂Cl and is partially soluble or insoluble in benzene, CHCl₃, and hexanes. Desiccation of this solid led to the collection of 0.45 g (0.939 mmol, 34% yield) of dry [Et₄N][Ta(CO)₆]. ¹H NMR (300 MHz, CD₃CN): δ 3.16 (q, 8H, J_{HH}=7.3 Hz, CH₂ of Et) , 1.21 (tt, 12H, J_{NH}=1.9 Hz, J_{HH}=7.3 Hz, CH₃ of Et). IR (HATR): 1817 cm⁻¹ (strong), 1905 cm⁻¹ (weak shoulder) CV: (CH₃CN) E_{p,a}=0.24 V. (DMA) E_{p,a}=0.25 V.

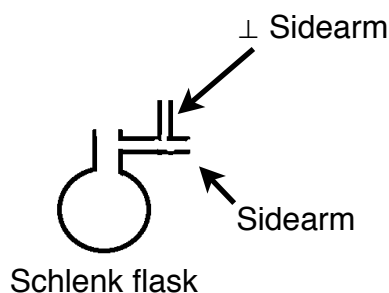


Figure 2.4: Depiction of 100 mL Schlenk flask.

Purification of TaCl₅ by sublimation

TaCl₅ (4.00 g, 11.2 mmol) under N₂ atmosphere was placed in a sublimation apparatus. The apparatus was sealed with a vacuum and an N₂ line was connected to cool the cold finger. The apparatus was heated to 120° C in an oil bath. Over the course of 1 hour, a significant amount of snow white solid crystalline needles formed on the end of the cold finger. The vacuum was carefully released and the solid was collected in a vial. While the solid was being collected, a white mist was noted to be emanating from the apparatus. The clean cold finger was replaced, the vacuum was applied, and sublimation

was continued. Care was taken not to allow too much solid to collect on the cold finger due to the tenuous nature of the connection between the cold finger and the purified TaCl_5 . At the end of the sublimation, a mass of black solid was noted in the bottom of the apparatus and a total of 2.44 g TaCl_5 was collected. Note: this amount will vary depending on the initial purity of the TaCl_5 .

2.9 References

- (1) Calderazzo, Fausto; Castellani, Manola; Pampaloni, Guido. *J. Chem. Soc. Dalton Trans.*, **1985**, 1989-1995.
- (2) Hayton, Trevor W.; Daff, James P.; Legzdins, Peter; Rettig, Steven J.; Patrick, Brian O. *Inorg. Chem.*, **2002**, 41, 4114-4126.
- (3) Reger, Daniel L.; Swift, Cornelius A.; Lebioda, Lukasz. *Inorganic Chemistry*. **1984**, 23, 349-354.
- (4) Based on a search of Strem Chemical Inc.; 6/30/2010.
- (5) Covert, Katharine J.; Neithamer, David R.; Zonneville, Marjanne J.; LaPointe, Robert E.; Schaller, Christopher P.; Wolczanski, Peter T. *Inorganic Chemistry*. **1991**, 30, 2494-2508.
- (6) Neithamer, David R.; Parkanyi, Laszlo; Mitchell, John F.; Wolczanski, Peter T. *J. Am. Chem. Soc.* **1988**, 110, 4421-4423.
- (7) Note that d^0/d^2 is listed instead of a single d-electron configuration because the structures as drawn in references 4 and 5 appear to be formal d^0 metal centers, but backbonding is invoked in the reference, requiring the presence of d-electrons.
- (8) Mashima, Kazushi; Oshiki, Toshiyuki; Tani, Kazuhide. *Organometallics*, **1997**, 16, 2760-2762.
- (9) Werner, Robert P. M.; Filbey, Allen H.; Manastyrskyj, Switlana A. *Inorganic Chemistry*, **1964**, 3, 298-300.

- (10) Reger, Daniel L.; Swift, Cornelius A.; Lebioda, Lukasz. *Inorg. Chem.*, **1984**, *23*, 349-354.
- (11) Mocella, Christopher J.; Delafuente, David A.; Keane, Joseph M.; Warner, Gretchen R.; Friedman, Lee R.; Sabat, Michal; Harman, W Dean. *Organometallics*, **2004**, *23*, 3772-3779.
- (12) Hubert-Pfalzgraf, Liliane G.; Tsunoda, Mitsukimi. *Polyhedron*, **1983**, *2*, 203-210.
- (13) It is still distinctly possible that a Ta(V) species including Tp could be formed. The [Tp*TaCl₃][TaCl₆] was made with a tin transmetalation reagent. Attempts at a direct substitution led to other products.¹⁴ Interested parties would be recommended to synthesize the proper Tp-Sn species and attempt a substitution at low temperature.¹⁵
- (14) Bradley, Donald C.; Hursthouse, Michael B.; Newton, Joy; Walker, Nigel P. *J. Chem. Soc. Chem. Commun.* **1984**, 188-190.
- (15) Lobbia, Giancarlo G.; Bonati, Flavio; Cecchi, Patrizio; Cingolani, Augusto; Lorenzotti, Adriana. *J. Organomet. Chem.*, **1989**, *378*, 139-146.
- (16) Calderazzo, Fausto; Englert, Ullrich; Pampaloni, Guido; Pelizzi, Giancarlo; Zamboni, Roberto. *Inorg. Chem.* **1983**, *22*, 1865-1870.
- (17) Ellis, John E.; Warnock, Garry F.; Barybin, Mikhail V.; Pomije, Marie K. *Chem. Eur. J.* **1995**, *1*, 521-527.
- (18) Dewey, Christopher G.; Ellis, John E.; Fjare, Kristi L.; Pfahl, Kathryn M.; Warnock, Garry F. P. *Organometallics*, **1983**, *2*, 388-391.

- (19) It should be noted that the two counterions, Et_4N^+ and Na^+ , are compared because Calderazzo does not report the synthesis of the Et_4N^+ species.
- (20) Note that the selection of $[\text{Et}_4\text{N}]^+$ as the counterion was based on the stability and yield reported for $[\text{Et}_4\text{N}][\text{Ta}(\text{CO})_6]$ when compared to species with different cations. Other cations which have been used include $[\text{n-Bu}_4\text{N}]^+$, $[\text{Na}(\text{diglyme})_2]^+$, Na^+ , and $[\text{PPh}_4]^+$. *Caution:* The unsolvated Na^+ species is pyrophoric.¹⁸
- (21) Koeslag, Mary Ann; Baird, Michael C.; Lovelace, Sherri; Geiger, William E. *Organometallics*, **1996**, 15, 3289-3302.
- (22) Fornalczyk, Michael; Susmilch, Frank; Priebisch, Wolfgang; Rehder, Dieter. *Journal of Organometallic Chemistry*, **1992**, 426, 159-172.
- (23) Brennessel, William W.; Ellis, John E.; Pomije, Marie K.; Sussman, Victor J.; Urnezius, Eugenijus; Young, Victor G. *J. Am. Chem. Soc.*, **2002**, 124, 10258-10259 Pombeiro, A. J. L. *Inorg. Chim. Acta*, **1985**, 103, 95
- (24) Lever, A.B.P. *Inorganic Chemistry* **1990**, 29, 1271-1285.
- (25) Welch, Kevin D.; Harrison, Daniel P.; Lis, Edward C., Jr.; Liu, Weijun; Salomon, Rebecca J.; Harman, W. Dean. *Organometallics*, **2007**, 26, 2791-2794.
- (26) Davidson, A.; Ellis, J.E. *Journal of Organometallic Chemistry*, **1971**, 31, 239-247.
- (27) Ellis, John E.; Fjare, Kristi L.; Warnock, Garry F. *Inorganica Chimica Acta*, **1995**, 240, 379-384.
- (28) Bernieri, Paolo; Calderazzo, Fausto; Englert, Ulli; Pampaloni, Guido. *Journal of Organometallic Chemistry*, **1998**, 562, 61-69.

(29) Luetkens, Melvin, L. Jr.; Santure, David J.; Huffman, John C.; Sattelberger, Alfred P.

J. Chem. Soc. Chem. Commun. **1985**, 552-553.

(30) McGeary, M. J.; Gamble, A. S.; Templeton, J. L. *Organometallics*, **1988**, 7,

271-279.

Chapter 3:

Part A: Ligand Substitution via Photolysis

Part B: Ligand Substitution via Oxidation

3a.1 Introduction

In order to synthesize a metal fragment capable of sufficient π donation to disrupt aromaticity, a very particular ligand set is required. A metal center too rich in electron density will perform oxidative addition, whereas a metal center too poor in electron density will not donate sufficiently into the aromatic π^* orbitals to disrupt the aromaticity.¹ The fact that neither the $\{\text{Os}(\text{NH}_3)_5\}^{2+}$ nor the $\{\text{TpW}(\text{PMe}_3)(\text{NO})\}$ metal fragment could be modified in any way and maintain its dearomatizing capability is a testament to the fine tuning of electron density that is required.¹ All methods of controlling and modifying the ligand set would need to be explored in order to give us the best opportunity to mold the $[\text{Et}_4\text{N}][\text{Ta}(\text{CO})_6]$ starting material into a tantalum-based dearomatization agent.

Metal carbonyl compounds are well known for their photochemical reactivity. By irradiating with UV or visible light an electron in a d_π orbital can be excited to the d_σ level, which weakens the M-CO bond and promotes dissociation (**Figure 3a.1**).^{2,3}

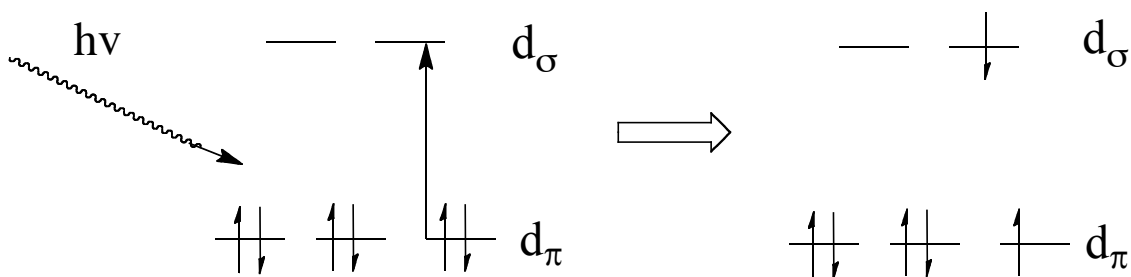


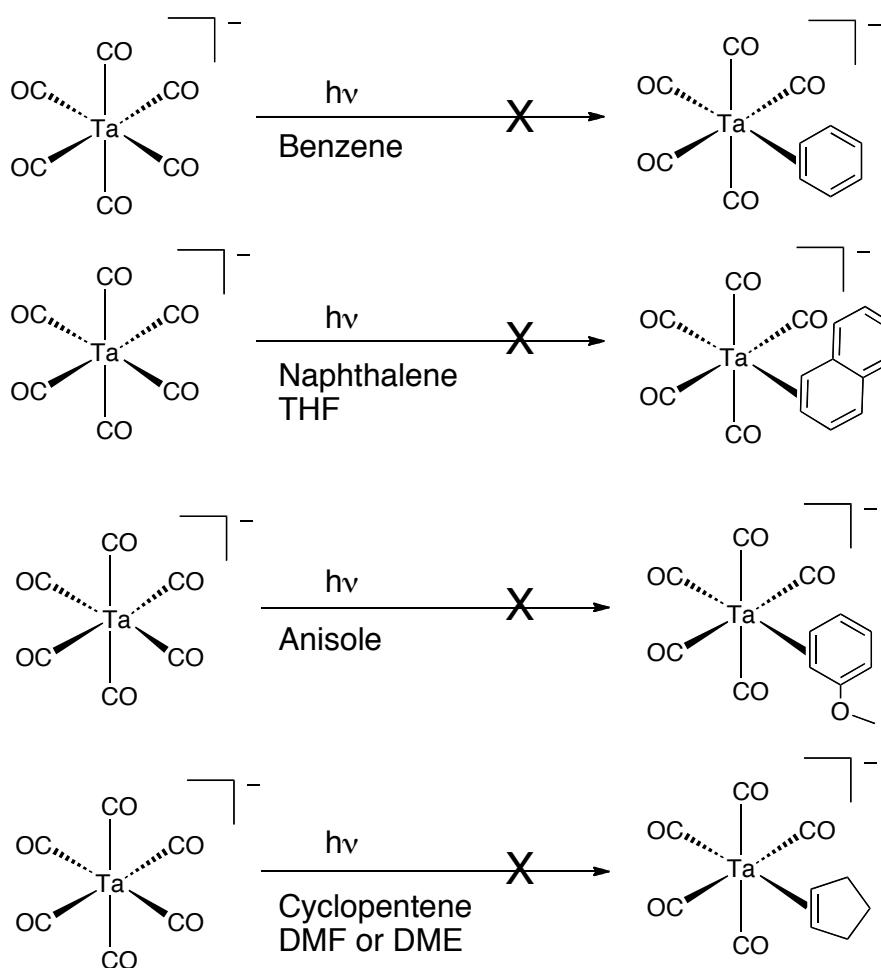
Figure 3a.1: Molecular Orbital diagram of electron promotion.

As concluded in Chapter 2, $[\text{Et}_4\text{N}][\text{Ta}(\text{CO})_6]^-$ is stable to thermal substitution. Two methods have been discussed to circumvent this problem and substitute a single carbonyl: reduction and photolysis. Reduction of **1** to the Ta(-3) species $[\text{Ta}(\text{CO})_5]^{3-}$ followed by oxidation with NH_4Cl makes the substitutionally labile $[\text{Ta}(\text{CO})_5\text{NH}_3]^-$.⁴ However, the conditions required for the reduction were too harsh for the laboratory equipment readily available; thus, we focused on the photolysis method. There is literature precedent claiming that **1** is amenable to photochemical substitution.⁵ Furthermore, there were visual cues noted during the attempted thermal substitution that suggested that **1** was undergoing photochemical substitution, even when irradiated with only ambient light. It was hypothesized that through photochemical substitution of one or more carbonyl ligands, the necessary electronics for dearomatization could be achieved.

3a.2 Direct substitution

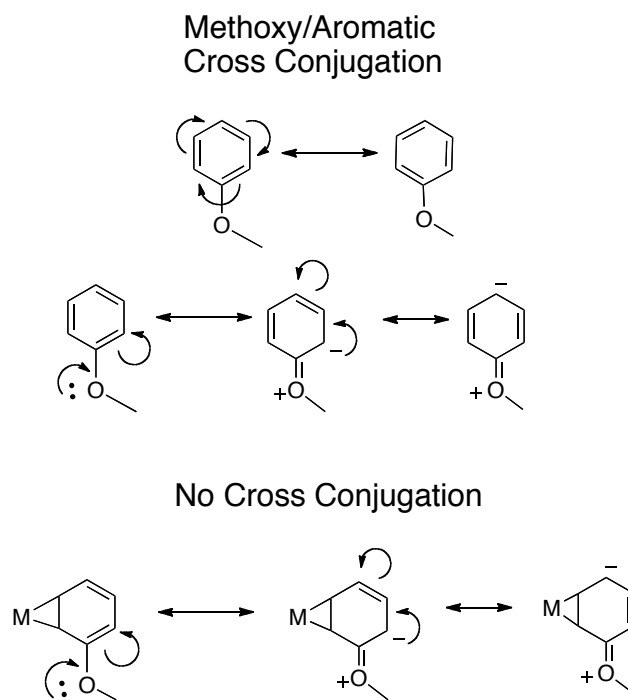
It was first attempted to directly substitute a carbonyl for a dihapto-coordinating ligand. There was some evidence that a $\{\text{Ta}(\text{CO})_5\}^-$ metal fragment may have been π basic enough to disrupt the aromaticity without further modification of the ligand set (See Chapter 2). This belief was based on a comparison between $[\text{Ta}(\text{CO})_6]^-$ and $\text{TpW}(\text{PMe}_3)(\text{NO})(\text{CO})$. Electrochemical measurements found that $[\text{Ta}(\text{CO})_6]^-$ has an anodic peak potential 80 mV more reducing than $\text{TpW}(\text{PMe}_3)(\text{NO})(\text{CO})$ [$E_{p,a}=0.24$ V and 0.32 V, respectively].⁶⁻⁷ There was also a striking difference in the ν_{CO} for each compound. Infrared measurements found that $[\text{Ta}(\text{CO})_6]^-$ has a ν_{CO} 47 cm^{-1} lower than $\text{TpW}(\text{PMe}_3)(\text{NO})(\text{CO})$ [1817 cm^{-1} and 1864 cm^{-1} , respectively].⁶⁻⁷ This suggested that the Ta species

actually provided significantly more back donation than the $\text{TpW}(\text{PMe}_3)(\text{NO})(\text{CO})$. This may have been an incorrect assumption based on the fact that the $\text{TpW}(\text{PMe}_3)(\text{NO})(\text{CO})$ ν_{CO} would be a reflection of the singular CO stretch, whereas the ν_{CO} of the $[\text{Ta}(\text{CO})_6]^-$ would be a reflection of a motion involving all six CO ligands. Because the $\{\text{TpW}(\text{PMe}_3)(\text{NO})\}$ was a known dearomatization agent, and it appeared that $\{\text{Ta}(\text{CO})_5\}^-$ was more electron rich, it was hypothesized that an aromatic ligand could replace a carbonyl in **1** and also disrupt aromaticity.



Scheme 3a.1: Photochemical reactions of **1** and C-C double bond containing π acids. The illustrated products were not obtained.

To test this hypothesis, a long-wave UV light source was applied to **1** partially dissolved in benzene. No reaction was noted, and as seen in **Scheme 3a.1**, the desired product was not obtained. It was reasoned that perhaps if naphthalene was used in place of benzene, dihapto coordination might be noted because of the smaller energetic cost associated with dearomatization of naphthalene relative to benzene.⁸ After irradiation with UV light, a color change was noted in the reaction solution, but no new products were identified. It was later discovered through control reactions that the color change that was observed (yellow solution to orange solution) was noted even in the presence of only solvent (THF, DME, CH₃CN). No products were identified from these reactions. When naphthalene failed, anisole was used. The hope was that the stabilization afforded by conjugation of the unbound portion of the ring would ‘recoup’ some of the energetic cost of dearomatization (**Scheme 3a.2**), but no reaction was noted using this experimental setup.



Scheme 3a.2: Illustration of a metal binding to disrupt dearomatization and allow for conjugation of the methoxy moiety into the remaining diene. In the top illustration, one would expect the aromaticity-maintaining resonance structures to be heavily favored over the methoxy donating structures.

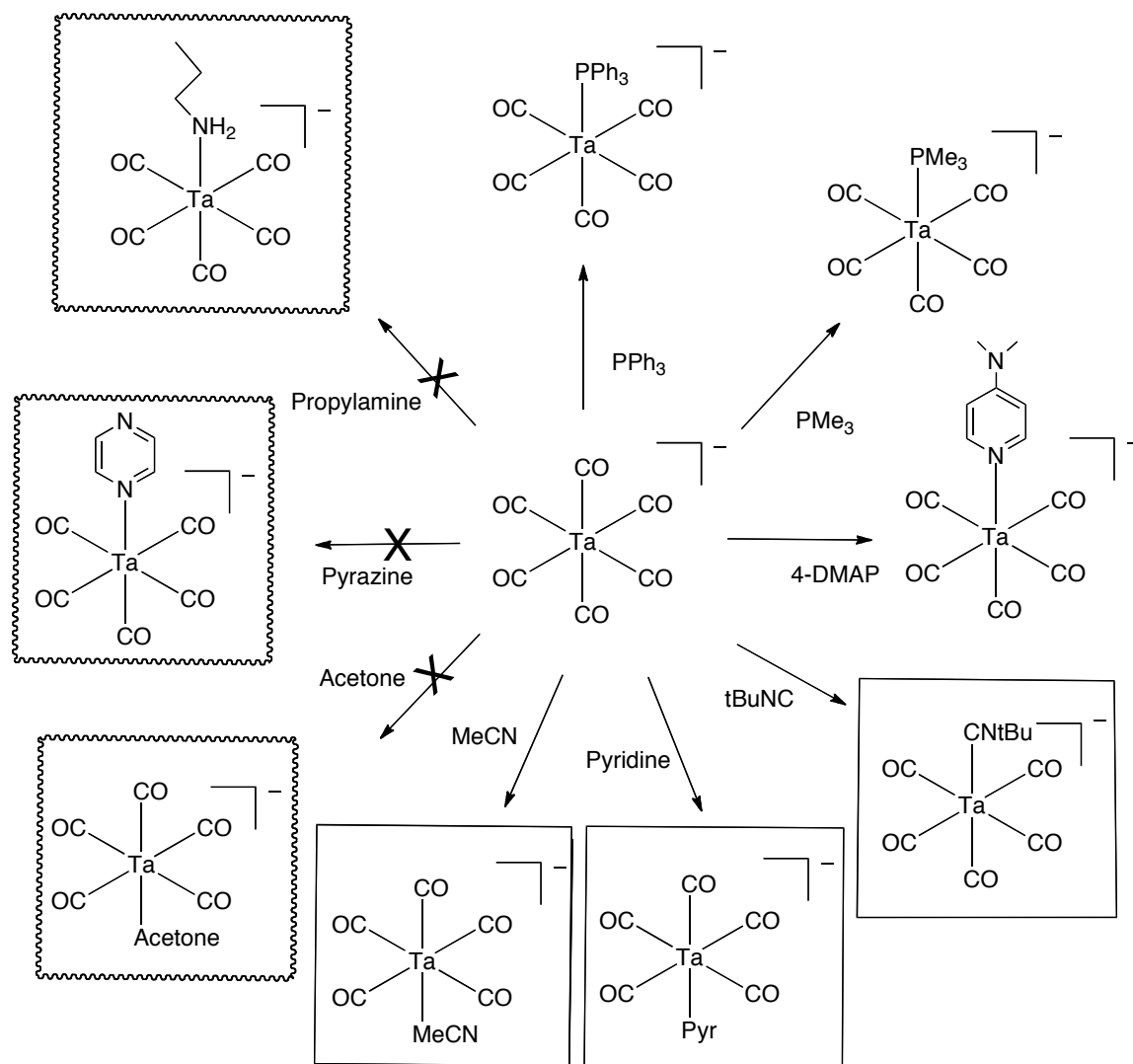
Finally, cyclopentene was used in hopes of achieving dihapto coordination without need for dearomatization. It was assumed that cyclopentene represented the most easily bound C-C double bond in a cyclic system that could be used. The reaction was attempted in DMF, DME, and in neat cyclopentene, but again the desired product seen in **Scheme 3a.1** was not formed. It was ultimately concluded that the direct substitution of a CO for a π acid would not occur under these photolytic conditions. However, it should be noted that it is possible that these reactions were run in sealed flasks; it may have been that due to the partial pressure of CO in the reaction flask (present because of the

carbonyl ligands lost from the metal center), CO was capable of out-competing the organic ligands for the open coordination site. We did not test for this possibility.

3a.3 Substitution of carbonyls for monodentate σ donors

Because the direct substitution failed, we endeavored to synthesize pentacarbonyl species in which a CO had been photolytically substituted for a σ -donor ligand.

Production of σ complexes would allow us to probe the electron-richness of these species, to attempt to substitute another carbonyl for a π acid after σ donor addition, and to validate the experimental setup used as one capable of producing new pentacarbonyl compounds.



Scheme 3a.3: Photolysis with monodentate σ donors. Each reaction was performed using a compact fluorescent lightbulb (CFL). The product compounds not boxed in were successfully isolated and characterized. Those that are boxed in with straight lines were not definitively characterized, but spectroscopic and/or electrochemical evidence was found supporting their synthesis. Those boxed in wavy lines were not obtained in any manner.

The first target was $[\text{Et}_4\text{N}][\text{Ta}(\text{CO})_5\text{PPh}_3]$ (**2**). A solution of **1** and **2** in THF irradiated with long wave UV light from a CFL spontaneously produced X-ray diffraction

quality crystals whose solution can be seen below (**Figure 3a.2**). This was the product expected from **Scheme 3a.2**. Two other reactions gave products that were successfully elucidated. The use of PMe_3 and the use of 4-DMAP resulted in identifiable, collectable products. It should be noted that the yield of the collected products were unfortunately low (~20%) and often times indications of decomposition were present. This was consistent with the literature report that the substituted anions of tantalum decompose under extended exposure to UV light.⁵ When five equivalents of PPh_3 or PMe_3 were used instead of one, a second product was noted. It was assumed to be the disubstituted product based on ^{31}P NMR data. In the case of PMe_3 substitution, the disubstituted species had an $E_{p,a} = -0.63$ V. This disubstitution made it difficult to cleanly synthesize one species; often starting material, monosubstituted, and disubstituted products were all present in the same reaction mixture. While polysubstitution with monodentate ligands may have been an attractive pathway, it was not pursued. Reaction with the isocyanide tBuNC , pyridine, and acetonitrile gave products that had identifiable, reasonable electrochemical or infrared signatures, but whose structure could not be unequivocally identified. These results can be seen below in section **3a.5**, **Table 3a.1**. One piece of data, though, deserves mention at this point. The ν_{CN} of the tBuNC product was recorded to be 2090 cm^{-1} , which matches a literature reported value.⁴ When this is compared to the $\text{TpW}(\text{PMe}_3)(\text{NO})(\text{tBuNC})$ ν_{CN} value of 1787 cm^{-1} , there appears to be a surprisingly small amount of back bonding into the C-N triple bond.⁶ This may be explained in part by the increase in stretching frequency associated with sigma donation by an isocyanide. Because the lone pair of the isocyanide has some antibonding character, the more

strongly an isocyanide donates electron density through a sigma bond, the higher this ν_{CN} becomes. This makes it more difficult to identify the level of back donation into the C-N triple bond. Moreover, additional observation supports the hypothesis that the $\{\text{Ta}(\text{CO})_5\}^-$ fragment may be quite amenable to accepting sigma donation, which could explain the surprisingly high observed ν_{CN} value (vide infra).³ When **1** was irradiated in the presence of propylamine or pyrazine ligands, an unidentified mass of white solid was created along with excessive evolution of a gas assumed to be $\text{CO}_{(\text{g})}$. It has been reported in the literature that protonated pyridines are capable of oxidizing the tantalum species. There may have been impurities, such as H_2O , that led to protonation of these nitrogen species and subsequent decomposition of the $[\text{Ta}(\text{CO})_6]^-$, and neither of these reactions were pursued further. When **1** was irradiated in the presence of acetone, no identifiable products were obtained.

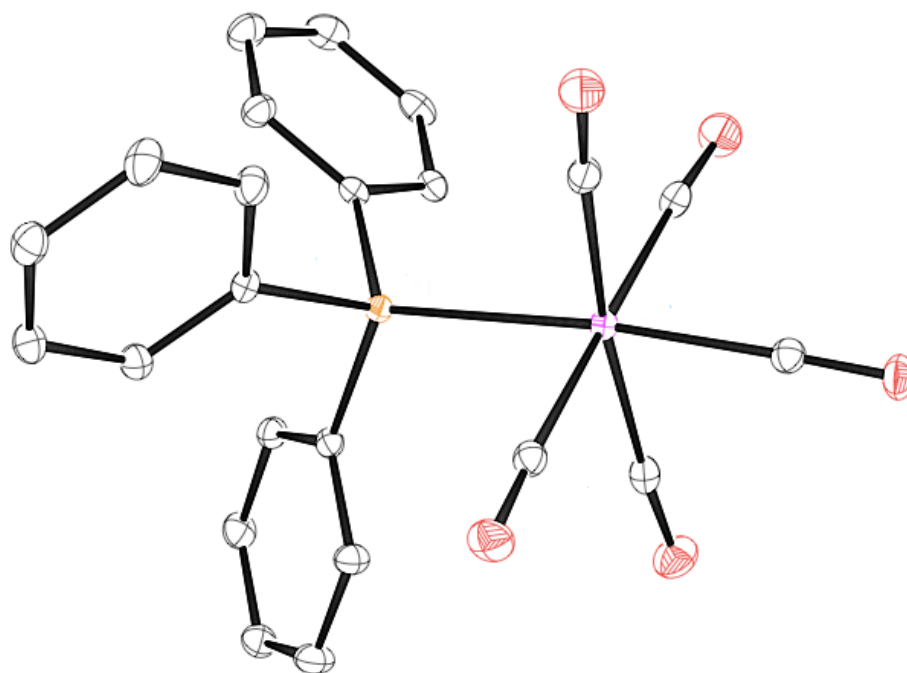


Figure 3a.2: Crystal structure of $[\text{Et}_4\text{N}][\text{Ta}(\text{CO})_5\text{PPh}_3]$ (**2**).

Each of the species which showed a possibility of having formed the desired product was also irradiated with UV light in the presence of naphthalene in hopes of synthesizing the $[\text{Ta}(\text{CO})_4\text{X}(\eta^2\text{-naphthalene})]$ complex. None of these reactions were successful. Note that this includes the PMe_3 and PPh_3 species in solution where the disubstituted products would also have been present.

3a.4 Substitution of 4-DMAP

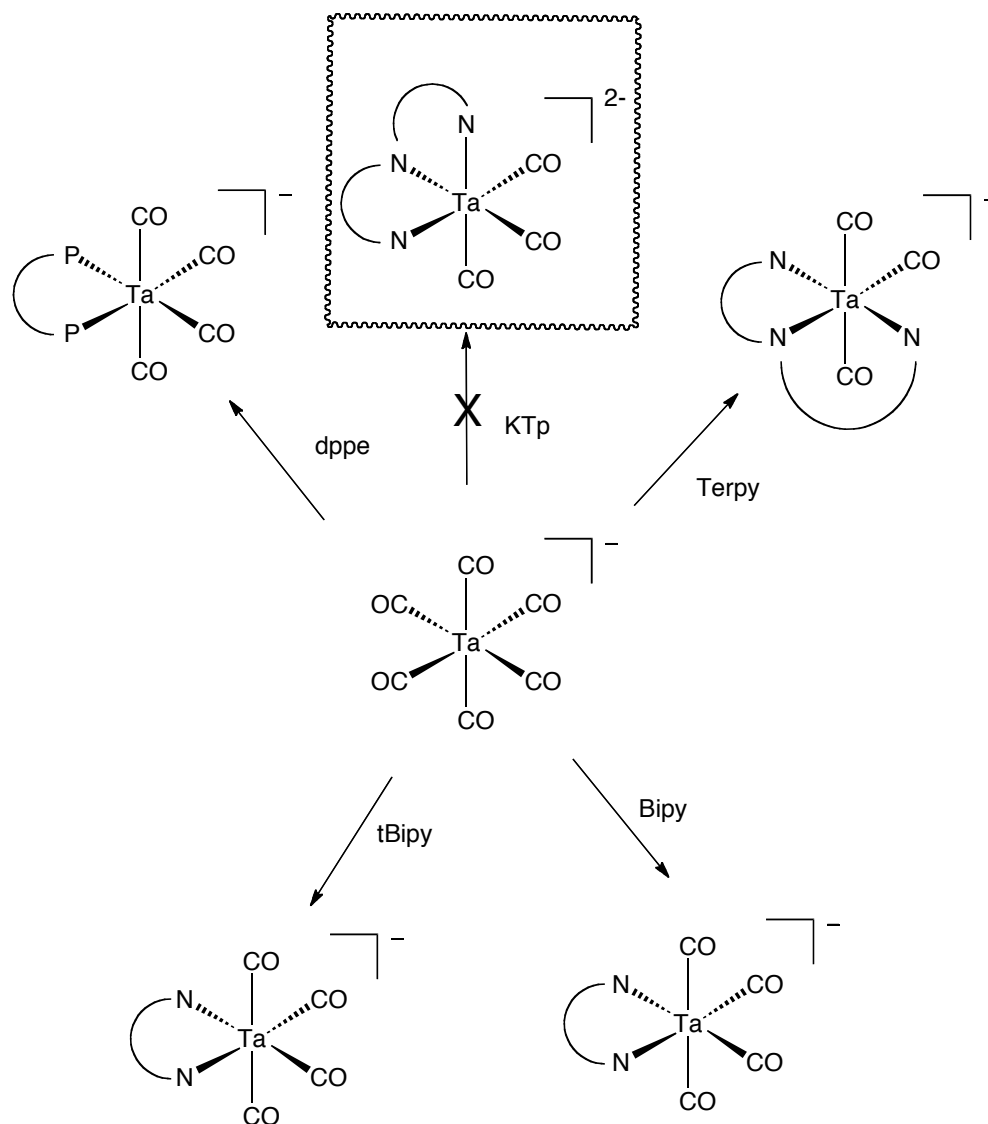
The 4-DMAP ligand in $[\text{Et}_4\text{N}][\text{Ta}(\text{CO})_5(4\text{-DMAP})]$ was found to be labile, similar to the reported $[\text{Ta}(\text{CO})_5\text{NH}_3]^-$ species that was synthesized using Birch conditions.⁴ Treatment of $[\text{Ta}(\text{CO})_5(4\text{-DMAP})]^-$ with PPh_3 quickly gave $[\text{Ta}(\text{CO})_5(\text{PPh}_3)]^-$. The ability to substitute one ligand for another gave us the opportunity to attempt to add a π acid like cyclopentene again without having to rely on photolysis.

Treatment of $[\text{Ta}(\text{CO})_5(4\text{-DMAP})]^-$ with neat cyclopentene, cyclopentene in DMF or THF, or naphthalene did not result in the desired product. It was concluded that the $\{\text{Ta}(\text{CO})_5\}^-$ metal fragment was simply not electron-rich enough to bind an aromatic or even an alkene in a dihapto fashion. This was surprising when considering the $\text{TpW}(\text{PMe}_3)(\text{NO})(\text{CO})/[\text{Ta}(\text{CO})_6]^-$ comparison. However, a comparison of the electrochemistry between $[\text{Ta}(\text{CO})_5(4\text{-DMAP})]^-$ and $\text{TpW}(\text{PMe}_3)(\text{NO})(\kappa^1\text{-N-pyridine})$ reveals a different trend. The $E_{\text{p,a}}$ of $[\text{Ta}(\text{CO})_5(4\text{-DMAP})]^-$ was found to be -0.50 V, whereas the $E_{1/2}$ of $\text{TpW}(\text{PMe}_3)(\text{NO})(\kappa^1\text{-N-pyridine})$ was found to be -0.78 V.⁹ Because we were considering the $\{\text{Ta}(\text{CO})_5\}^-$ fragment to be more electron rich than the $\{\text{TpW}(\text{PMe}_3)(\text{NO})\}$ fragment, we would have expected the $E_{\text{p,a}}$ of $[\text{Ta}(\text{CO})_5(4\text{-DMAP})]^-$ to be more negative than for the $\text{TpW}(\text{PMe}_3)(\text{NO})(\kappa^1\text{-N-pyridine})$ because the 4-DMAP ligand is more σ donating than pyridine. Also, the $\Delta E_{\text{p,a}}$ between $[\text{Ta}(\text{CO})_6]^-/[\text{Ta}(\text{CO})_5(4\text{-DMAP})]^-$ was found to be much smaller (0.74 V) than the ΔE between the $\text{TpW}(\text{PMe}_3)(\text{NO})(\text{CO})/\text{TpW}(\text{PMe}_3)(\text{NO})(\kappa^1\text{-N-pyridine})$ (1.10 V). It was suggested that these observations were a result of having five strong π acids present. It was hypothesized that despite its strong back bonding, the $\{\text{Ta}(\text{CO})_5\}^-$ was much more accommodating of electron donation because of the five π acids present capable of stabilizing the additional charge. This hypothesis led us to believe a more electron rich metal with fewer π acids was going to be necessary.

3a.5 Substitution of carbonyls for polydentate σ donors

When it became clear that $\{\text{Ta}(\text{CO})_5\}^-$ and $\{\text{Ta}(\text{CO})_4\text{X}\}^-$ fragments were not going to bind aromatics, we turned to polydentate ligands to try to increase the electron-richness

of the metal fragment. The following photochemical reactions were attempted using polydentate ligands (**Scheme 3a.4**).



Scheme 3a.4: Photochemical reactions attempted with polydentate ligands. The reaction with KTp was the only reaction to give no indication that the illustrated product was formed.

The first reaction attempted was photolysis in the presence of KTp. When **1** was irradiated in the presence of KTp in THF, some reaction occurred, but no indication of the desired product seen in **Scheme 3a.4** was noted by CV, IR, or NMR. Because the product of the reaction with KTp was expected to produce a very electron rich species and a dianion, the reaction was also attempted in the presence of Diazald with the hope that the substitution of a carbonyl for a nitrosyl would stabilize and trap the nitrosylated congener. However, it was found in the presence of Diazald (with or without KTp), irradiation of **1** led to vigorous bubbling and the deposition of an unidentified white solid.

Photolysis was then performed in the presence of dppe. Irradiation of **1** in the presence of dppe led to the desired $[\text{Ta}(\text{CO})_4(\text{dppe})]^-$. Further irradiation in the presence of cyclopentene, though, did not lead to the desired $[\text{Ta}(\text{CO})_3(\text{dppe})(\eta^2\text{-cyclopentene})]^-$ product. When $[\text{Ta}(\text{CO})_4(\text{dppe})]^-$ was treated with Diazald, IR spectrum suggested a nitrosylated product might have formed, but $\text{Ta}(\text{CO})_3(\text{NO})(\text{dppe})$ was not isolated.

The three other polydentate ligands were employed during this study: 2,2'-bipyridyl (bipy), 4,4' tertbutyl-2,2'-bipyridyl (tBipy), and 2,2':6',2''-terpyridine (terpy). Exceptional effort was directed towards the synthesis of $[\text{Ta}(\text{CO})_4(\text{bipy})]^-$. The irradiation of **1** in the presence of bipy produced two different species, which were identified by their ^1H NMR signatures (See appendix). Each had four peaks, indicating that the two pyridine rings were equivalent in both cases. The compound which had its four ^1H NMR peaks on average further downfield was referred to as compound A, and the compound with its four peaks further upfield, compound B. Despite attempts to adjust conditions, such as number of bipyridyl equivalents, concentration, reaction time,

and dryness of solvent, it was clear that we were not able to control which product was obtained in a given experiment. Upon irradiation, the reaction solution would immediately turn a deep, opaque green, eventually becoming a bluish color. This strong color was attributed to a charge transfer often seen in coordination compounds containing bipyridine.⁹ However, despite this color, very little product was found in solution. Instead, large amounts of a black-blue crystalline solid were collected as they spontaneously deposited during irradiation. This solid was sparingly soluble in most solvents, and often peak broadness was noted during NMR experiments because of this insolubility and insufficient NMR solvent. When compound A had been formed, a blue color was noted upon addition of CD₃CN to the dry crystalline solid; compound B instead was a distinctly purple color. Anecdotally, once after irradiation, a reaction mixture had its solution decanted leaving only solid in the flask. The solid was dried, and as much solid as possible was removed from the flask; however, a residue of solid remained in the flask. The solid removed from the flask and the residue of solid that was stuck to the flask were separately analyzed. The solid not removed from the flask showed compound B and the solid removed from the flask compound A.

A recrystallization of the solid collected from an irradiation of **1** with bipy using solution of the blue solid layered with decane revealed the crystal structure below.

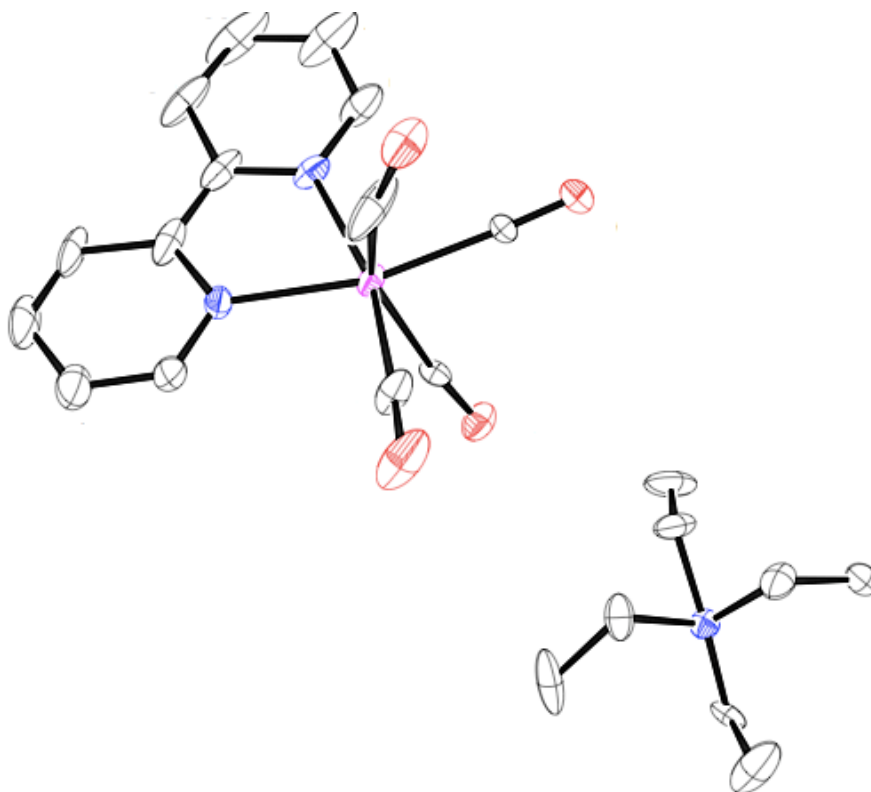


Figure 3a.3: X-ray structure of [Et₄N][Ta(CO)₄(bipy)].

NMR of the solid prior to recrystallization indicated that it was compound A, and thus A was, with some trepidation, assigned as [Et₄N][Ta(CO)₄(bipy)]. Because the crystals used for the X-ray diffraction could not be re-obtained for additional ¹H NMR examination, it was not undeniably confirmed that a small amount of compound B had not crystallized and been used in the diffraction instead of A. Between compounds A and B, the only recorded difference was in the ¹H HMR. IR and CV gave the same results whether it was compound A or B that had been noted previously. This led to the hypothesis that compound B was a binuclear species, although if it was bridging via carbonyls, the IR would likely look different.

Addition of Diazald to the reaction solution or the collected solid resulted in a loss of the deep color and no identifiable products both at room temperature and at -40°C . Photolysis of **1** in the presence of bipy and cyclopentene did not produce the desired $[\text{Ta}(\text{CO})_3(\text{bipy})(\eta^2\text{-cyclopentene})]^-$ either.

Irradiation of **1** with tBipy did produce a product with four new ^1H peaks, indicating that the two pyridyl rings were equivalent. However, the product was highly unstable; IR and CV were very difficult to obtain, and this species was not pursued further.

Irradiation of **1** with terpy generated a new product which was assigned as $[\text{Ta}(\text{CO})_3(\text{terpy})]^-$ by ^1H NMR and CV. Like the bipy products, the reaction solution quickly turned a deep blue color upon exposure to UV light. The somewhat more negative $E_{p,a}$ (**Table 3a.1**) was attributed to the additional π acidity associated with the larger π system of three pyridine rings. Attempts to nitrosylate this species failed both at room temperature and at -45°C , as well as attempts to substitute a fourth CO in favor of cyclopentene.¹¹

A table of the CV and IR data collected from each photolytic reaction in which data of interest could be obtained is seen in **Table 3a.1** below.

Ligand	Electrochemistry (E _{p,a} vs. NHE)	IR (cm ⁻¹)	Supporting NMR Data
PPh ₃	-0.16 V (in DCM)	1967, 1855, 1817	Yes
PMe ₃	-0.21 V / -0.63 V (in MeCN) ^h	Not Reported ^h	Yes
tBuNC	Not Collected ^a	2090, 1917, 1828 ^f	Yes
4-DMAP	-0.50 V (in DMA)	1959, 1844, 1774	Yes
Pyridine	-0.41 V (in DMA)	Not Collected ^c	No ^e
MeCN	-0.30 V (in MeCN)	1844, 1793	No ^e
bipy	-0.94 V (in MeCN)	Not Collected ^d	Yes, see appendix
tBipy	Not Collected ^a	Not Collected ^d	Yes, see appendix
terpy	-1.10 V (in MeCN) ^b	Not Collected ^d	Yes, see appendix
dppe	-0.44 V (in MeCN)	Not Reported ^g	Yes

Table 3a.1: Reported electrochemical and infrared data collected after irradiation of **1** with the listed ligand. This data reported does not necessarily correspond to the associated [Ta(CO)_{6-n}X_n]⁻ species.

^a Not collected because of apparent product instability

^b E_{p,a} reported using internal standard FeCp₂. Peak-to-peak separation of FeCp₂ E_{1/2} was 138 mV. Use of internal standard hampered by decomposition peaks after initial product E_{p,a}.

^c No peaks of interest seen in IR

^d Not collected due to air sensitivity

^e ¹H NMR shows no peaks supporting possibility of a [Ta(CO)₅X]⁻ species

^f IR stretches chosen from an IR spectrum with multiple products. Stretches determined using reported stretches in reference 4.

^g IR spectrum and CV analysis indicated that a [Ta(CO)₅(dppe)]⁻ species was also present, making it difficult to assign stretches to compounds. Reference 5 reports IR data for this compound.

^h IR spectrum and CV analysis indicated that [Ta(CO)₅(PMe₃)]⁻ and [Ta(CO)₄(PMe₃)₂]⁻ species were present, making it difficult to assign stretches to compounds. Reference 4 reports IR data for this compound.

It is surprising to note the potentials found for the σ donor complexes. At these negative potentials, we would expect the related metal fragments to either bind an aromatic or perform an oxidative addition. If these complexes did not react with aromatic molecules because they were too electron poor, the expectation that electrochemistry could be used to relate the electron richness of these systems to the electron richness of the other dearomatizing metal systems appears incorrect. However, there is another explanation that seems more likely. It may have been the case that photolysis was unable to open the coordination site trans to the σ donor. Once the first σ donor was added to the ligand set, we would expect that the carbonyl trans to the σ donor would be particularly difficult to remove relative to the other four carbonyl groups. This

is because, unlike the carbonyl trans to the σ donor, the other four carbonyl groups all have a strong trans influence on each other, weakening each of their M-CO bonds. Therefore, the photolysis would most likely open a coordination site cis to the σ donor. This site, while being a good coordination site for an additional σ donor, would be a poor site for the complexation of an aromatic ligand that requires significant π back donation to bind strongly because it is trans to another strong π acid (**Figure 3a.4**).

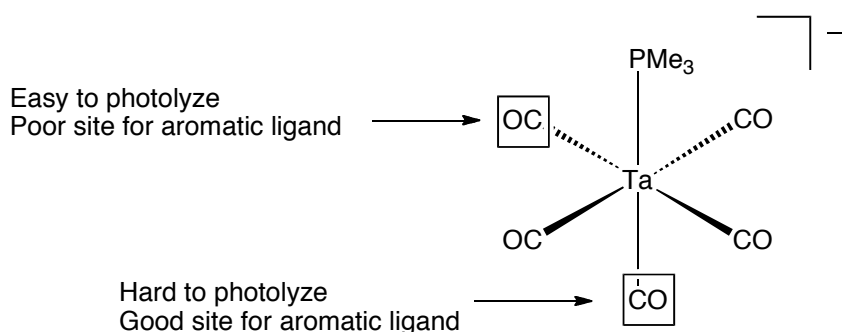


Figure 3a.4: Explanation for why complexation of an aromatic ligand to a metal fragment that *appeared* sufficiently electron-rich to bind an aromatic was not observed using photolysis.

This would explain why mono- and disubstitution were observed for PMe₃ and PPh₃, but no η^2 aromatic or organic complexes were observed when the monosubstituted products were photolyzed in the presence of aromatic molecules. Thus, it may be that these species were electron rich enough to react with the organic ligands, but the photolysis was incapable of opening an the proper coordination site for binding of the aromatic ligand. It also may have simply been that the CO_(g) present in the reaction solution was able to out-compete the aromatic ligands, but not additional σ donors.

3a.6 Conclusion

Photochemical substitution was shown to be capable of producing new compounds by irradiation of $[\text{Ta}(\text{CO})_6]^-$ with UV light. However, substitution of a carbonyl for a π acid (benzene, naphthalene, cyclopentene) was not observed. $[\text{Ta}(\text{CO})_5\text{X}]^-$ species were reported with CV, IR, and NMR data where possible; among these was the previously unreported, substitutionally labile $[\text{Ta}(\text{CO})_5(4\text{-DMAP})]^-$ (**3**). Substitution to give $[\text{Ta}(\text{CO})_4\text{X}(\eta^2\text{-}\pi\text{ acid})]^-$ failed. A number of polydentate ligands were also substituted to give $[\text{Ta}(\text{CO})_{4-n}(\text{X}_{2+n})]^-$ species ($n=0,1$). Substitution to give $[\text{Ta}(\text{CO})_{4-n}\text{X}_{2+n}(\eta^2\text{-}\pi\text{ acid})]^-$ also failed. Attempts to nitrosylate pentacarbonyl, tetracarbonyl, and tricarbonyl species failed. The yields of these reactions were always low and they were difficult to obtain as pure samples. The reactions were difficult to replicate from trial to trial. Even if one of the substituted species had been shown to bind cyclopentene in a dihapto fashion, it was clear that photolysis was not a good method to depend on if the synthesis of a tantalum dearomatization agent in any appreciable yield or purity was to be expected.

3b.1 Introduction to Ligand Substitution Via Oxidation

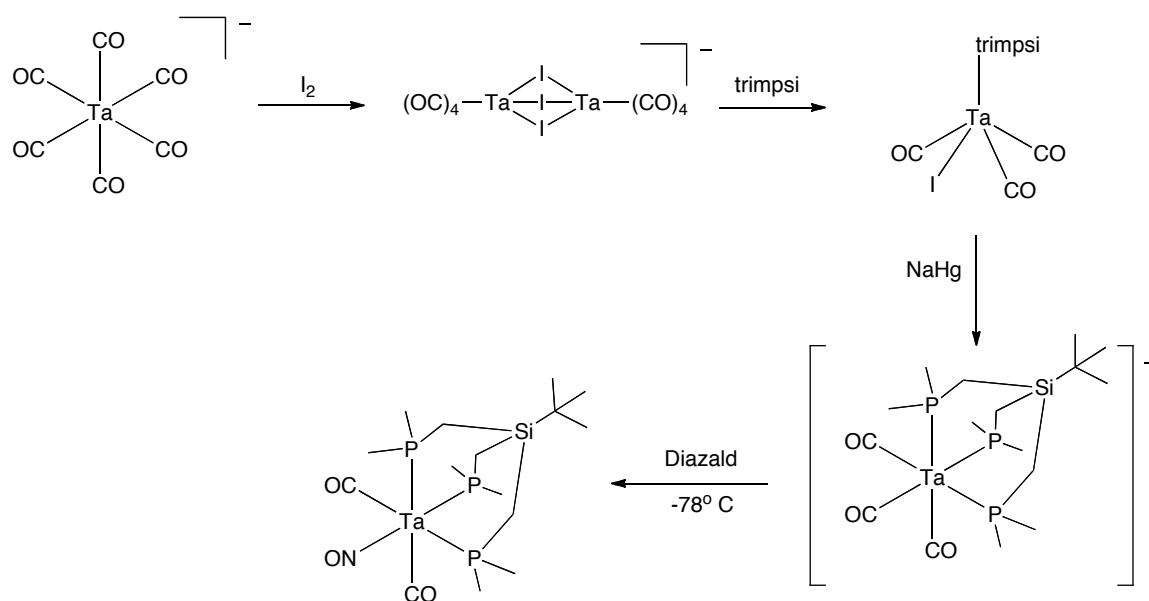
Both thermal substitution and photolytic substitution of $[\text{Ta}(\text{CO})_6]^-$ were attractive methods for the synthesis of a tantalum-based dearomatization agent because they were simple and maintained the desired Ta(-1) oxidation state. However, from the outset, it was clear that they were less versatile techniques than the oxidation chemistry of $[\text{Ta}(\text{CO})_6]^-$. This was most clearly illustrated by the dearth of publications that focused on $[\text{Ta}(\text{CO})_6]^-$ photolysis (one publication) or thermal substitution (one publication) relative to the number of publications employing the oxidation of $[\text{Ta}(\text{CO})_6]^-$ to modify the ligand set (12+ publications). Once it was clear that these first two methods were not going to be effective (see Chapter 3a), our attention was turned to oxidation chemistry.

Ligand substitution via oxidation refers to chemistry in which the first step is a $2e^-$ oxidation of $[\text{Ta}(\text{CO})_6]^-$. The loss of $2e^-$ labilizes the $[\text{Ta}(\text{CO})_6]^-$ ligand set, and when a halogen is present during the oxidation, two carbonyls are immediately lost to give the binuclear $[\text{Ta}_2(\mu\text{-X})_3(\text{CO})_8]^-$ ($\text{X}=\text{Cl}, \text{Br}, \text{I}$) seen in **Scheme 2.5** in Chapter 2.¹² One electron oxidations were not explored because of reports that they had been attempted many times and had almost always resulted in Ta(I) species.¹³ The $[\text{Ta}_2(\mu\text{-X})_3(\text{CO})_8]^-$ species is amenable to substitution to form monomeric tetracarbonyl, tricarbonyl, or even dicarbonyl tantalum species.^{12,14-15} Thus, as outlined in Chapter 1, the goal was to oxidize **1**, add a Tp or Tpm ligand to the Ta(I) species, reduce this species back to the Ta(-1) oxidation state, and finally add an aromatic species as a ligand to demonstrate dearomatization. At the Ta(-1) oxidation state, it was assumed that the initial

product would be extremely electron-rich and likely unstable, so nitrosylation would be necessary to stabilize the system. This assumption was supported by the electrochemistry reported from the suspected $[\text{Et}_4\text{N}][\text{Ta}(\text{CO})_4(\text{bipy})]$ and $[\text{Et}_4\text{N}][\text{Ta}(\text{CO})_4(\text{terpy})]$ complexes and a report by Legzdins that the tricarbonyl species postulated to be an intermediate in the $\text{Ta}(\text{trimpsi})(\text{CO})_2(\text{NO})$ synthesis was not isolable (**Scheme 3b.1**).

While there were many literature reports of Ta(I) species, there was only one report that matched the reduction and nitrosylation in this proposed synthesis. Legzdins and coworkers published the following synthesis of $(\text{trimpsi})\text{Ta}(\text{CO})_2(\text{NO})$

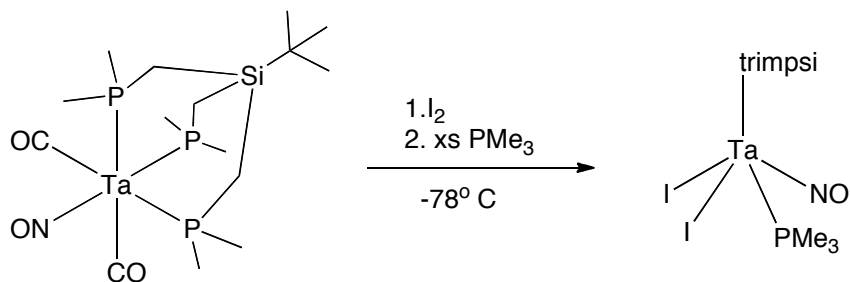
(**Scheme 3b.1**).¹⁴



Scheme 3b.1: Synthesis of $(\text{trimpsi})\text{Ta}(\text{CO})_2(\text{NO})$.¹⁴

Not only does the synthesis in **Scheme 3b.1** demonstrate that the reduction and nitrosylation can be performed, but it also uses a tridentate phosphine ligand which can be seen as analogous to the desired Tp and Tpm ligands. This left only the final step of

the proposed synthesis (**Scheme 2.6**) undemonstrated; there were no reports of photolysis on a dicarbonyl nitrosyl tantalum species to give a different product. Although the photolysis work described previously did not lead to a dearomatization agent, it did give us confidence that we could photolyze a CO if needed even if the energy of the light used had to be increased. The low yield of the photolyses coupled with the concession that these dicarbonyl nitrosyl species may bear very little analogy to the hexacarbonyl species photolyzed before led us to search for an alternative plan in case the photolysis failed. The focus of the alternative plan was to include a weakly σ donating ligand (such as a halogen) at the Ta(I) stage. It was hoped that upon reduction, this ligand would be lost in favor of a weakly π accepting aromatic species. Fortunately, additional work by Legzdins provided this pathway also although it comes at the cost of a number of additional steps in the synthesis scheme (**Scheme 3b.2**).



Scheme 3b.2: Ta(trimpsp)(CO)₂(NO) oxidation scheme.¹⁶

It was hypothesized that the PMe₃ seen in **Scheme 3b.2** could be replaced with a more π -acidic, less σ -donating ligand (e.g., P(OMe₃)).

3b.2 Electrochemistry and Computational Clues

The electrochemistry of the Ta(trimpsi)(CO)₂(NO) species measured at 0.01 V vs. NHE suggested that the species that had been targeted would at least be in the range of electron density that we were expecting (see Chapter 1). However, having not worked with trimpsi before, it was difficult to confidently predict the effect that replacing it with Tp or Tpm might have had on the overall electron density of the system. We turned to computational chemistry to assist us in making these predictions.

Using Gaussian 09, a number of calculations were performed on theoretical η^2 species, beginning with the TpW(PMe₃)(NO)(η^2 -benzene). The results of these calculations can be seen below (**Table 3b.1**).

Compound	C-C bond length (Å)	Average C ₄ -C ₁ -H bond angle (°)
Benzene	1.409	180
TaTp(NO)(NO)(η^2 -benzene)	1.417	173.9
Ta(CO) ₅ (η^2 -benzene) ⁻	1.419	174.25
Ta(CO) ₄ (PPh ₃)(η^2 -benzene) ⁻	1.424	170.7
Ta(CO) ₄ (PMe ₃)(η^2 -benzene) ⁻	1.427	169.9
Ta(PMe ₃) ₃ (CO)(NO)(η^2 -benzene)*	1.437	163.5
Ta(trimpsi)(CO)(NO)(η^2 -benzene)	1.439	163.2
TaTpm(CO)(NO)(η^2 -benzene)	1.440	163.81
TaTpm(CO) ₂ (η^2 -benzene)	1.459	159.16
TaTp(CO)(NO)(η^2 -benzene) ⁻	1.466	156.6
Os(NH ₃) ₅ (η^2 -benzene) ²⁺ *	1.438	171.9
TpW(PMe ₃)(NO)(η^2 -benzene) †	1.471	153.2

Table 3b.1: Calculations hypothetical η^2 -coordinated benzene complexes of tantalum.

* Calculation did not converge to a solution; however, C-C bond length and C-H bond angle were constant after two days. Lack of convergence attributed to PMe₃ rotations.

† Calculation performed by Daniel Harrison

* Calculation performed by Daniel Harrison, also, See reference 17.

The likelihood of a species to successfully form a stable species in which a dihapto coordinated benzene ligand was present was judged based on a comparison to

calculations performed on the $\text{TpW}(\text{PMe}_3)(\text{NO})(\eta^2\text{-benzene})$ species. The two parameters that were analyzed were the length of the C-C bond bound to the metal and the average $\text{C}_4\text{-C}_1\text{-H}$ bond angle observed for the two bound carbons (**Figure 3b.1**). These were chosen because distortion of these two carbons towards sp^3 is indicative of significant metal donation.¹

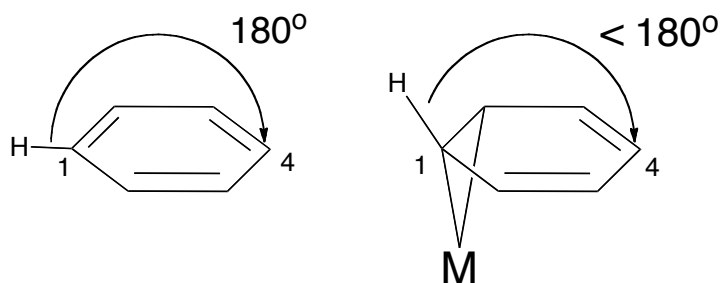


Figure 3b.1: Angle measured in C-H bond angle measurement.

The first species calculated were with the $\{\text{Ta}(\text{CO})_5\}^-$, $\{\text{Ta}(\text{CO})_4\text{PMe}_3\}^-$, and $\{\text{Ta}(\text{CO})_4\text{PPh}_3\}^-$ metal fragments whose usefulness in synthesizing a dearomatization agent had already been discounted experimentally in Chapter 3b. The calculations agreed with experimental result; as seen in **Table 3b.1**, these species reported a C-C bond distance and C-H bond angle quite different from the $\text{TpW}(\text{PMe}_3)(\text{NO})(\eta^2\text{-benzene})$. Next were the neutral $\{\text{Ta}(\text{PMe}_3)(\text{CO})(\text{NO})\}$, $\{\text{Ta}(\text{trimpSi})(\text{CO})(\text{NO})\}$, and $\{\text{Ta}(\text{Tpm})(\text{CO})(\text{NO})\}$. Calculations on these species returned C-C bond distances with an intermediate distortion between the unperturbed benzene and the strongly dearomatizing tungsten metal fragment and very near the bond length very near the distortion of the benzene in $\text{Os}(\text{NH}_3)_5(\eta^2\text{-benzene})^{2+}$. The $\{\text{TaTp}(\text{NO})_2\}$ metal fragment showed very little distortion due to the strong π acidity of the nitrosyl ligands. Finally, the two

negatively charged species, $\{\text{Ta}(\text{Tpm})(\text{CO})_2\}^-$ and $\{\text{Ta}(\text{Tp})(\text{CO})(\text{NO})\}^-$ showed benzene distortions much closer to the $\{\text{TpW}(\text{PMe}_3)(\text{NO})\}^-$. The fact that $\text{TaTpm}(\text{CO})_2(\eta^2\text{-benzene})^-$ did not show a greater distortion was surprising. It was expected that without the nitrosyl, this species would be far too electron rich. This assumption was based on the logic that if the electrochemistry of the desired species was expected to show an oxidative wave in the range of -0.15 V, and the $[\text{Ta}(\text{CO})_3\text{terpy}]^-$ complex had an $E_{p,a} = -1.10$ V, then replacing the terpy with a less π acidic ligand and removing an additional CO would certainly be far too electron rich. In fact, based on the change of $[\text{W}]\text{-CO}$ to $[\text{W}]\text{-}\eta^2\text{-benzene}$, the trimpsi species electrochemically appeared to be quite favorable. Most importantly, the Gaussian calculations supported the assertion made in Chapter 1 that a Tp or Tpm ligand could be useful in the synthesis of a tantalum-based dearomatization agent. It should be noted that the calculations performed would not have necessarily revealed that a species was electron rich enough to perform C-H activation.

3b.3 Addition of Tp and Tpm

With the promise of a Tp or Tpm species not discounted by the computational results, the process of synthesizing Tp and Tpm Ta(I) species was undertaken. It was predicted that treatment of $[\text{Ta}_2(\mu\text{-I})_3(\text{CO})_8]^-$ with either Tp and Tpm would produce compounds analogous to the trimpsi species. When **1** was treated with I_2 followed by KTp in DME, red crystalline solid was spontaneously deposited after treatment of the reaction solution with hexanes. X-ray quality crystals were collected and the structure in **Figure 3b.2** was solved by X-ray diffraction. While the data collected via X-ray diffraction were sufficient to confirm the connectivity of the product, they were not high

enough quality to use the bond length and bond angle data to further analyze the molecule.

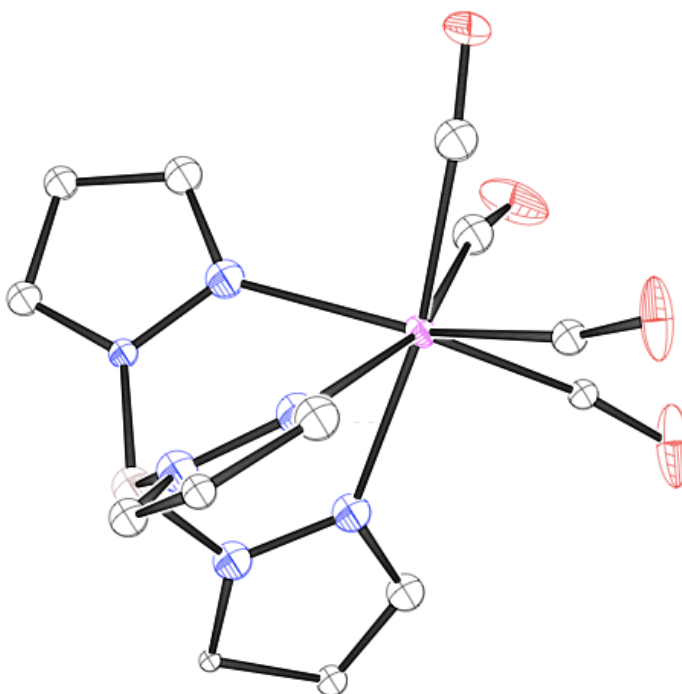


Figure 3b.2: Crystal structure of TaTp(CO)₄ (**4**).

This is the second mononuclear tantalum species featuring a Tp ligand and the first in the Ta(I) oxidation state. The electrochemistry of TaTp(CO)₄ revealed an anodic peak potential at 1.01 V, as expected for a Ta(I) species. Infrared spectroscopy showed 3 carbonyl stretches at 2006 cm⁻¹, 1890 cm⁻¹, and 1851 cm⁻¹. When compared to the reported ν_{CO} stretches for TaCp(CO)₄, (2025 cm⁻¹, 1922 cm⁻¹), the Tp species appears to be more back bonding.¹² The number of stretches also is of some interest. The infrared spectrum of TaCp(CO)₄ suggests a local C_{4v} symmetry (A₁ + E), and based on the crystal structure, this also might have been predicted for **5**. However, it appears the Tp has a greater influence on the environment of the carbonyls based on the additional stretching

frequency that was observed. Another interesting point are the presence of only 3 pyrazole peaks in the ^1H and ^{13}C NMR, as well as only one CO resonance in the ^{13}C NMR. This indicated that each of the pyrazole rings and each of the CO ligands is equivalent on the NMR. This would not be possible without some fluctuonality in the molecule (**Figure 3b.3**).

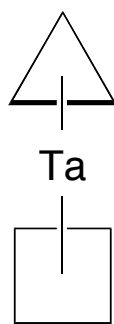


Figure 3b.3: Schematic representation of $\text{TaCp}(\text{CO})_4$. Each point of the triangle represents a pyrazole ring, and each point of the square represents a carbonyl. In this static system, it is impossible for each pyrazole ring to be equivalent.

It was hypothesized that this is a result of the three pyrazole rings spinning freely about the B-Ta molecular axis. The trimpsi ligand in $\text{Ta}(\text{trimpsi})(\text{CO})_3\text{I}$ also displayed fluctuonality. The fact that all four carbonyl ligands remained on the metal center suggested that the Tp ligand was more donating than the trimpsi ligand, confirming the prediction made using Gaussian. This may have been in part due to the negative charge of the Tp ligand.

The same procedure was repeated with Tpm in place of the Tp. Because Tpm is a neutral molecule, like trimpsi, it was predicted that unlike **5**, the resulting species would

be analogous to the Ta(trimpsi)(CO)₃I . Using the analogous procedure, a new compound was synthesized and crystals were grown. X-ray quality crystals were recovered and the structure in **Figure 3b.4** was solved by X-ray diffraction.

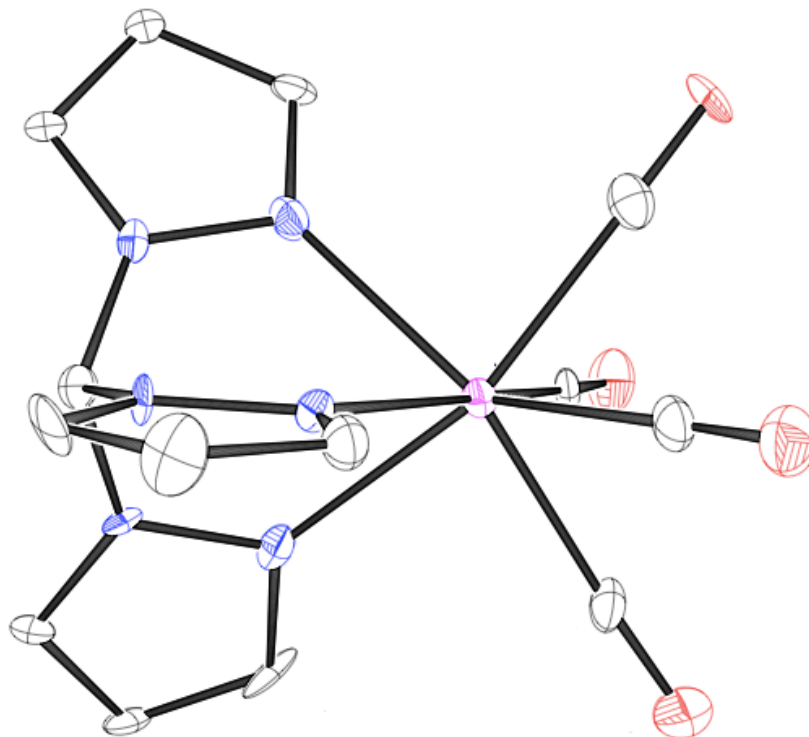


Figure 3b.4: Crystal structure of [TaTpM(CO)₄]I (**5**). This image omits the I⁻ counterion.

This is the first mononuclear tantalum complex to include a Tpm ligand.

Electrochemical measurements indicated an anodic peak potential at 1.41 V. When compared to TpW(CO)₂NO ($E_{p,a}=1.21$ V)/[TpMw(CO)₂NO]⁺ ($E_{p,a}=1.46$ V), the change in electrochemical potential were similar (TpW/TpmW $\Delta E_{p,a}=0.25$ V; TpTa/TpmTa $\Delta E_{p,a}=0.40$ V).¹⁸ IR spectroscopy gave 2 stretches at 2025 and 1886 cm⁻¹; almost

identical to the TaCp(CO)₄ IR spectrum. ¹H and ¹³C NMR again indicated that the pyrazole rings were equivalent, meaning there was fluxionality in the molecule.

The presence of the fourth carbonyl in both cases presented a problem. The expected next step towards a tantalum dearomatization agent was reduction of the Tp or Tpm product. Because the fourth CO remained instead of being replaced by a halogen or other weakly bound ligand, it was not clear which ligand would be forced to dissociate after reduction if the 18e⁻ rule was to be obeyed. Despite this, reduction of both TaTp(CO)₄ and TaTpm(CO)₄I was attempted. It was hypothesized that perhaps the chelation of the Tp and Tpm ligands would favor the loss of a CO even though the addition of one or two electrons should bolster the strength of the Ta-CO bond.

TaTp(CO)₄ was treated with Na⁰, which led to the formation of a new product with carbonyl stretching frequencies at 1874 and 1751 cm⁻¹. Addition of Diazald led to no change in the infrared spectrum. The product was too unstable for CV analysis.

When TaTpm(CO)₄⁺ was treated with Na⁰, new carbonyl stretching frequencies at 1986 cm⁻¹ and 1840 cm⁻¹ were observed. Treatment with Diazald again led to no reaction.

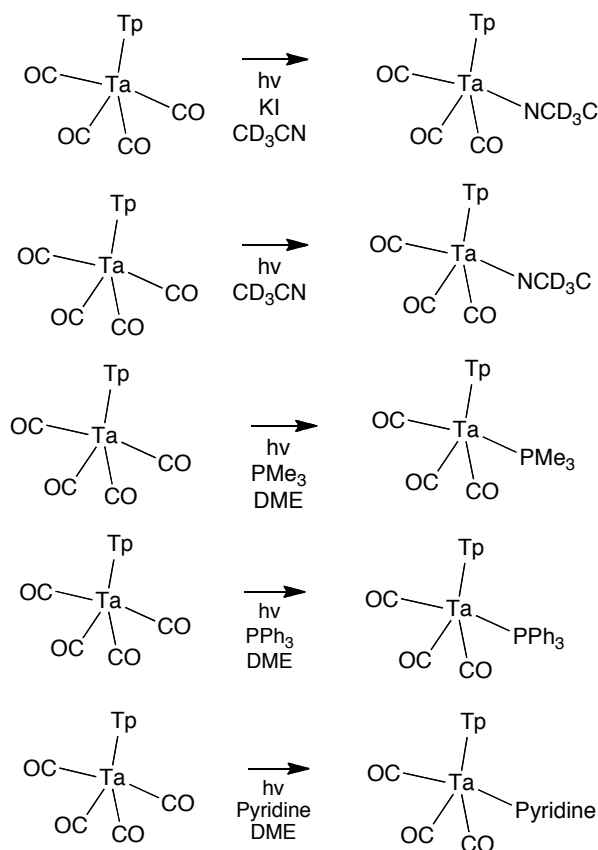
While there may still be some value in these reductions, they were abandoned in favor of what was viewed as a more favorable path to a Ta(-1) species (*vide infra*).

3b.4 Removal of a CO

Thermolysis of TaTp(CO)₄ was attempted using a microwave reactor. Because the trimpsi species was amenable to losing the fourth carbonyl in favor of an iodide and even losing another carbonyl in favor of an alkyne, it was hypothesized that it might be possible to force the dissociation of a carbonyl by heating.¹⁴⁻¹⁵ TaTp(CO)₄ was heated to

160° C in DME. A slight color change in solution was noted with the deposition of a white solid. Infrared spectroscopy reveals that no new carbonyl species had been formed. When TaTp(CO)₄ was heated to 120° C in DME in the presence of PMe₃, new peaks were noted in the IR spectrum that indicated that a tricarbonyl species had formed, but a single new product was not obtained. At 170° C, degradation of **4** was noted in the presence of Diazald.

We then returned to photolysis as a method of removing a carbonyl from the Ta(I) species. TaTp(CO)₄ was photolyzed under the conditions seen in **Scheme 3b.3**.



Scheme 3b.3: Photolysis reactions attempted with TaTp(CO)₄ and predicted products.

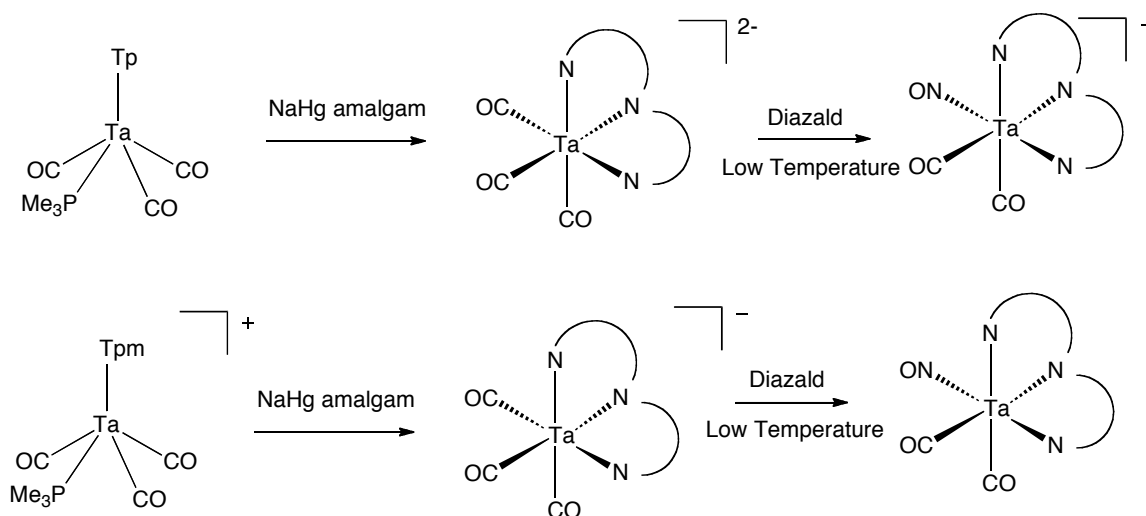
In the case of the irradiation of TaTp(CO)₄ in the presence of CD₃CN at -40° C, there were new ¹H NMR signals obtained (see appendix for NMR). Unlike previous experiments, there were six ¹H pyrazole peaks observed in which corresponded to two equivalent pyrazole rings and one inequivalent. The same NMR spectrum was obtained both in the presence and absence of iodide. Electrochemistry revealed an E_{p,a}=0.72 V, which was a reasonable shift from the E_{p,a}=1.01 V of TaTp(CO)₄. The IR showed new peaks at 1921 cm⁻¹, 1813 cm⁻¹, and an anomalous peak at 1732 cm⁻¹. The 1732 cm⁻¹ peak is particularly low energy for a CO stretch, especially because no reduction took place and the published CO stretches for Ta(CO)₃(PMe₃)₃I were in the 1920 cm⁻¹ - 1800 cm⁻¹ range. When TaTp(CO)₄ was irradiated in the presence of pyridine, results were ambiguous, but a new set of pyridine signals were noted in the ¹H NMR along with an E_{p,a}=0.35 V, suggesting the desired product may have been formed. When TaTp(CO)₄ was irradiated in the presence of PMe₃ and PPh₃, new signals were seen in the ³¹P NMR and in the IR spectrum that suggested that tricarbonyl compounds where PMe₃ or PPh₃ had substituted for a carbonyl had been synthesized.

We attempted to reduce and nitrosylate the product of the PMe₃ and PPh₃ photolysis reactions with Na⁰ or NaHg amalgam and Diazald. No nitrosylated products were observed, but new anodic peak potentials were noted at approximately -0.38 V for the reduction of the PPh₃ product and -0.30 V for the reduction of the PMe₃ product.¹⁹ No crystal structure could be obtained, without which it was difficult to say with certainty the products that had been produced by the photolysis. The photolysis method was again

abandoned because of difficulties determining reaction length and obtaining products in a reasonable yield and purity. However, at the same time that the photolysis method was being explored, another method was being explored which confirmed the identity of the $\text{TaTp}(\text{CO})_3(\text{PMe}_3)$ product and by analogy the $\text{TaTp}(\text{CO})_3(\text{PPh}_3)$ product.

It was reported by Sattelberger that the addition of PMe_3 to $[\text{Ta}_2(\mu\text{-X})_3(\text{CO})_8]^-$ gave the tricarbonyl species $\text{Ta}(\text{CO})_3(\text{PMe}_3)_3\text{I}$.²⁰ It was further reported by Templeton that the treatment of $\text{Ta}(\text{CO})_3(\text{PMe}_3)_3\text{I}$ with diphenylacetylene gave $\text{Ta}(\text{CO})_2(\text{diphenylacetylene})(\text{I})(\text{PMe}_3)_2$. It was hypothesized from these results that the PMe_3 ligands of $\text{Ta}(\text{CO})_3(\text{PMe}_3)_3\text{I}$ were labile enough to be substituted for a Tp or Tpm ligand to give the $\text{KTpTa}(\text{CO})_3\text{I}$ or $\text{TpTa}(\text{CO})_3\text{PMe}_3$ (or the Tpm congeners). Treatment of **1** with I_2 , followed by PMe_3 and then KTp (or Tpm) gave $\text{TpTa}(\text{CO})_3\text{PMe}_3$ (**6**) or $[\text{TpmTa}(\text{CO})_3\text{PMe}_3]\text{I}$ (**7**). These products were identified by IR, NMR and CV. High resolution mass spectrometry confirmed the identity of **7**. These are the first two tantalum tricarbonyl species to include Tp and Tpm ligands. The goal of creating a Ta(I) species with three carbonyls and a σ donor ligand was achieved. This procedure was also attempted using PPh_3 in place of PMe_3 , but it seemed that the predicted intermediate $\text{Ta}(\text{CO})_3(\text{PPh}_3)_3\text{I}$ had trouble forming.

The next step in the proposed scheme is the reduction of **6** and **7** (**Scheme 3b.4**).



Scheme 3b.4: Proposed synthesis to dicarbonyl nitrosyl d^6 complexes from **6** and **7**.

When **6** was treated with NaHg amalgam, new CO stretching frequencies were noted at 1863 cm^{-1} and 1736 cm^{-1} . Also, a new $E_{p,a}$ was noted at -0.30 V , suggesting that a $[\text{TpTa}(\text{CO})_3]^{2-}$ compound likely was not present. ^1H NMR of this species showed free Tp and a new product. This does not rule out the possibility of additional paramagnetic $17e^-$ species. An $18e^-$, d^6 metal species with these ligands was expected to have a much more negative reduction potential. Treatment of this reduced compound with Diazald, both at room temperature and -70°C led to the collection of a new IR spectrum with peaks at 2017 cm^{-1} , 1655 cm^{-1} , and 1577 cm^{-1} . It was tempting to suggest that the two low energy peaks were the result of a dinitrosylation with the remaining 2017 cm^{-1} peak representing the stretch of a lone carbonyl.

When $[\text{TaTpm}(\text{CO})_3\text{PMe}_3]^+$ was treated with NaHg amalgam, new CO stretching frequencies were noted at 1886 cm^{-1} and 1774 cm^{-1} . ^1H NMR analysis of this compound showed only free Tpm, suggesting that at least some of the starting material had

decomposed. This does not rule out the formation of a $17e^-$ species, which may not be observed in the NMR due to paramagnetism. Treatment of this species with Diazald at room temperature and -50°C led to complete decomposition.

The reduction of the $\text{Ta}(\text{CO})_3(\text{PMe}_3)_3\text{I}$ species reported by Sattelberger was also attempted, but to no avail. Because of the similarity between this compound and the $\text{Ta}(\text{trimpsi})(\text{CO})_3\text{I}$, it was concluded the the chelation was required to maintain a stable structure. Treatment of $[\text{Ta}_2(\mu\text{-X})_3(\text{CO})_8]^-$ with the tridentate terpy species led to an unstable product. However, an IR spectrum with stretches at 1913, 1832, and 1778 cm^{-1} suggest the expected $\text{Ta}(\text{terpy})(\text{CO})_3\text{I}$ species was present.

3b.5 Conclusion

The oxidation method for modifying the ligand set of **1** has resulted in early success. Through oxidation of $[\text{Ta}(\text{CO})_6]^-$, no fewer than four 7-coordinate Tp or Tpm complexed Ta(I) species have been synthesized. Previously, only one tantalum complex had been reported with either Tp or Tpm ligands. Three of these species are tricarbonyl species, which we have hypothesized can be reduced back to the Ta(-1) oxidation state where they can be nitrosylated. There is some evidence that a dinitrosylated tantalum species has also been synthesized. The predictions made about the ability of a number of different metal fragments using Gaussian 09 appear to be useful, but whose accuracy will become more clear when Ta(-1) species are isolated and characterized. More effort needs to be directed towards the reduction and nitrosylation of the Tp and Tpm compounds made.

3ab.1 Experimental

General Methods

NMR spectra were obtained on a 300 or 500 MHz spectrometer (Varian INOVA). All chemical shifts are reported in ppm. Proton and carbon shifts are referenced to tetramethylsilane (TMS) utilizing residual ^1H or ^{13}C signals of the deuterated solvents as an internal standard. Phosphorus NMR signals are referenced to 85% H_3PO_4 ($\delta = 0.00$) using a triphenylphosphate external standard ($\delta = -16.58$) unless noted. Coupling constants (J) are reported in hertz (Hz). Infrared spectra (IR) were recorded on a MIDAC Prospect Series (Model PRS) spectrometer as a glaze on a Horizontal Attenuated Total Reflectance (HATR) accessory (Pike Industries). Electrochemical experiments were performed under a dinitrogen atmosphere using a BAS Epsilon EC-2000 potentiostat. Cyclic voltammetry data was taken at ambient temperature at 100 mV/s (25 °C) in a standard three-electrode cell with a glassy carbon working electrode using tetrabutylammonium hexafluorophosphate (TBAH) as an electrolyte (approx. 0.5 M in an appropriate solvent). All potentials are reported versus NHE (Normal Hydrogen Electrode) using cobaltocenium hexafluorophosphate ($E_{1/2} = -0.78$ V) or ferrocene ($E_{1/2} = +0.55$ V) as an internal standard. The peak-to-peak separation was 100 mV or less for all reversible couples. Photolyses were performed using either a 15 W or a 26 W compact fluorescent light bulb, which included radiation at $\lambda=360$ nm. High resolution mass spectrometry analyses were obtained from the University of Richmond on a Bruker BioTOF-Q running in ESI mode from samples dissolved in acetonitrile solution. Peak positions were calibrated against an acetonitrile/water solution containing sodium trifluoroacetate (NaTFA), with some trifluoroacetic acid added. Mass spectra are reported for M^+ cationic complexes using $[\text{Na}(\text{NaTFA})_x]^+$ clusters as an external standard. Unless otherwise noted, all synthetic reactions were performed in a glovebox under a dry nitrogen atmosphere. Dichloromethane (DCM) and benzene were purified by

passage through a column packed with activated alumina. Dissolve tetrahydrofuran (THF) was used as received. These and other solvents and liquid reagents were thoroughly purged with nitrogen prior to use. Deuterated solvents were used as received from Cambridge Isotopes. Tpm was prepared using a modified procedure from the synthesis described by Reger et al. (vide infra).²¹ All calculations performed herein were executed using Gaussian 09, revision A.02 on an Apple MacBook Pro running Windows 7 in parallel with Apple OS X.²² For each molecule of interest, the following procedure was applied. A rough approximation of the compound was assembled in GaussView 5.0.8. The clean command was then applied. A calculation was prepared by selecting the B3LYP method with default spin and the LanL2DZ basis set.^{23,24} Care was taken to ensure the charge for the molecule was correct and in all cases, spin was set to singlet. An optimization of the structure was run, with the options optimize to a *minimum* and calculate force constants *never* selected.

[Et₄N][Ta(CO)₅PPh₃] (2)

The synthesis of [Et₄N][Ta(CO)₅PPh₃] via photolysis of [Ta(CO)₆]⁻ has been reported previously.^{4,5}

PPh₃ (0.019 g, 0.072 mmol) was dissolved in ~0.5 mL THF. The resulting clear solution was added to [Et₄N][Ta(CO)₆] (0.030 g, 0.0625 mmol). This solution was photolyzed using a 15 W CFL. The solution changed from bright yellow to neon orange. The deposition of neon orange crystals was noted. These crystals were collected (0.020 g, 0.0280 mmol, 45% unoptimized yield) and purity was confirmed by ¹H and ³¹P NMR. ¹H NMR (300 MHz, CD₂Cl₂): δ 7.55 (m, 6H, Ph protons), 7.33 (m, 9H, Ph protons), 3.22 (q, 8H, J_{HH}=7.4 Hz, CH₂ of Et) 1.21 (tt, 12H, J_{NH}=1.9 Hz, J_{HH}=7.4 Hz, methyl of Et). ³¹P

NMR (121 MHz, CD₂Cl₂): δ 34.9 (s, 1P, PPh₃). IR (HATR): 1967 cm⁻¹ (weak, sharp), 1855 cm⁻¹ (strong, sharp), 1817 cm⁻¹ (strong, sharp). CV (CH₂Cl₂): E_{p,a} = -0.16 V.

Crystallographic tables appear in Appendix.

[Et₄N][Ta(CO)₅(4-DMAP)] (3)

[Et₄N][Ta(CO)₆] (0.049 g, 0.102 mmol) was dissolved in DME. 4-DMAP (0.008 g, 0.0655 mmol) was dissolved in DME and added to solution of **1** at room temperature. This solution was placed under a 26 W CFL. Irradiation of this solution led to heating, and the temperature was carefully maintained below 50° C. After 3 hours, some crystal deposition was noticed. After 2 days, the brown-orange solution was decanted and the crystalline solid was dried and collected. Yield: 0.022 g (38%). Note: **3** was unstable in CD₃CN, initial purity of 0.022 g not clear. ¹H NMR (300 MHz, CD₃CN): δ 8.51 (m, 2H, 4-DMAP ring protons), 6.36 (m, 2H, 4-DMAP ring protons), 3.22 (q, 8H, J_{HH}=7.0 Hz, CH₂ of Et) 2.96 (s, 6H, N-Me) 1.21 (t, 12H, J_{HH}=7.0 Hz, methyl of Et). IR (HATR): 1959 cm⁻¹ (medium, sharp), 1844 cm⁻¹ (strong, broad), 1844 cm⁻¹ (strong, broad). CV (DMA): E_{p,a} = -0.50 V.

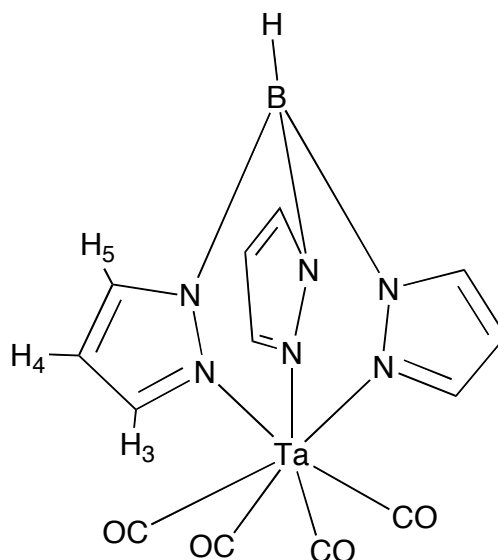
TaTp(CO)₄(4)

Figure 3ab.1: Depiction of compound **4**.

1 (0.100 g, 0.209 mmol) was dissolved in 1.5 mL DME in a 30 mL test tube. The resulting yellow solution was cooled to -45°C and stirred. I_2 (0.054 g, 0.213 mmol) was dissolved in 1.5 mL DME. The resulting dark red solution was cooled to -40°C and added to the solution of **1**, giving a dark red, turbid solution almost immediately. After 35 minutes, KTp in 1 mL chilled DME was added to the solution. This solution was stirred at -45°C for 25 minutes. After 25 minutes, the test tube was removed from the cold bath, and the reaction mixture was allowed to warm with stirring for 80 minutes. The mixture was then filtered, and the filtrate was evaporated. The residue was redissolved in ~ 6 mL DME. This solution was transferred to a four dram vial, and evaporation began again. This led to the deposition of a red, crystalline solid. The solid

was desiccated to a constant mass of 0.073 g (69% yield). On a 0.050 g scale, a nearly identical procedure gave 68% yield of a product whose purity was confirmed by NMR. ^1H NMR (300 MHz, CD_3CN): δ 8.15 (d, 3H, $J_{\text{HH}}=2.2$ Hz, H_3), 7.86 (d, 3H, $J_{\text{HH}}=2.2$ Hz, H_5), 6.32 (t, 3H, $J_{\text{HH}}=2.2$ Hz, H_4), 4.52 (m, 1H, B-H). ^{13}C NMR $\{^1\text{H}\}$ (CD_3CN): δ 253.6 (s, CO), 147.5 (s, C_3), 138.1 (s, C_5), 107.5 (s, C_4). IR (HATR): $\nu_{\text{CO}} = 2006\text{ cm}^{-1}$ (medium, sharp), 1890 cm^{-1} (strong, sharp), 1851 cm^{-1} (strong, sharp). Note: Occasionally the 1890 cm^{-1} peak is observed as a shoulder of the 1851 cm^{-1} peak. CV: (CH_3CN) $E_{\text{p,a}} = 1.01\text{ V}$. $E_{\text{p,c}} = -1.59\text{ V}$. Crystallographic tables appear in Appendix

[Ta(TpM)(CO) $_4$] $^+$ I $^-$ (5)

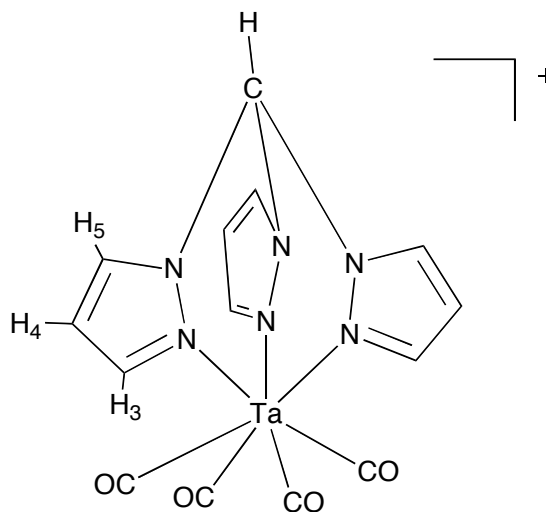


Figure 3ab.2: Depiction of compound **5**.

1 (0.052 g, 0.108 mmol) was dissolved in 1.5 mL DME in a 30 mL test tube. The resulting yellow solution was cooled to -45°C and stirred. I_2 (0.027 g, 0.104 mmol) was dissolved in 1.5 mL DME. The resulting dark red solution was cooled to -50°C and added to the solution of **1**, giving a dark red, turbid solution almost immediately. After

15 minutes, Tpm (0.048 g, 0.224 mmol) was dissolved in DME and added to reaction mixture. This lightened the color of the reaction mixture. After 10 minutes, the reaction was allowed to warm to room temperature. Reaction mixture was filtered with a 15 mL fine fritted glass funnel. The filtrate was orange-yellow. The precipitate was noted to be spontaneously forming in the filtrate. Excess hexanes were added, causing additional precipitation. The solid collected on 15 mL fine fritted glass funnel. 0.041 g (~60% crude yield). ^1H NMR indicated 80-85% purity, thus, the actual yield was lower. ^1H NMR (300 MHz, CD_3CN): δ 10.89 (s, 1H, H₆), 8.72 (d, 3H, $J_{\text{HH}}=2.7$ Hz, H₅), 8.32 (d, 3H, $J_{\text{HH}}=2.2$ Hz, H₃), 6.57 (t, 3H, $J_{\text{HH}}=2.7$ Hz, H₄). ^{13}C NMR $\{^1\text{H}\}$ (CD_3CN): δ 149.9 (s, C₃), 135.9 (s, C₅), 109.6 (s, C₄), 75.0 (s, C₆), CO Resonance not observed. IR (HATR): $\nu_{\text{CO}} = 2021$ cm^{-1} (weak, sharp), 1917 cm^{-1} (medium, sharp), 1894 cm^{-1} (strong, sharp). CV: (CH_3CN) $E_{\text{p,a}} = 1.45$ V. Crystallographic tables appear in Appendix

TaTp(CO)₃PMe₃ (6)

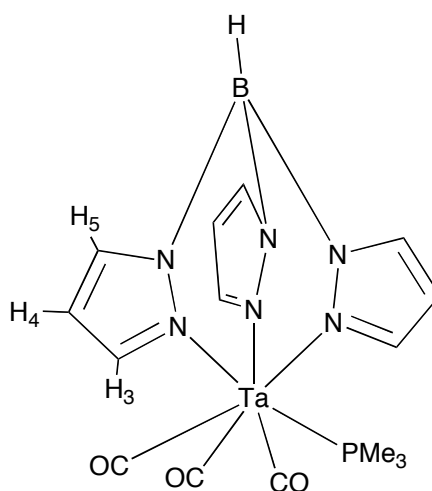


Figure 3ab.3: Depiction of compound 6.

1 (0.099 g, 0.206 mmol) was dissolved in 2 mL DME in a 30 mL test tube. The resulting yellow solution was cooled to -40° C and stirred. I₂ (0.054 g, 0.213 mmol) was dissolved in 1.75 mL DME. The resulting dark red solution was cooled to -40° C and added to the solution of **1**, giving a dark red, turbid solution almost immediately. After 20 minutes, PMe₃ (0.077 g, 1.012 mmol) in 0.5 mL DME was added to the reaction mixture. The reaction flask was removed from the cold bath. After 10 minutes, KTp (0.053 g, 0.210 mmol) in 0.75 mL DME was added to the reaction mixture. Reaction allowed to stir for 25 minutes, then it was filtered over a 15 mL fine fritted glass funnel. The solid was washed 2 x 2mL with DME. The red filtrate was evaporated, leaving a red oily residue. The residue was dissolved in 3 mL and transferred to a 4 dram vial. Red crystalline solid began to deposit spontaneously. 0.060 g of solid collected (52% yield). Pure by ¹H NMR except for the solvent peaks. ¹H-NMR (CD₃CN): δ 8.09 (d, 3H, J_{HH}=1.9 Hz, H₃), 7.78 (d, 3H, J_{HH}=2.3 Hz, H₅), 6.31 (t, 3H, J_{HH}=2.2 Hz, H₄), 4.47 (m, 1H, B-H), 1.38 (d, 9H, J_{PH}=8.1 Hz, PMe₃). ¹³C-NMR {¹H} (CD₃CN): δ 147.0 (s, C₃), 137.6 (s, C₅), 106.9 (s, C₄), 16.6 (d, J_{PC}=27.7 Hz, PMe₃). CO Resonances not observed. ³¹P NMR {¹H} (CD₃CN): δ -11.04 (s, 1P). IR (HATR): ν_{CO} = 1917 cm⁻¹ (medium, sharp), 1790 cm⁻¹ (strong, broad). CV: (CH₃CN) E_{p,a} = 0.49 V.

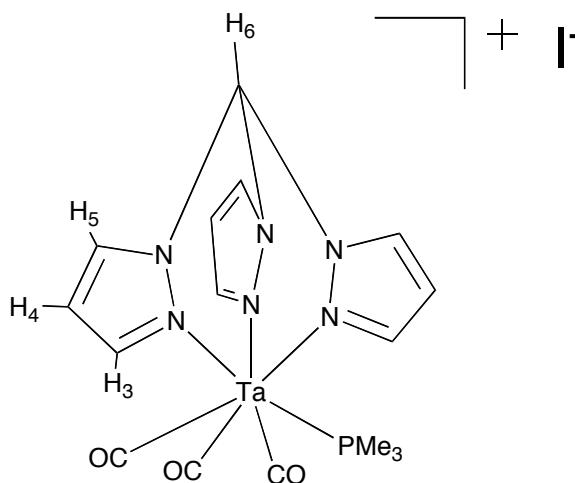
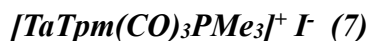


Figure 3ab.4: Depiction of 7.

1 (0.099 g, 0.206 mmol) was dissolved in 2 mL DME in a 30 mL test tube. The resulting yellow solution was cooled to -40°C and stirred. I_2 (0.054 g, 0.213 mmol) was dissolved in 1.5 mL DME. The resulting dark red solution was cooled to -40°C and added to the solution of **1**, giving a dark red, turbid solution almost immediately. After 30 minutes, PMe_3 (0.062 g, 0.815 mmol) in 0.5 mL DME was chilled to -40°C and added to the heterogenous reaction solution, at which point the solution immediately became a much lighter orange turbid mixture. This mixture was allowed to stir for 20 minutes before Tpm (0.237 g, 1.106 mmol) was dissolved in ~ 3 mL chilled DME and added to the reaction mixture. No physical change was noted. The mixture was then allowed to warm to room temperature and stir overnight. The mixture was then filtered over a 15 mL medium porosity fritted glass funnel. A peach solid and red solution were collected. The peach solid was washed with DME until the washings were collected as nearly clear solutions, leaving a white solid once dried. The red filtrate was evaporated, then

redissolved in ~5 mL DME. Excess hexanes (~7 mL) were added, causing a precipitation to occur. Using a clean 15 mL medium porosity fritted glass funnel, a solid the color of the tangy orange sherbet in Dreyer's Orange Cream Sherbet™ (and not the color of the vanilla light ice cream) was collected, along with a red filtrate. This filtrate was evaporated and dissolved in minimal DME, at which point excess hexanes were again added and another batch of solid was collected. This procedure was repeated once more to collect a total mass of 0.048 g (42%) of **7** which was pure by NMR and CV. An m/z peak at 555.07257 was observed with high resolution mass spectrometry. This was further than 5 ppm away from the predicted 555.07307. Peaks smaller than the molecular ion were successfully identified as fragmentation peaks. Unidentified peaks at $m/z=803.53577$ and $m/z=627.35604$ were also observed by HRMS. $^1\text{H-NMR}$ (CD_3CN): δ 10.11 (s, 1H, H_6), 8.53 (dd, 3H, $J_{\text{HH}}=0.6, 2.7$ Hz, H_5), 8.26 (d, 3H, $J_{\text{HH}}=2.5$ Hz, H_3), 6.54 (t, 3H, $J=2.6$ Hz, H_4) 1.48 (d, $J_{\text{PH}}=9.0$ Hz, PMe_3). $^{13}\text{C-NMR}$ $\{^1\text{H}\}$ (CD_3CN): δ 75.8 (s, 1C, C_6), δ 135.7 (s, 3C, C_5), δ 149.5 (s, 3C, C_3), 109.5 (s, 3C, C_4) 16.4 (d, $J_{\text{PC}}=30.0$ Hz, PMe_3). CO resonances were not observed. $^{31}\text{P-NMR}$ $\{^1\text{H}\}$ (CD_3CN): δ -11.28 (s, 1P). IR (HATR): $\nu_{\text{CO}} = 1932$ cm^{-1} (medium, sharp), 1809 cm^{-1} (strong, broad). CV: (CH_3CN) $E_{\text{p,a}} = 0.62$ V. HRMS, calculated, observed, ppm difference. 555.0731, 555.0726, 0.9. Peaks smaller than the molecular ion were successfully identified as fragmentation peaks. Unidentified peaks at $m/z=803.53577$ and $m/z=627.35604$ were also observed by HRMS. High resolution mass spectrometry data available in appendix.

Tris(1-pyrazoyl)methane (9)

The following procedure was derived from the procedure reported by Reger et al. in 2000.²¹

This procedure was executed outside of a glovebox. Pyrazole (19.97 g, 0.293 mol) was added to a 1L round bottom flask with a side arm. A positive pressure of N₂ was applied through sidearm. Bu₄NBr (4.63 g, 0.014 mol) was added to flask. H₂O (294 mL) was also added. The mixture was stirred with magnetic stir bar. After 5 minutes, Na₂CO₃ addition began (188 g, 1.77 mol). Portions of the total 188 g were added over the course of 30 minutes. A yellowish solution was noted. Note: this reaction was exothermic and will noticeably heat the flask. CHCl₃ (150 mL) was added, and a reflux was set up. After 3 days, the solution was yellow and brown. The heating device used for reflux was turned off. When the reaction flask had cooled to room temperature, the mixture was filtered over a 350 mL M fritted glass funnel. Et₂O (500 mL) and H₂O (300 mL) were added to the filtrate. Using a 4L separatory funnel, the aqueous and organic layers of the filtrate were separated. The aqueous layer was extracted 2x200 mL Et₂O and added to the organic layer. The organic layer was treated with activated charcoal and MgSO₄. This mixture was filtered over celite. The filtrate was a light yellow. This solution was evaporated by rotary evaporation. A small amount of water remained after evaporation of the organic solvent along with a yellow solid. CH₂Cl₂ used to dissolve solid. MgSO₄ was added to remove this water. The solution was filtered over a 60 mL medium fritted glass funnel. A yellow filtrate was collected and evaporated to give ~15g

of a yellow solid. ^1H NMR of this solid indicated that free pyrazole was present in the product as an impurity. The solid was dissolved in 300 mL Et_2O . This solution was extracted 5 x 50 mL with a saturated $\text{NaHCO}_3(\text{aq})$ solution. The ether solution was evaporated. The solid was collected and desiccated. 9.183 g of solid collected. A small amount of free pyrazole remained as observed in ^1H NMR. Additional $\text{NaHCO}_3(\text{aq})$ extraction would likely solve this problem. Tpm approximated by ^1H NMR to be 90-95% pure. ^1H -NMR (CD_3CN): δ 8.63 (s, 1H, H_6), 7.73 (d, 3H, $J_{\text{HH}}=2.44$ Hz, H_5), 7.69 (d, 3H, $J_{\text{HH}}=1.55$ Hz, H_3), 6.44 (m, 3H, H_4). ^1H -NMR (CDCl_3): δ 8.43 (s, 1H, H_6), 7.67 (d, 3H, $J_{\text{HH}}=2.6$ Hz, H_5 or H_3), 7.57 (d, 3H, $J_{\text{HH}}=1.7$ Hz, H_5 or H_3), 6.37 (dd, 3H, $J_{\text{HH}}=2.6$, 1.7 Hz H_4). ^{13}C -NMR (CD_3CN): δ 83.7 (s, 1C, C_6), 130.8 (s, 3C, C_5), 142.3 (s, 3C, C_3), 108.0 (s, 3C, C_4).

3ab.2 References

- 1) Keane, J. M; Harman, W. D. *Organometallics* **2005**, 24, 1786-1798
- 2) Wrighton, Mark. *Chemical Reviews* **1974**, Vol. 74, No. 4, 401-430.
- 3) Crabtree, Robert H. *The Organometallic Chemistry of the Transition Metals, Fourth Edition*. John Wiley & Sons: Hoboken, NJ. 2005.
- 4) Ellis, John E.; Fjare, Kristi L.; Warnock, Garry F. *Inorganica Chimica Acta*, **1995**, 240, 379-384.
- 5) Davidson, A.; Ellis, J.E. *Journal of Organometallic Chemistry*, **1971**, 31, 239-247.
- 6) Welch, Kevin D.; Harrison, Daniel P.; Lis, Edward C., Jr.; Liu, Weijun; Salomon, Rebecca J.; Harman, W. Dean. *Organometallics*, **2007**, 26, 2791-2794.
- 7) [Ta(CO)₆]⁻ data collected in this work
- 8) Carey, F.A.; Sundberg, R.J.. *Advanced Organic Chemistry Part A: Structure and Mechanisms, Fifth Ed.*; Springer Press: New York, 2007.
- 9) Harman, W. Hill. *Distinguished Majors Thesis*; University of Virginia: Charlottesville, 2005.
- 10) Ford, P.; Rudd, D. F. P.; Gaunder, R.; Taube, H. *J. Am. Chem. Soc.* **1968**, 90 (5), 1187.
- 11) Work with terpy performed by Andrew Walden
- 12) Calderazzo, Fausto; Castellani, Manola; Pampaloni, Guido. *J. Chem. Soc. Dalton Trans.*, **1985**, 1989-1995.
- 13) Koeslag, Mary Ann; Baird, Michael C.; Lovelace, Sherri; Geiger, William E. *Organometallics*, **1996**, 15, 3289-3302.

- 14) Hayton, Trevor W.; Daff, James P.; Legzdins, Peter; Rettig, Steven J.; Patrick, Brian O. *Inorg. Chem.*, **2002**, 41, 4114-4126.
- 15) McGearry, M. J.; Gamble, A. S.; Templeton, J. L. *Organometallics*, **1988**, 7, 271-279.
- 16) Hayton, Trevor W.; Legzdins, Peter; Rettig, Steven J.; Patrick, Brian O. *Inorg. Chem.*, **2002**, 41, 5388-5396.
- 17) Trindle, Carl; Sacks, Gavin; Harman, W. Dean. *International Journal of Quantum Chemistry* **2003**, Vol. 92, 457-469.
- 18) Ha, Yunkyoun; Dilsky, Stefan; Graham, Peter M.; Liu, Weijun; Reichart, Timothy M.; Sabat, Michal; Keane, Joseph M.; Harman, W. Dean. *Organometallics* **2006**, 25, 5184-5187.
- 19) It was surprising to observe that the reduction of the PPh₃ product had an E_{p,a} more reducing than the PMe₃ product. However, ³¹P NMR data showed that the reduction of the PPh₃ product led to a new product with PPh₃ still in the ligand set, whereas reduction of the PMe₃ product led to a species without PMe₃ in the ligand set. Thus, the two products were structurally unrelated and a prediction of the relative potentials of these compounds would be difficult.
- 20) Luetkens, Melvin, L. Jr.; Santure, David J.; Huffman, John C.; Sattelberger, Alfred P. *J. Chem. Soc. Chem. Commun.* **1985**, 552-553.
- 21) Reger, Daniel L.; Grattan, T. Christian; Brown, Kenneth J.; Little, Christine A.; Lamba, Jaydeep J.S.; Rheingold, Arnold L.; Sommer, Roger D. *Journal of Organometallic Chemistry* **2000**, 607, 120-128

22) Gaussian 09, Revision **A.02**, M. J. Frisch, G. W. Trucks, H. B. Schlegel, G. E.

Scuseria, M. A. Robb, J. R. Cheeseman, G. Scalmani, V. Barone, B.

Mennucci, G. A. Petersson, H. Nakatsuji, M. Caricato, X. Li, H. P. Hratchian,

A. F. Izmaylov, J. Bloino, G. Zheng, J. L. Sonnenberg, M. Hada, M. Ehara, K.

Toyota, R. Fukuda, J. Hasegawa, M. Ishida, T. Nakajima, Y. Honda, O. Kitao,

H. Nakai, T. Vreven, J. A. Montgomery, Jr., J. E. Peralta, F. Ogliaro, M.

Bearpark, J. J. Heyd, E. Brothers, K. N. Kudin, V. N. Staroverov, R.

Kobayashi, J. Normand, K. Raghavachari, A. Rendell, J. C. Burant, S. S.

Iyengar, J. Tomasi, M. Cossi, N. Rega, J. M. Millam, M. Klene, J. E. Knox, J.

B. Cross, V. Bakken, C. Adamo, J. Jaramillo, R. Gomperts, R. E. Stratmann,

O. Yazyev, A. J. Austin, R. Cammi, C. Pomelli, J. W. Ochterski, R. L. Martin,

K. Morokuma, V. G. Zakrzewski, G. A. Voth, P. Salvador, J. J. Dannenberg, S.

Dapprich, A. D. Daniels, O. Farkas, J. B. Foresman, J. V. Ortiz, J. Cioslowski,

and D. J. Fox, Gaussian, Inc., Wallingford CT, 2009.

23) a)A.D. Becke, *J. Chem. Phys.*, **98**, (1993), 5648. b)P.J. Stevens, F.J. Devlin, C.F.

Chabalowski, M.J. Frisch, *J. Phys. Chem.*, **98**, (1994) 11623.

24) a)T. H. Dunning Jr. and P. J. Hay, in *Modern Theoretical Chemistry*, Ed. H. F.

Schaefer III, Vol. 3 (Plenum, New York, 1976) 1-28. b)P. J. Hay and W. R.

Wadt, "Ab initio effective core potentials for molecular calculations -

potentials for the transition-metal atoms Sc to Hg," *J. Chem. Phys.*, **82** (1985)

270-83. c)P. J. Hay and W. R. Wadt, "Ab initio effective core potentials for

molecular calculations - potentials for K to Au including the outermost core

orbitals," *J. Chem. Phys.*, **82** (1985) 299-310. d) W. R. Wadt and P. J. Hay, "Ab initio effective core potentials for molecular calculations - potentials for main group elements Na to Bi," *J. Chem. Phys.*, **82** (1985) 284-98.

Conclusion

Aromatic compounds are valuable precursors to a number of compounds of synthetic interest when the stability inherent to them can be overcome. One way to disrupt this aromaticity is to complex the aromatic molecule to a strongly π -basic metal fragment. We have synthesized a number of these metal fragments in the past, including $\{\text{Os}(\text{NH}_3)_5\}^{2+}$, $\{\text{TpRe}(\text{CO})(\text{MeIm})\}$, and $\{\text{TpW}(\text{PMe}_3)(\text{NO})\}$. We noticed a trend in each of these metal systems: as we moved from late 3rd row metals to early 3rd row metals, the activation of the dihapto-coordinated species became greater. Thus, we hypothesized that we could synthesize a tantalum-based dearomatization agent that would be even more activating towards aromatic molecules. This also gave us the opportunity to test the hypothesis that the identity of the metal in the metal fragment does not preclude the synthesis of a dearomatizing metal fragment as long as the proper ligand set was chosen. Two unknown metal fragments, $\{\text{TpTa}(\text{CO})(\text{NO})\}^-$ and $\{\text{TpmTa}(\text{CO})(\text{NO})\}$ were targeted as possible dearomatizing metal fragments.

$[\text{Et}_4\text{N}][\text{Ta}(\text{CO})_6]$ was chosen as the starting material for the synthesis of these target compounds. Because this compound was already fairly electron rich, as determined by electrochemical measurements, $\{\text{Ta}(\text{CO})_5\}^-$, $\{\text{Ta}(\text{CO})_4\text{X}\}^-$, and $\{\text{Ta}(\text{CO})_3\text{X}_2\}^-$ were probed to determine if they might instead act as dearomatizing agents. These species were synthesized using photolytic methods, but none of them displayed the ability to bind an arene or an olefin.

In order to arrive at the target compounds, it was determined that the $[\text{Et}_4\text{N}][\text{Ta}(\text{CO})_6]$ starting material would have to be oxidized in order to easily modify the ligand

set. Using this method, $\text{TaTp}(\text{CO})_4$, $[\text{Ta}(\text{TpM})(\text{CO})_4]^+ \text{I}^-$, $\text{TaTp}(\text{CO})_3\text{PMe}_3$, and $[\text{TaTpM}(\text{CO})_3\text{PMe}_3]^+ \text{I}^-$ were synthesized. The tricarbonyl species were of particular interest because it was not difficult to imagine them going through d^6 , $18e^-$, tricarbonyl intermediates that would be electron rich enough to nitrosylate and produce the desired metal fragments bound to an additional carbonyl ligand. More effort needs to be placed into the reduction and nitrosylation of these species. Initial results suggest that this process can be executed successfully.

Appendix

Tantalum (V) Trimer Crystallographic Data...	A-2
[Et ₄ N][Ta(CO) ₅ (PPh ₃)] (2) Crystallographic Data...	A-15
[Et ₄ N][Ta(CO) ₄ (bipy)] Crystallographic Data...	A-26
TaTp(CO) ₄ (5) Crystallographic Data...	A-34
[TaTp(CO) ₄]I (6) Crystallographic Data...	A-42
[Et ₄ N][Ta(CO) ₆] (1) Infrared Spectrum/Cyclic Voltammogram...	A-50
High Resolution Mass Spectrum of [TaTp(CO) ₃ PMe ₃] ⁺ (8)...	A-52
NMR Data from Table 3a.1 ...	A-54
¹ H NMR Data for 5 ...	A-58
¹ H NMR Data for 6 ...	A-59
¹ H NMR Data for 7 ...	A-60
¹ H NMR Data for 8 ...	A-61
Unpublished Synthesis of <i>tert</i> -BuSi(CH ₂ PMe ₂) ₃ (trimpsi) from Dr. Greg Girolami...	A-62

Crystallographic data for Ta (V) Trimer

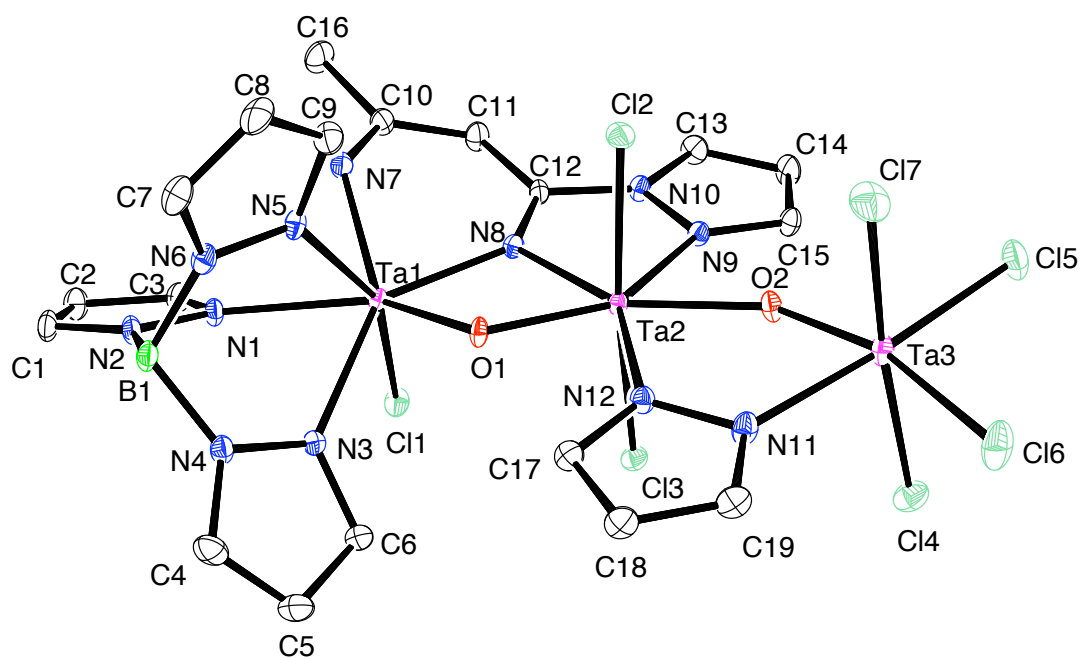


Table 1. Crystal data and structure refinement for C₂₃H₂₈BN₁₄O₂Cl₇Ta₃.

Empirical formula	C ₂₃ H ₂₈ B Cl ₇ N ₁₄ O ₂ Ta ₃	
Formula weight	1334.40	
Temperature	153(2) K	
Wavelength	0.71073 Å	
Crystal system	Monoclinic	
Space group	P2(1)/c	
Unit cell dimensions	a = 15.1623(3) Å	
	b = 15.4902(4) Å	β = 109.235(1)°.
	c = 17.0654(4) Å	
Volume	3784.35(15) Å ³	
Z	4	
Density (calculated)	2.342 Mg/m ³	
Absorption coefficient	9.193 mm ⁻¹	
F(000)	2492	
Crystal size	0.43 x 0.31 x 0.10 mm ³	
Theta range for data collection	1.82 to 36.42°.	
Index ranges	-22 ≤ h ≤ 22, -15 ≤ k ≤ 25, -24 ≤ l ≤ 23	
Reflections collected	42608	
Independent reflections	12142 [R(int) = 0.0364]	
Completeness to theta = 36.42°	95.7 %	
Absorption correction	Empirical	
Max. and min. transmission	0.4600 and 0.1100	
Refinement method	Full-matrix least-squares on F ²	
Data / restraints / parameters	12142 / 0 / 428	
Goodness-of-fit on F ²	0.871	
Final R indices [I > 2σ(I)]	R1 = 0.0306, wR2 = 0.1024	
R indices (all data)	R1 = 0.0365, wR2 = 0.1090	
Largest diff. peak and hole	3.052 and -2.118 e.Å ⁻³	

Table 2. Atomic coordinates ($\times 10^4$) and equivalent isotropic displacement parameters ($\text{\AA}^2 \times 10^3$) for $\text{C}_{23}\text{H}_{28}\text{BN}_{14}\text{O}_2\text{Cl}_7\text{Ta}_3$. $U(\text{eq})$ is defined as one third of the trace of the orthogonalized U^{ij} tensor.

	x	y	z	$U(\text{eq})$
Ta(1)	1837(1)	5334(1)	3527(1)	14(1)
Ta(2)	2095(1)	3261(1)	3583(1)	14(1)
Ta(3)	2628(1)	1004(1)	4233(1)	21(1)
Cl(1)	204(1)	5309(1)	3127(1)	22(1)
Cl(2)	3519(1)	3281(1)	3295(1)	22(1)
Cl(3)	632(1)	3093(1)	3775(1)	20(1)
Cl(4)	1088(1)	703(1)	4235(1)	30(1)
Cl(5)	2397(1)	18(1)	3138(1)	36(1)
Cl(6)	3164(1)	15(1)	5386(1)	40(1)
Cl(7)	4190(1)	1160(1)	4299(1)	40(1)
O(1)	2386(2)	4329(2)	4193(2)	16(1)
O(2)	2243(2)	1970(2)	3613(2)	20(1)
N(1)	1557(3)	6786(2)	3547(2)	19(1)
N(2)	2036(3)	7329(2)	4170(2)	21(1)
N(3)	1734(2)	5637(2)	4777(2)	19(1)
N(4)	2218(3)	6282(2)	5290(2)	20(1)
N(5)	3244(2)	5858(2)	4101(2)	19(1)
N(6)	3495(2)	6479(2)	4689(2)	21(1)
N(7)	2021(3)	5855(2)	2457(2)	21(1)
N(8)	1626(2)	4299(2)	2746(2)	16(1)
N(9)	1403(2)	2752(2)	2285(2)	17(1)
N(10)	1141(2)	3356(2)	1670(2)	17(1)
N(11)	2830(3)	2000(2)	5174(2)	22(1)
N(12)	2721(2)	2857(2)	4923(2)	18(1)
N(13)	3211(4)	7490(3)	2775(3)	42(1)
N(14)	5729(11)	4791(11)	3145(10)	173(6)
C(1)	1744(3)	8146(3)	3963(3)	25(1)
C(2)	1078(3)	8151(3)	3194(3)	26(1)
C(3)	977(3)	7281(3)	2960(3)	22(1)
C(4)	2060(4)	6221(3)	6024(3)	30(1)

C(5)	1472(4)	5552(3)	5995(3)	32(1)
C(6)	1274(3)	5192(3)	5201(3)	25(1)
C(7)	4426(3)	6570(3)	4950(3)	30(1)
C(8)	4793(3)	5991(3)	4522(4)	34(1)
C(9)	4036(3)	5561(3)	3993(3)	27(1)
C(10)	1626(3)	5669(3)	1652(2)	22(1)
C(11)	1225(3)	4873(3)	1364(2)	22(1)
C(12)	1308(3)	4214(2)	1931(2)	17(1)
C(13)	774(3)	2971(3)	918(2)	25(1)
C(14)	773(3)	2107(3)	1048(2)	26(1)
C(15)	1194(3)	1997(3)	1916(2)	20(1)
C(16)	1606(4)	6367(3)	1036(3)	34(1)
C(17)	2919(3)	3341(3)	5608(2)	22(1)
C(18)	3172(3)	2817(3)	6308(2)	26(1)
C(19)	3110(3)	1985(3)	6008(2)	25(1)
C(20)	4336(6)	8595(6)	3701(5)	70(2)
C(21)	3721(4)	7986(4)	3177(4)	43(1)
C(22)	4774(12)	6130(10)	2236(11)	152(6)
C(23)	5317(10)	5331(9)	2719(9)	108(4)
B(1)	2745(4)	6949(3)	4961(3)	22(1)

Table 3. Bond lengths [\AA] and angles [$^\circ$] for $\text{C}_{23}\text{H}_{28}\text{BN}_{14}\text{O}_2\text{Cl}_7\text{Ta}_3$.

Ta(1)-O(1)	1.945(3)
Ta(1)-N(8)	2.042(3)
Ta(1)-N(7)	2.098(3)
Ta(1)-N(5)	2.190(3)
Ta(1)-N(3)	2.238(3)
Ta(1)-N(1)	2.291(3)
Ta(1)-Cl(1)	2.3409(10)
Ta(1)-Ta(2)	3.2326(2)
Ta(2)-O(1)	1.926(3)
Ta(2)-O(2)	2.010(3)
Ta(2)-N(8)	2.113(3)
Ta(2)-N(9)	2.257(3)
Ta(2)-N(12)	2.257(3)
Ta(2)-Cl(3)	2.3609(9)
Ta(2)-Cl(2)	2.3672(10)
Ta(3)-O(2)	1.815(3)
Ta(3)-N(11)	2.174(4)
Ta(3)-Cl(7)	2.3458(13)
Ta(3)-Cl(5)	2.3493(11)
Ta(3)-Cl(4)	2.3830(11)
Ta(3)-Cl(6)	2.4133(11)
N(1)-C(3)	1.335(5)
N(1)-N(2)	1.363(4)
N(2)-C(1)	1.348(5)
N(2)-B(1)	1.539(6)
N(3)-C(6)	1.350(5)
N(3)-N(4)	1.370(5)
N(4)-C(4)	1.354(5)
N(4)-B(1)	1.523(6)
N(5)-N(6)	1.351(5)
N(5)-C(9)	1.354(6)
N(6)-C(7)	1.341(5)
N(6)-B(1)	1.544(6)

N(7)-C(10)	1.337(5)
N(8)-C(12)	1.320(5)
N(9)-C(15)	1.317(5)
N(9)-N(10)	1.365(4)
N(10)-C(13)	1.357(5)
N(10)-C(12)	1.398(5)
N(11)-C(19)	1.345(5)
N(11)-N(12)	1.387(5)
N(12)-C(17)	1.338(5)
N(13)-C(21)	1.144(8)
N(14)-C(23)	1.148(18)
C(1)-C(2)	1.368(6)
C(2)-C(3)	1.400(6)
C(4)-C(5)	1.358(7)
C(5)-C(6)	1.403(6)
C(7)-C(8)	1.383(7)
C(8)-C(9)	1.376(7)
C(10)-C(11)	1.390(6)
C(10)-C(16)	1.502(6)
C(11)-C(12)	1.383(5)
C(13)-C(14)	1.356(7)
C(14)-C(15)	1.416(5)
C(17)-C(18)	1.389(6)
C(18)-C(19)	1.379(7)
C(20)-C(21)	1.417(10)
C(22)-C(23)	1.563(19)
O(1)-Ta(1)-N(8)	72.42(12)
O(1)-Ta(1)-N(7)	131.44(13)
N(8)-Ta(1)-N(7)	76.72(13)
O(1)-Ta(1)-N(5)	82.50(12)
N(8)-Ta(1)-N(5)	120.17(13)
N(7)-Ta(1)-N(5)	81.73(14)
O(1)-Ta(1)-N(3)	76.28(12)
N(8)-Ta(1)-N(3)	137.93(12)

N(7)-Ta(1)-N(3)	145.02(13)
N(5)-Ta(1)-N(3)	81.94(13)
O(1)-Ta(1)-N(1)	145.39(12)
N(8)-Ta(1)-N(1)	142.19(12)
N(7)-Ta(1)-N(1)	73.33(13)
N(5)-Ta(1)-N(1)	77.70(13)
N(3)-Ta(1)-N(1)	73.07(12)
O(1)-Ta(1)-Cl(1)	111.44(9)
N(8)-Ta(1)-Cl(1)	82.76(9)
N(7)-Ta(1)-Cl(1)	100.58(11)
N(5)-Ta(1)-Cl(1)	156.55(10)
N(3)-Ta(1)-Cl(1)	83.29(9)
N(1)-Ta(1)-Cl(1)	80.64(9)
O(1)-Ta(1)-Ta(2)	33.21(8)
N(8)-Ta(1)-Ta(2)	39.73(9)
N(7)-Ta(1)-Ta(2)	110.99(10)
N(5)-Ta(1)-Ta(2)	105.34(9)
N(3)-Ta(1)-Ta(2)	103.09(9)
N(1)-Ta(1)-Ta(2)	174.89(9)
Cl(1)-Ta(1)-Ta(2)	95.67(2)
O(1)-Ta(2)-O(2)	146.76(10)
O(1)-Ta(2)-N(8)	71.20(12)
O(2)-Ta(2)-N(8)	141.63(11)
O(1)-Ta(2)-N(9)	141.20(12)
O(2)-Ta(2)-N(9)	71.92(11)
N(8)-Ta(2)-N(9)	70.01(12)
O(1)-Ta(2)-N(12)	75.27(12)
O(2)-Ta(2)-N(12)	72.08(11)
N(8)-Ta(2)-N(12)	146.29(12)
N(9)-Ta(2)-N(12)	143.31(13)
O(1)-Ta(2)-Cl(3)	94.47(9)
O(2)-Ta(2)-Cl(3)	89.36(9)
N(8)-Ta(2)-Cl(3)	93.18(9)
N(9)-Ta(2)-Cl(3)	86.78(9)
N(12)-Ta(2)-Cl(3)	85.97(9)

O(1)-Ta(2)-Cl(2)	92.20(9)
O(2)-Ta(2)-Cl(2)	85.26(9)
N(8)-Ta(2)-Cl(2)	88.61(9)
N(9)-Ta(2)-Cl(2)	87.79(9)
N(12)-Ta(2)-Cl(2)	96.11(9)
Cl(3)-Ta(2)-Cl(2)	173.32(3)
O(1)-Ta(2)-Ta(1)	33.57(8)
O(2)-Ta(2)-Ta(1)	179.46(9)
N(8)-Ta(2)-Ta(1)	38.14(9)
N(9)-Ta(2)-Ta(1)	107.78(9)
N(12)-Ta(2)-Ta(1)	108.16(9)
Cl(3)-Ta(2)-Ta(1)	90.17(2)
Cl(2)-Ta(2)-Ta(1)	95.18(3)
O(2)-Ta(3)-N(11)	77.58(12)
O(2)-Ta(3)-Cl(7)	93.97(11)
N(11)-Ta(3)-Cl(7)	89.83(11)
O(2)-Ta(3)-Cl(5)	97.91(9)
N(11)-Ta(3)-Cl(5)	175.35(9)
Cl(7)-Ta(3)-Cl(5)	89.37(5)
O(2)-Ta(3)-Cl(4)	91.96(10)
N(11)-Ta(3)-Cl(4)	92.15(11)
Cl(7)-Ta(3)-Cl(4)	174.03(5)
Cl(5)-Ta(3)-Cl(4)	89.10(5)
O(2)-Ta(3)-Cl(6)	162.96(9)
N(11)-Ta(3)-Cl(6)	85.50(9)
Cl(7)-Ta(3)-Cl(6)	87.88(5)
Cl(5)-Ta(3)-Cl(6)	99.05(5)
Cl(4)-Ta(3)-Cl(6)	86.67(5)
Ta(2)-O(1)-Ta(1)	113.22(13)
Ta(3)-O(2)-Ta(2)	147.87(15)
C(3)-N(1)-N(2)	106.3(3)
C(3)-N(1)-Ta(1)	129.2(3)
N(2)-N(1)-Ta(1)	124.3(3)
C(1)-N(2)-N(1)	109.3(3)
C(1)-N(2)-B(1)	131.5(4)

N(1)-N(2)-B(1)	119.1(3)
C(6)-N(3)-N(4)	107.0(3)
C(6)-N(3)-Ta(1)	127.9(3)
N(4)-N(3)-Ta(1)	124.9(2)
C(4)-N(4)-N(3)	108.7(4)
C(4)-N(4)-B(1)	131.5(4)
N(3)-N(4)-B(1)	119.6(3)
N(6)-N(5)-C(9)	107.3(3)
N(6)-N(5)-Ta(1)	126.2(3)
C(9)-N(5)-Ta(1)	126.2(3)
C(7)-N(6)-N(5)	109.2(4)
C(7)-N(6)-B(1)	130.5(4)
N(5)-N(6)-B(1)	120.3(3)
C(10)-N(7)-Ta(1)	131.9(3)
C(12)-N(8)-Ta(1)	133.7(3)
C(12)-N(8)-Ta(2)	124.2(3)
Ta(1)-N(8)-Ta(2)	102.13(14)
C(15)-N(9)-N(10)	106.1(3)
C(15)-N(9)-Ta(2)	137.8(3)
N(10)-N(9)-Ta(2)	116.0(2)
C(13)-N(10)-N(9)	110.5(3)
C(13)-N(10)-C(12)	134.0(4)
N(9)-N(10)-C(12)	115.5(3)
C(19)-N(11)-N(12)	107.9(3)
C(19)-N(11)-Ta(3)	133.4(3)
N(12)-N(11)-Ta(3)	118.6(2)
C(17)-N(12)-N(11)	107.3(3)
C(17)-N(12)-Ta(2)	128.9(3)
N(11)-N(12)-Ta(2)	123.0(2)
N(2)-C(1)-C(2)	109.4(4)
C(1)-C(2)-C(3)	104.2(4)
N(1)-C(3)-C(2)	110.9(4)
N(4)-C(4)-C(5)	109.5(4)
C(4)-C(5)-C(6)	105.5(4)
N(3)-C(6)-C(5)	109.4(4)

N(6)-C(7)-C(8)	108.6(4)
C(9)-C(8)-C(7)	105.5(4)
N(5)-C(9)-C(8)	109.4(4)
N(7)-C(10)-C(11)	123.4(4)
N(7)-C(10)-C(16)	117.5(4)
C(11)-C(10)-C(16)	119.1(4)
C(12)-C(11)-C(10)	118.6(4)
N(8)-C(12)-C(11)	125.5(4)
N(8)-C(12)-N(10)	113.3(3)
C(11)-C(12)-N(10)	120.9(3)
C(14)-C(13)-N(10)	107.5(4)
C(13)-C(14)-C(15)	105.4(4)
N(9)-C(15)-C(14)	110.4(4)
N(12)-C(17)-C(18)	110.0(4)
C(19)-C(18)-C(17)	105.1(4)
N(11)-C(19)-C(18)	109.7(4)
N(13)-C(21)-C(20)	177.6(7)
N(14)-C(23)-C(22)	173.0(17)
N(4)-B(1)-N(2)	106.4(4)
N(4)-B(1)-N(6)	108.6(3)
N(2)-B(1)-N(6)	106.7(3)

Symmetry transformations used to generate equivalent atoms:

Table 4. Anisotropic displacement parameters ($\text{\AA}^2 \times 10^3$) for C₂₃H₂₈BN₁₄O₂Cl₇Ta₃. The anisotropic displacement factor exponent takes the form: $-2\pi^2 [h^2 a^{*2} U^{11} + \dots + 2 h k a^* b^* U^{12}]$

	U ¹¹	U ²²	U ³³	U ²³	U ¹³	U ¹²
Ta(1)	14(1)	12(1)	14(1)	0(1)	3(1)	-1(1)
Ta(2)	15(1)	13(1)	13(1)	0(1)	3(1)	-1(1)
Ta(3)	24(1)	14(1)	21(1)	1(1)	4(1)	1(1)
Cl(1)	15(1)	19(1)	30(1)	0(1)	4(1)	0(1)
Cl(2)	17(1)	24(1)	27(1)	-4(1)	8(1)	-2(1)
Cl(3)	17(1)	22(1)	21(1)	0(1)	7(1)	-3(1)
Cl(4)	30(1)	35(1)	26(1)	0(1)	8(1)	-10(1)
Cl(5)	52(1)	20(1)	32(1)	-5(1)	12(1)	4(1)
Cl(6)	53(1)	24(1)	31(1)	9(1)	-2(1)	5(1)
Cl(7)	24(1)	43(1)	52(1)	-2(1)	10(1)	6(1)
O(1)	21(1)	9(1)	15(1)	1(1)	0(1)	1(1)
O(2)	26(1)	13(1)	18(1)	-1(1)	3(1)	4(1)
N(1)	23(2)	13(2)	21(1)	-4(1)	6(1)	-3(1)
N(2)	29(2)	13(2)	20(1)	-4(1)	8(1)	-2(1)
N(3)	22(2)	17(2)	19(1)	-3(1)	8(1)	-3(1)
N(4)	25(2)	16(2)	17(1)	-1(1)	5(1)	-1(1)
N(5)	18(2)	14(1)	23(2)	-1(1)	3(1)	-3(1)
N(6)	20(2)	20(2)	19(1)	-2(1)	2(1)	-5(1)
N(7)	29(2)	16(2)	19(1)	-1(1)	9(1)	-2(1)
N(8)	16(1)	13(2)	16(1)	1(1)	4(1)	0(1)
N(9)	21(2)	15(2)	13(1)	-1(1)	4(1)	-3(1)
N(10)	20(2)	15(2)	13(1)	-1(1)	2(1)	-3(1)
N(11)	29(2)	17(2)	16(1)	4(1)	2(1)	1(1)
N(12)	20(2)	17(2)	17(1)	-2(1)	4(1)	-1(1)
C(1)	36(2)	12(2)	27(2)	-1(1)	11(2)	-2(2)
C(2)	31(2)	16(2)	31(2)	3(2)	8(2)	5(2)
C(3)	21(2)	19(2)	23(2)	0(1)	3(2)	-1(2)
C(4)	38(3)	35(2)	18(2)	-1(2)	10(2)	3(2)
C(5)	36(3)	37(3)	28(2)	3(2)	18(2)	-1(2)
C(6)	30(2)	22(2)	26(2)	2(2)	16(2)	0(2)

C(7)	22(2)	29(2)	31(2)	-2(2)	-2(2)	-11(2)
C(8)	17(2)	29(3)	56(3)	2(2)	11(2)	-4(2)
C(9)	17(2)	26(2)	37(2)	-4(2)	7(2)	-3(2)
C(10)	31(2)	18(2)	18(2)	4(1)	8(2)	3(2)
C(11)	32(2)	18(2)	15(2)	2(1)	4(2)	0(2)
C(12)	21(2)	12(2)	19(2)	-2(1)	7(1)	-1(1)
C(13)	29(2)	27(2)	15(2)	-6(2)	3(2)	-6(2)
C(14)	34(2)	22(2)	17(2)	-7(2)	3(2)	-7(2)
C(15)	23(2)	16(2)	18(2)	-1(1)	2(1)	-4(1)
C(16)	52(3)	25(2)	25(2)	9(2)	15(2)	-2(2)
C(17)	20(2)	23(2)	20(2)	-1(1)	4(2)	-3(2)
C(18)	29(2)	29(2)	16(2)	1(2)	4(2)	-4(2)
C(19)	25(2)	31(2)	15(2)	6(2)	1(1)	0(2)
B(1)	30(2)	14(2)	20(2)	-3(2)	7(2)	-5(2)

Table 5. Hydrogen coordinates ($\times 10^4$) and isotropic displacement parameters ($\text{\AA}^2 \times 10^{-3}$) for C₂₃H₂₈BN₁₄O₂Cl₇Ta₃.

	x	y	z	U(eq)
H(7A)	1915	6436	2490	25
H(7B)	2652	5803	2549	25
H(1)	1966	8641	4300	30
H(2)	758	8635	2888	32
H(3)	553	7071	2453	27
H(4)	2320	6590	6488	36
H(5)	1244	5366	6423	38
H(6)	877	4711	4995	29
H(7)	4776	6967	5359	36
H(8)	5433	5908	4581	41
H(9)	4065	5124	3612	33
H(11)	901	4784	790	27
H(13)	557	3254	395	30
H(14)	539	1669	643	31
H(15)	1309	1455	2192	24
H(16A)	1234	6855	1119	50
H(16B)	1327	6142	472	50
H(16C)	2245	6561	1116	50
H(17)	2890	3954	5615	26
H(18)	3349	2994	6872	31
H(19)	3245	1478	6340	30
H(20A)	3972	9067	3825	104
H(20B)	4755	8826	3422	104
H(20C)	4704	8312	4220	104
H(22A)	4779	6592	2630	229
H(22B)	4128	5965	1932	229
H(22C)	5076	6335	1843	229
H(1B)	3150(60)	7410(50)	5610(50)	120(30)

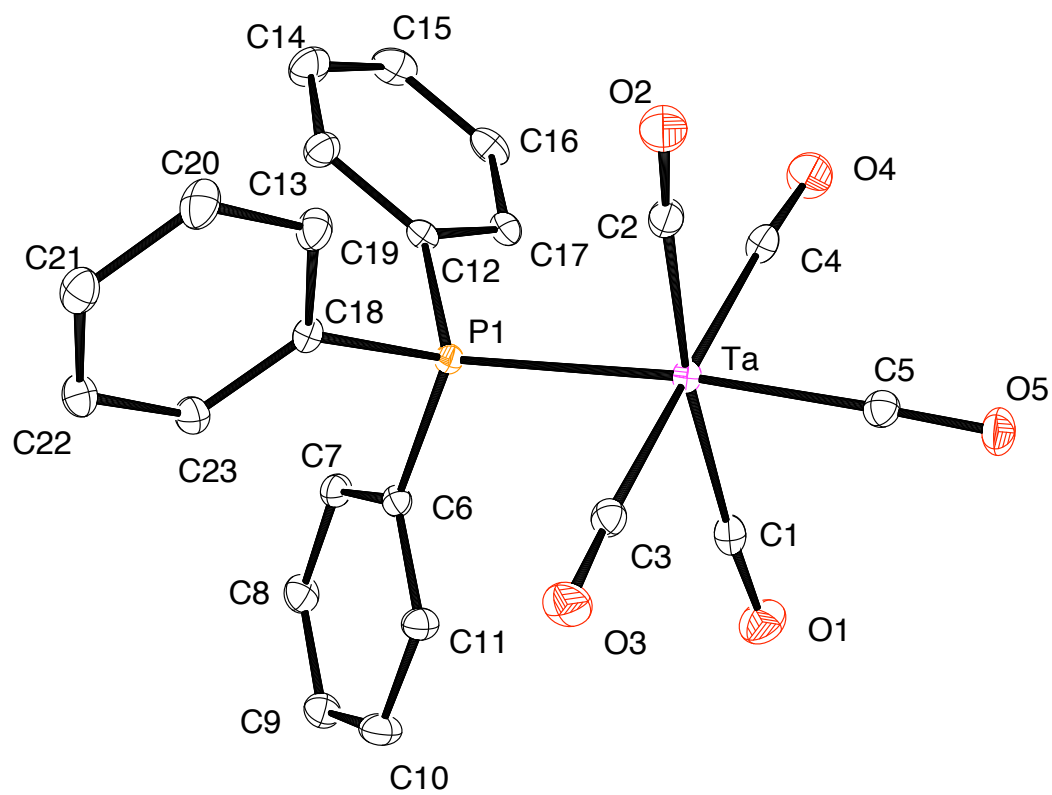
Crystallographic data for $[\text{Et}_4\text{N}][\text{Ta}(\text{CO})_5(\text{PPh}_3)]$ (2)

Table 1. Crystal data and structure refinement for C₃₁H₃₅N₅O₅PTa.

Empirical formula	C ₃₁ H ₃₅ N ₅ O ₅ P Ta	
Formula weight	713.52	
Temperature	153(2) K	
Wavelength	0.71073 Å	
Crystal system	Monoclinic	
Space group	P2(1)/n	
Unit cell dimensions	a = 9.2208(1) Å	
	b = 33.9625(5) Å	β = 93.935(1)°.
	c = 9.6452(1) Å	
Volume	3013.38(6) Å ³	
Z	4	
Density (calculated)	1.573 Mg/m ³	
Absorption coefficient	3.739 mm ⁻¹	
F(000)	1424	
Crystal size	0.38 x 0.21 x 0.14 mm ³	
Theta range for data collection	1.20 to 34.59°.	
Index ranges	-13 ≤ h ≤ 12, -48 ≤ k ≤ 54, -14 ≤ l ≤ 13	
Reflections collected	34868	
Independent reflections	9705 [R(int) = 0.0327]	
Completeness to theta = 34.59°	97.3 %	
Absorption correction	Empirical	
Max. and min. transmission	0.6226 and 0.3307	
Refinement method	Full-matrix least-squares on F ²	
Data / restraints / parameters	9705 / 0 / 356	
Goodness-of-fit on F ²	0.703	
Final R indices [I > 2σ(I)]	R1 = 0.0266, wR2 = 0.0813	
R indices (all data)	R1 = 0.0381, wR2 = 0.0945	
Largest diff. peak and hole	0.936 and -1.369 e.Å ⁻³	

Table 2. Atomic coordinates ($\times 10^4$) and equivalent isotropic displacement parameters ($\text{\AA}^2 \times 10^3$) for C₃₁H₃₅NO₅PTa. U(eq) is defined as one third of the trace of the orthogonalized U^{ij} tensor.

	x	y	z	U(eq)
Ta	2469(1)	8580(1)	1797(1)	17(1)
P(1)	3456(1)	9191(1)	3217(1)	16(1)
O(1)	5148(3)	8010(1)	2812(3)	39(1)
O(2)	-283(3)	9006(1)	145(3)	35(1)
O(3)	4458(3)	8855(1)	-669(2)	34(1)
O(4)	413(3)	8262(1)	4163(3)	41(1)
O(5)	1594(2)	7792(1)	114(2)	31(1)
N(1)	7213(3)	8013(1)	8320(3)	26(1)
C(1)	4212(3)	8228(1)	2531(3)	24(1)
C(2)	699(3)	8870(1)	785(3)	23(1)
C(3)	3738(3)	8767(1)	215(3)	22(1)
C(4)	1164(3)	8388(1)	3361(3)	25(1)
C(5)	1889(3)	8086(1)	708(3)	22(1)
C(6)	5381(3)	9162(1)	3851(3)	18(1)
C(7)	5895(3)	9290(1)	5174(3)	23(1)
C(8)	7367(3)	9265(1)	5586(3)	28(1)
C(9)	8345(3)	9119(1)	4694(3)	29(1)
C(10)	7856(4)	8996(1)	3376(3)	30(1)
C(11)	6376(3)	9014(1)	2953(3)	23(1)
C(12)	2591(3)	9316(1)	4815(3)	19(1)
C(13)	2084(3)	9691(1)	5113(3)	26(1)
C(14)	1466(4)	9769(1)	6357(3)	34(1)
C(15)	1328(4)	9472(1)	7313(3)	34(1)
C(16)	1831(3)	9096(1)	7040(3)	28(1)
C(17)	2448(3)	9021(1)	5797(3)	22(1)
C(18)	3415(3)	9660(1)	2263(3)	18(1)
C(19)	2123(4)	9772(1)	1523(3)	27(1)
C(20)	2051(4)	10123(1)	778(3)	30(1)
C(21)	3271(4)	10362(1)	747(3)	28(1)
C(22)	4547(4)	10253(1)	1476(3)	28(1)

C(23)	4626(3)	9906(1)	2229(3)	24(1)
C(24)	7459(4)	8196(1)	9761(3)	33(1)
C(25)	7993(4)	7917(1)	10902(4)	41(1)
C(26)	6564(5)	8334(1)	7377(4)	39(1)
C(27)	6272(6)	8213(1)	5869(4)	50(1)
C(28)	6217(4)	7659(1)	8349(3)	30(1)
C(29)	4747(4)	7740(1)	8860(4)	44(1)
C(30)	8640(4)	7867(1)	7796(4)	33(1)
C(31)	9739(4)	8180(1)	7521(4)	44(1)

Table 3. Bond lengths [\AA] and angles [$^\circ$] for C₃₁H₃₅NO₅PTa.

Ta-C(5)	2.032(3)
Ta-C(3)	2.084(3)
Ta-C(1)	2.088(3)
Ta-C(2)	2.089(3)
Ta-C(4)	2.098(3)
Ta-P(1)	2.6141(7)
P(1)-C(12)	1.834(3)
P(1)-C(18)	1.837(3)
P(1)-C(6)	1.840(3)
O(1)-C(1)	1.155(4)
O(2)-C(2)	1.157(4)
O(3)-C(3)	1.156(3)
O(4)-C(4)	1.154(4)
O(5)-C(5)	1.174(3)
N(1)-C(28)	1.513(4)
N(1)-C(26)	1.517(4)
N(1)-C(30)	1.524(4)
N(1)-C(24)	1.526(4)
C(6)-C(11)	1.398(4)
C(6)-C(7)	1.399(4)
C(7)-C(8)	1.391(4)
C(8)-C(9)	1.381(4)
C(9)-C(10)	1.384(5)
C(10)-C(11)	1.398(4)
C(12)-C(17)	1.392(4)
C(12)-C(13)	1.393(4)
C(13)-C(14)	1.389(4)
C(14)-C(15)	1.379(5)
C(15)-C(16)	1.387(5)
C(16)-C(17)	1.386(4)
C(18)-C(23)	1.396(4)
C(18)-C(19)	1.398(4)
C(19)-C(20)	1.391(4)

C(20)-C(21)	1.391(4)
C(21)-C(22)	1.380(5)
C(22)-C(23)	1.384(4)
C(24)-C(25)	1.509(5)
C(26)-C(27)	1.517(5)
C(28)-C(29)	1.500(5)
C(30)-C(31)	1.503(5)
C(5)-Ta-C(3)	90.75(11)
C(5)-Ta-C(1)	82.59(11)
C(3)-Ta-C(1)	87.95(11)
C(5)-Ta-C(2)	88.71(11)
C(3)-Ta-C(2)	88.58(11)
C(1)-Ta-C(2)	170.58(11)
C(5)-Ta-C(4)	88.29(11)
C(3)-Ta-C(4)	178.88(11)
C(1)-Ta-C(4)	92.50(12)
C(2)-Ta-C(4)	90.82(11)
C(5)-Ta-P(1)	174.80(8)
C(3)-Ta-P(1)	87.12(8)
C(1)-Ta-P(1)	92.58(8)
C(2)-Ta-P(1)	95.98(8)
C(4)-Ta-P(1)	93.88(8)
C(12)-P(1)-C(18)	102.99(12)
C(12)-P(1)-C(6)	101.43(12)
C(18)-P(1)-C(6)	101.50(12)
C(12)-P(1)-Ta	117.90(9)
C(18)-P(1)-Ta	115.53(9)
C(6)-P(1)-Ta	115.14(8)
C(28)-N(1)-C(26)	111.6(3)
C(28)-N(1)-C(30)	106.8(2)
C(26)-N(1)-C(30)	110.4(3)
C(28)-N(1)-C(24)	111.0(2)
C(26)-N(1)-C(24)	106.3(2)
C(30)-N(1)-C(24)	110.9(3)

O(1)-C(1)-Ta	172.8(3)
O(2)-C(2)-Ta	174.4(2)
O(3)-C(3)-Ta	177.3(2)
O(4)-C(4)-Ta	175.5(3)
O(5)-C(5)-Ta	177.2(3)
C(11)-C(6)-C(7)	118.7(3)
C(11)-C(6)-P(1)	118.2(2)
C(7)-C(6)-P(1)	123.1(2)
C(8)-C(7)-C(6)	120.3(3)
C(9)-C(8)-C(7)	120.6(3)
C(8)-C(9)-C(10)	119.7(3)
C(9)-C(10)-C(11)	120.3(3)
C(6)-C(11)-C(10)	120.3(3)
C(17)-C(12)-C(13)	118.0(3)
C(17)-C(12)-P(1)	118.2(2)
C(13)-C(12)-P(1)	123.8(2)
C(14)-C(13)-C(12)	121.0(3)
C(15)-C(14)-C(13)	120.0(3)
C(14)-C(15)-C(16)	119.9(3)
C(17)-C(16)-C(15)	119.8(3)
C(16)-C(17)-C(12)	121.2(3)
C(23)-C(18)-C(19)	118.7(3)
C(23)-C(18)-P(1)	122.7(2)
C(19)-C(18)-P(1)	118.6(2)
C(20)-C(19)-C(18)	120.3(3)
C(21)-C(20)-C(19)	120.2(3)
C(22)-C(21)-C(20)	119.6(3)
C(21)-C(22)-C(23)	120.6(3)
C(22)-C(23)-C(18)	120.5(3)
C(25)-C(24)-N(1)	115.4(3)
C(27)-C(26)-N(1)	114.6(3)
C(29)-C(28)-N(1)	115.1(3)
C(31)-C(30)-N(1)	116.0(3)

Symmetry transformations used to generate equivalent atoms:

Table 4. Anisotropic displacement parameters ($\text{\AA}^2 \times 10^3$) for C31H35NO5PTa. The anisotropic displacement factor exponent takes the form: $-2\pi^2 [h^2 a^{*2} U^{11} + \dots + 2 h k a^* b^* U^{12}]$

	U ¹¹	U ²²	U ³³	U ²³	U ¹³	U ¹²
Ta	20(1)	15(1)	18(1)	0(1)	1(1)	-1(1)
P(1)	16(1)	15(1)	18(1)	0(1)	1(1)	0(1)
O(1)	39(1)	34(1)	44(1)	1(1)	-4(1)	11(1)
O(2)	30(1)	32(1)	41(1)	3(1)	-7(1)	3(1)
O(3)	35(1)	35(1)	32(1)	8(1)	11(1)	0(1)
O(4)	47(2)	38(1)	39(1)	3(1)	22(1)	-5(1)
O(5)	36(1)	24(1)	32(1)	-8(1)	1(1)	-7(1)
N(1)	33(1)	21(1)	24(1)	-1(1)	2(1)	0(1)
C(1)	29(2)	21(1)	22(1)	-1(1)	2(1)	-5(1)
C(2)	26(1)	19(1)	24(1)	-1(1)	4(1)	0(1)
C(3)	23(1)	19(1)	25(1)	2(1)	0(1)	1(1)
C(4)	31(2)	19(1)	24(1)	-3(1)	3(1)	2(1)
C(5)	23(1)	21(1)	23(1)	1(1)	1(1)	1(1)
C(6)	18(1)	17(1)	20(1)	2(1)	-1(1)	0(1)
C(7)	22(1)	21(1)	25(1)	-5(1)	-1(1)	0(1)
C(8)	25(1)	29(1)	29(2)	-4(1)	-7(1)	-3(1)
C(9)	19(1)	29(2)	39(2)	-1(1)	-4(1)	0(1)
C(10)	19(1)	38(2)	34(2)	-3(1)	3(1)	3(1)
C(11)	20(1)	27(1)	24(1)	-2(1)	1(1)	2(1)
C(12)	15(1)	23(1)	19(1)	0(1)	1(1)	-2(1)
C(13)	28(2)	24(1)	27(1)	-2(1)	6(1)	3(1)
C(14)	39(2)	32(2)	30(2)	-9(1)	10(1)	4(1)
C(15)	30(2)	51(2)	21(1)	-8(1)	8(1)	-2(1)
C(16)	23(1)	40(2)	22(1)	4(1)	1(1)	-8(1)
C(17)	20(1)	23(1)	24(1)	0(1)	0(1)	-3(1)
C(18)	23(1)	15(1)	17(1)	0(1)	1(1)	1(1)
C(19)	27(1)	20(1)	32(2)	1(1)	-6(1)	1(1)
C(20)	36(2)	22(1)	32(2)	6(1)	-9(1)	4(1)
C(21)	36(2)	22(1)	26(1)	5(1)	4(1)	1(1)
C(22)	31(2)	21(1)	33(2)	6(1)	7(1)	-3(1)

C(23)	24(1)	22(1)	26(1)	2(1)	2(1)	-1(1)
C(24)	43(2)	32(2)	25(2)	-8(1)	2(1)	-9(1)
C(25)	34(2)	61(2)	27(2)	1(2)	2(1)	3(2)
C(26)	60(2)	25(2)	31(2)	2(1)	-6(2)	8(2)
C(27)	82(3)	33(2)	33(2)	3(1)	-14(2)	12(2)
C(28)	34(2)	24(1)	31(2)	-3(1)	2(1)	-4(1)
C(29)	35(2)	53(2)	44(2)	-12(2)	7(2)	-4(2)
C(30)	34(2)	36(2)	30(2)	0(1)	6(1)	2(1)
C(31)	43(2)	54(2)	36(2)	6(2)	9(2)	-14(2)

Table 5. Hydrogen coordinates ($\times 10^4$) and isotropic displacement parameters ($\text{\AA}^2 \times 10^{-3}$) for C₃₁H₃₅NO₅PTa.

	x	y	z	U(eq)
H(7)	5235	9394	5793	28
H(8)	7704	9350	6490	34
H(9)	9349	9103	4983	35
H(10)	8528	8898	2756	36
H(11)	6046	8926	2051	28
H(13)	2163	9897	4454	31
H(14)	1138	10027	6550	41
H(15)	890	9524	8157	41
H(16)	1752	8892	7703	34
H(17)	2780	8762	5612	27
H(19)	1291	9607	1529	32
H(20)	1166	10199	289	36
H(21)	3226	10600	228	33
H(22)	5379	10417	1460	34
H(23)	5512	9834	2727	28
H(24A)	8174	8412	9711	40
H(24B)	6533	8314	10017	40
H(25A)	7242	7720	11047	61
H(25B)	8207	8065	11764	61
H(25C)	8878	7785	10638	61
H(26A)	5639	8422	7739	47
H(26B)	7235	8562	7417	47
H(27A)	7192	8148	5472	75
H(27B)	5799	8431	5345	75
H(27C)	5634	7982	5817	75
H(28A)	6085	7549	7398	36
H(28B)	6701	7455	8950	36
H(29A)	4860	7853	9796	66
H(29B)	4197	7494	8887	66

H(29C)	4223	7926	8232	66
H(30A)	9090	7681	8489	40
H(30B)	8418	7718	6925	40
H(31A)	9335	8357	6791	66
H(31B)	10623	8056	7218	66
H(31C)	9974	8330	8373	66

Table 1. Crystal data and structure refinement for C₁₈H₂₈N₃O₄Ta.

Empirical formula	C ₁₈ H ₂₈ N ₃ O ₄ Ta
Formula weight	531.38
Temperature	153(2) K
Wavelength	0.71073 Å
Crystal system	Orthorhombic
Space group	Pnma
Unit cell dimensions	a = 17.4599(8) Å b = 14.2794(7) Å c = 8.9634(4) Å
Volume	2234.73(2) Å ³
Z	4
Density (calculated)	1.579 Mg/m ³
Absorption coefficient	4.943 mm ⁻¹
F(000)	1048
Crystal size	0.31 x 0.12 x 0.11 mm ³
Theta range for data collection	2.33 to 33.34°
Index ranges	-25 ≤ h ≤ 26, -20 ≤ k ≤ 20, -9 ≤ l ≤ 13
Reflections collected	23364
Independent reflections	3745 [R(int) = 0.1229]
Completeness to theta = 33.34°	93.5 %
Absorption correction	Empirical
Max. and min. transmission	0.6124 and 0.3095
Refinement method	Full-matrix least-squares on F ²
Data / restraints / parameters	3745 / 0 / 166
Goodness-of-fit on F ²	1.327
Final R indices [I > 2σ(I)]	R1 = 0.0732, wR2 = 0.2025
R indices (all data)	R1 = 0.1390, wR2 = 0.2242
Largest diff. peak and hole	2.168 and -3.033 e.Å ⁻³

Table 2. Atomic coordinates ($\times 10^4$) and equivalent isotropic displacement parameters ($\text{\AA}^2 \times 10^3$) for C₁₈H₂₈N₃O₄Ta. U(eq) is defined as one third of the trace of the orthogonalized U^{ij} tensor.

	x	y	z	U(eq)
Ta	1543(1)	2500	8519(1)	33(1)
O(1)	2988(6)	2500	6335(12)	48(3)
O(2)	1202(9)	784(9)	6338(11)	103(5)
O(3)	-279(9)	2144(14)	8398(17)	64(6)
N(1)	1775(5)	1604(7)	10500(11)	42(2)
N(2)	4465(6)	2500	1634(13)	35(3)
C(1)	1751(8)	662(11)	10454(17)	66(4)
C(2)	1835(13)	81(17)	11660(20)	109(8)
C(3)	1972(10)	496(17)	13048(19)	107(9)
C(4)	2001(8)	1435(14)	13133(14)	75(5)
C(5)	1909(6)	2002(11)	11854(12)	57(4)
C(6)	2542(7)	2500	7224(16)	28(3)
C(7)	1320(8)	1424(9)	7093(13)	54(3)
C(8)	374(12)	2500	8569(19)	99(11)
C(9)	5054(11)	1814(11)	2310(30)	36(5)
C(9A)	4056(14)	1881(19)	2870(30)	56(7)
C(10)	4647(11)	1132(12)	3443(19)	90(6)
C(11)	3801(13)	2000(20)	830(30)	55(6)
C(11A)	4922(10)	1933(12)	560(30)	38(5)
C(12)	4266(13)	1251(12)	-337(19)	108(8)

Table 3. Bond lengths [\AA] and angles [$^\circ$] for $\text{C}_{18}\text{H}_{28}\text{N}_3\text{O}_4\text{Ta}$.

Ta-C(7)#1	2.036(11)
Ta-C(7)	2.036(11)
Ta-C(8)	2.04(2)
Ta-C(6)	2.096(13)
Ta-N(1)#1	2.226(9)
Ta-N(1)	2.226(9)
O(1)-C(6)	1.114(16)
O(2)-C(7)	1.156(15)
O(3)-O(3)#1	1.02(4)
O(3)-C(8)	1.26(2)
N(1)-C(1)	1.347(17)
N(1)-C(5)	1.360(15)
N(2)-C(11A)	1.49(2)
N(2)-C(11A)#1	1.49(2)
N(2)-C(11)	1.54(3)
N(2)-C(11)#1	1.54(3)
N(2)-C(9)#1	1.543(18)
N(2)-C(9)	1.543(18)
N(2)-C(9A)#1	1.59(2)
N(2)-C(9A)	1.59(2)
C(1)-C(2)	1.37(2)
C(2)-C(3)	1.40(3)
C(3)-C(4)	1.34(3)
C(4)-C(5)	1.413(17)
C(5)-C(5)#1	1.42(3)
C(8)-O(3)#1	1.26(2)
C(9)-C(10)	1.58(3)
C(9)-C(11A)	1.59(3)
C(9)-C(9A)	1.82(3)
C(9)-C(9)#1	1.96(3)
C(9A)-C(10)	1.57(3)
C(9A)-C(9A)#1	1.77(6)
C(9A)-C(11)	1.89(3)

C(11)-C(11)#1	1.41(6)
C(11)-C(12)	1.70(3)
C(11)-C(11A)	1.97(3)
C(11A)-C(11A)#1	1.62(3)
C(11A)-C(12)	1.71(3)
C(7)#1-Ta-C(7)	98.0(8)
C(7)#1-Ta-C(8)	79.8(5)
C(7)-Ta-C(8)	79.8(5)
C(7)#1-Ta-C(6)	79.1(4)
C(7)-Ta-C(6)	79.1(4)
C(8)-Ta-C(6)	147.6(6)
C(7)#1-Ta-N(1)#1	95.9(5)
C(7)-Ta-N(1)#1	165.8(4)
C(8)-Ta-N(1)#1	99.5(5)
C(6)-Ta-N(1)#1	106.9(4)
C(7)#1-Ta-N(1)	165.8(4)
C(7)-Ta-N(1)	95.9(5)
C(8)-Ta-N(1)	99.5(5)
C(6)-Ta-N(1)	106.9(4)
N(1)#1-Ta-N(1)	70.1(5)
O(3)#1-O(3)-C(8)	66.2(10)
C(1)-N(1)-C(5)	116.8(12)
C(1)-N(1)-Ta	122.9(10)
C(5)-N(1)-Ta	120.2(8)
C(11A)-N(2)-C(11A)#1	66.0(16)
C(11A)-N(2)-C(11)	81.4(13)
C(11A)#1-N(2)-C(11)	110.6(15)
C(11A)-N(2)-C(11)#1	110.6(15)
C(11A)#1-N(2)-C(11)#1	81.4(13)
C(11)-N(2)-C(11)#1	55(2)
C(11A)-N(2)-C(9)#1	103.9(13)
C(11A)#1-N(2)-C(9)#1	63.1(13)
C(11)-N(2)-C(9)#1	167.8(14)
C(11)#1-N(2)-C(9)#1	113.2(13)

C(11A)-N(2)-C(9)	63.1(13)
C(11A)#1-N(2)-C(9)	103.9(13)
C(11)-N(2)-C(9)	113.2(13)
C(11)#1-N(2)-C(9)	167.8(14)
C(9)#1-N(2)-C(9)	78.9(15)
C(11A)-N(2)-C(9A)#1	174.2(15)
C(11A)#1-N(2)-C(9A)#1	112.8(13)
C(11)-N(2)-C(9A)#1	104.2(15)
C(11)#1-N(2)-C(9A)#1	74.5(13)
C(9)#1-N(2)-C(9A)#1	70.9(13)
C(9)-N(2)-C(9A)#1	112.4(16)
C(11A)-N(2)-C(9A)	112.8(13)
C(11A)#1-N(2)-C(9A)	174.2(15)
C(11)-N(2)-C(9A)	74.5(13)
C(11)#1-N(2)-C(9A)	104.2(15)
C(9)#1-N(2)-C(9A)	112.4(16)
C(9)-N(2)-C(9A)	70.9(13)
C(9A)#1-N(2)-C(9A)	68(2)
N(1)-C(1)-C(2)	125.2(18)
C(1)-C(2)-C(3)	118(2)
C(4)-C(3)-C(2)	118.7(15)
C(3)-C(4)-C(5)	121.4(16)
N(1)-C(5)-C(4)	120.3(15)
N(1)-C(5)-C(5)#1	114.7(7)
C(4)-C(5)-C(5)#1	125.0(10)
O(1)-C(6)-Ta	168.0(12)
O(2)-C(7)-Ta	176.7(13)
O(3)-C(8)-O(3)#1	47.7(19)
O(3)-C(8)-Ta	154.6(11)
O(3)#1-C(8)-Ta	154.6(11)
N(2)-C(9)-C(10)	110.1(14)
N(2)-C(9)-C(11A)	56.7(10)
C(10)-C(9)-C(11A)	129.5(15)
N(2)-C(9)-C(9A)	55.7(11)
C(10)-C(9)-C(9A)	54.6(12)

C(11A)-C(9)-C(9A)	97.4(13)
N(2)-C(9)-C(9)#1	50.6(7)
C(10)-C(9)-C(9)#1	128.1(11)
C(11A)-C(9)-C(9)#1	83.8(9)
C(9A)-C(9)-C(9)#1	87.0(10)
C(10)-C(9A)-N(2)	108.2(16)
C(10)-C(9A)-C(9A)#1	132.9(11)
N(2)-C(9A)-C(9A)#1	56.1(11)
C(10)-C(9A)-C(9)	55.0(12)
N(2)-C(9A)-C(9)	53.4(10)
C(9A)#1-C(9A)-C(9)	93.0(10)
C(10)-C(9A)-C(11)	122(2)
N(2)-C(9A)-C(11)	51.6(11)
C(9A)#1-C(9A)-C(11)	84.6(11)
C(9)-C(9A)-C(11)	87.8(15)
C(9)-C(10)-C(9A)	70.4(12)
C(11)#1-C(11)-N(2)	62.6(11)
C(11)#1-C(11)-C(12)	129.2(10)
N(2)-C(11)-C(12)	102.6(15)
C(11)#1-C(11)-C(9A)	95.4(11)
N(2)-C(11)-C(9A)	53.9(11)
C(12)-C(11)-C(9A)	114.9(18)
C(11)#1-C(11)-C(11A)	93.0(10)
N(2)-C(11)-C(11A)	48.2(10)
C(12)-C(11)-C(11A)	54.7(11)
C(9A)-C(11)-C(11A)	82.9(14)
N(2)-C(11A)-C(9)	60.1(12)
N(2)-C(11A)-C(11A)#1	57.0(8)
C(9)-C(11A)-C(11A)#1	96.1(9)
N(2)-C(11A)-C(12)	104.9(13)
C(9)-C(11A)-C(12)	120.1(14)
C(11A)#1-C(11A)-C(12)	124.8(10)
N(2)-C(11A)-C(11)	50.4(10)
C(9)-C(11A)-C(11)	91.9(14)
C(11A)#1-C(11A)-C(11)	87.0(10)

C(12)-C(11A)-C(11)	54.6(12)
C(11)-C(12)-C(11A)	70.7(12)

Symmetry transformations used to generate equivalent atoms: #1 x,-y+1/2,z

Table 4. Anisotropic displacement parameters ($\text{\AA}^2 \times 10^3$) for C18H28N3O4Ta. The anisotropic displacement factor exponent takes the form: $-2\pi^2 [h^2 a^{*2} U^{11} + \dots + 2 h k a^* b^* U^{12}]$

	U ¹¹	U ²²	U ³³	U ²³	U ¹³	U ¹²
Ta	32(1)	46(1)	20(1)	0	0(1)	0
O(1)	37(6)	72(8)	36(6)	0	3(4)	0
O(2)	166(12)	87(8)	56(7)	-26(6)	31(7)	-86(9)
O(3)	32(8)	114(19)	46(9)	3(9)	-2(6)	5(8)
N(1)	45(5)	48(5)	33(5)	12(4)	10(4)	14(4)
N(2)	31(6)	39(6)	35(7)	0	1(5)	0
C(1)	84(9)	69(9)	46(7)	16(7)	26(7)	36(7)
C(2)	126(15)	127(17)	73(12)	51(12)	49(11)	88(14)
C(3)	90(12)	170(20)	64(10)	69(12)	25(9)	86(13)
C(4)	50(7)	148(17)	27(6)	35(8)	3(5)	41(9)
C(5)	29(5)	112(11)	28(5)	13(6)	2(4)	1(6)
C(6)	19(5)	21(6)	44(8)	0	-1(5)	0
C(7)	78(8)	50(7)	33(6)	-9(5)	5(6)	-40(6)
C(8)	34(9)	240(40)	26(9)	0	-4(7)	0
C(9)	37(9)	11(7)	58(14)	10(8)	-17(9)	5(6)
C(9A)	55(14)	61(15)	52(15)	26(13)	2(12)	-18(11)
C(10)	102(12)	82(11)	87(12)	61(10)	-43(10)	-47(10)
C(11)	38(11)	84(17)	44(14)	2(13)	5(10)	-18(11)
C(11A)	30(9)	20(9)	65(15)	5(9)	4(9)	7(7)
C(12)	190(20)	80(11)	55(10)	-21(9)	34(12)	-83(12)

Table 1. Crystal data and structure refinement for C₁₃H₁₀BN₆O₄Ta.

Empirical formula	C ₁₃ H ₁₀ B N ₆ O ₄ Ta	
Formula weight	506.03	
Temperature	153(2) K	
Wavelength	0.71074 Å	
Crystal system	Monoclinic	
Space group	P2 ₁	
Unit cell dimensions	a = 7.598(1) Å	
	b = 13.090(1) Å	β = 109.151(3)°.
	c = 8.755(1) Å	
Volume	822.56(16) Å ³	
Z	2	
Density (calculated)	2.043 Mg/m ³	
Absorption coefficient	6.713 mm ⁻¹	
F(000)	480	
Crystal size	0.31 x 0.23 x 0.11 mm ³	
Theta range for data collection	2.91 to 31.44°.	
Index ranges	-10 ≤ h ≤ 10, -19 ≤ k ≤ 19, -12 ≤ l ≤ 12	
Reflections collected	4782	
Independent reflections	4782 [R(int) = 0.0792]	
Completeness to theta = 31.44°	91.3 %	
Refinement method	Full-matrix least-squares on F ²	
Data / restraints / parameters	4782 / 1 / 175	
Goodness-of-fit on F ²	1.125	
Final R indices [I > 2σ(I)]	R ₁ = 0.0556, wR ₂ = 0.1088	
R indices (all data)	R ₁ = 0.0926, wR ₂ = 0.1248	
Largest diff. peak and hole	3.160 and -1.730 e.Å ⁻³	

Table 2. Atomic coordinates ($\times 10^4$) and equivalent isotropic displacement parameters ($\text{\AA}^2 \times 10^3$) for C₁₃H₁₀BN₆O₄Ta. U(eq) is defined as one third of the trace of the orthogonalized U^{ij} tensor.

	x	y	z	U(eq)
Ta	4249(1)	2084(4)	1901(1)	19(1)
O(1)	5950(50)	662(17)	-240(30)	65(8)
O(2)	1170(40)	580(20)	-470(30)	67(8)
O(3)	1050(40)	3500(30)	-470(30)	95(12)
O(4)	6140(40)	3456(17)	-210(30)	50(7)
N(1)	5940(30)	3195(11)	3870(30)	17(5)
N(2)	6170(30)	3017(15)	5450(20)	18(5)
N(3)	5920(30)	971(15)	3810(20)	17(5)
N(4)	6290(30)	1114(14)	5450(30)	14(4)
N(5)	2563(11)	2065(18)	3593(10)	20(2)
N(6)	3327(10)	2060(30)	5225(8)	17(2)
C(1)	7290(30)	3830(15)	6200(20)	23(5)
C(2)	7710(30)	4495(16)	5370(30)	18(5)
C(3)	6800(30)	4075(16)	3790(30)	24(6)
C(4)	7270(20)	401(12)	6410(20)	10(3)
C(5)	7630(30)	-299(17)	5180(30)	21(5)
C(6)	6770(30)	82(12)	3720(30)	22(6)
C(7)	2009(13)	2070(40)	5934(12)	24(2)
C(8)	272(13)	2100(40)	4711(11)	24(2)
C(9)	704(16)	2100(20)	3305(14)	28(3)
C(10)	5160(20)	1174(11)	459(18)	18(3)
C(11)	2130(30)	1215(16)	420(30)	34(5)
C(12)	2380(30)	3129(16)	360(30)	33(5)
C(13)	5640(20)	2922(12)	610(20)	22(4)
B(1)	5461(15)	2070(20)	6026(14)	18(2)

Table 3. Bond lengths [\AA] and angles [$^\circ$] for C₁₃H₁₀BN₆O₄Ta.

Ta-C(10)	2.016(15)
Ta-C(11)	2.05(2)
Ta-C(13)	2.092(16)
Ta-C(12)	2.11(2)
Ta-N(5)	2.254(9)
Ta-N(3)	2.26(2)
Ta-N(1)	2.30(2)
O(1)-C(10)	1.19(3)
O(2)-C(11)	1.20(3)
O(3)-C(12)	1.14(3)
O(4)-C(13)	1.16(3)
N(1)-C(3)	1.34(3)
N(1)-N(2)	1.35(3)
N(2)-C(1)	1.39(3)
N(2)-B(1)	1.50(3)
N(3)-C(6)	1.35(3)
N(3)-N(4)	1.39(3)
N(4)-C(4)	1.31(3)
N(4)-B(1)	1.56(3)
N(5)-C(9)	1.352(13)
N(5)-N(6)	1.354(10)
N(6)-C(7)	1.340(11)
N(6)-B(1)	1.541(13)
C(1)-C(2)	1.24(3)
C(1)-H(1)	0.9300
C(2)-C(3)	1.44(3)
C(2)-H(2)	0.9300
C(3)-H(3)	0.9300
C(4)-C(5)	1.50(3)
C(4)-H(4)	0.9300
C(5)-C(6)	1.33(3)
C(5)-H(5)	0.9300
C(6)-H(6)	0.9300

C(7)-C(8)	1.401(13)
C(7)-H(7)	0.9300
C(8)-C(9)	1.374(14)
C(8)-H(8)	0.9300
C(9)-H(9)	0.9300
B(1)-H(1B)	1.23(11)
C(10)-Ta-C(11)	68.5(7)
C(10)-Ta-C(13)	68.5(5)
C(11)-Ta-C(13)	112.2(8)
C(10)-Ta-C(12)	106.3(7)
C(11)-Ta-C(12)	74.3(6)
C(13)-Ta-C(12)	70.6(7)
C(10)-Ta-N(5)	142.3(7)
C(11)-Ta-N(5)	85.1(7)
C(13)-Ta-N(5)	149.0(7)
C(12)-Ta-N(5)	91.1(7)
C(10)-Ta-N(3)	81.8(7)
C(11)-Ta-N(3)	104.2(8)
C(13)-Ta-N(3)	118.4(7)
C(12)-Ta-N(3)	170.1(8)
N(5)-Ta-N(3)	79.1(7)
C(10)-Ta-N(1)	128.5(7)
C(11)-Ta-N(1)	162.9(8)
C(13)-Ta-N(1)	79.5(7)
C(12)-Ta-N(1)	99.3(7)
N(5)-Ta-N(1)	79.1(7)
N(3)-Ta-N(1)	79.3(3)
C(3)-N(1)-N(2)	108(2)
C(3)-N(1)-Ta	131.8(17)
N(2)-N(1)-Ta	120.7(14)
N(1)-N(2)-C(1)	102.1(19)
N(1)-N(2)-B(1)	123.0(15)
C(1)-N(2)-B(1)	134.6(18)
C(6)-N(3)-N(4)	103.8(18)

C(6)-N(3)-Ta	132.7(14)
N(4)-N(3)-Ta	123.6(15)
C(4)-N(4)-N(3)	116.4(19)
C(4)-N(4)-B(1)	125.1(18)
N(3)-N(4)-B(1)	118.4(18)
C(9)-N(5)-N(6)	104.9(9)
C(9)-N(5)-Ta	131.4(7)
N(6)-N(5)-Ta	123.6(6)
C(7)-N(6)-N(5)	111.2(8)
C(7)-N(6)-B(1)	128.6(7)
N(5)-N(6)-B(1)	120.2(7)
C(2)-C(1)-N(2)	119(2)
C(2)-C(1)-H(1)	120.4
N(2)-C(1)-H(1)	120.2
C(1)-C(2)-C(3)	99(2)
C(1)-C(2)-H(2)	130.4
C(3)-C(2)-H(2)	130.3
N(1)-C(3)-C(2)	112(2)
N(1)-C(3)-H(3)	124.2
C(2)-C(3)-H(3)	124.2
N(4)-C(4)-C(5)	100.2(16)
N(4)-C(4)-H(4)	129.9
C(5)-C(4)-H(4)	129.8
C(6)-C(5)-C(4)	108.2(18)
C(6)-C(5)-H(5)	125.9
C(4)-C(5)-H(5)	125.9
C(5)-C(6)-N(3)	111.3(19)
C(5)-C(6)-H(6)	124.4
N(3)-C(6)-H(6)	124.3
N(6)-C(7)-C(8)	107.8(8)
N(6)-C(7)-H(7)	126.1
C(8)-C(7)-H(7)	126.0
C(9)-C(8)-C(7)	104.0(9)
C(9)-C(8)-H(8)	128.0
C(7)-C(8)-H(8)	127.9

N(5)-C(9)-C(8)	112.0(10)
N(5)-C(9)-H(9)	124.0
C(8)-C(9)-H(9)	124.0
O(1)-C(10)-Ta	170(2)
O(2)-C(11)-Ta	167(2)
O(3)-C(12)-Ta	162(3)
O(4)-C(13)-Ta	169(2)
N(2)-B(1)-N(6)	107(2)
N(2)-B(1)-N(4)	109.0(7)
N(6)-B(1)-N(4)	108.8(16)
N(2)-B(1)-H(1B)	112(10)
N(6)-B(1)-H(1B)	101(5)
N(4)-B(1)-H(1B)	117(10)

Table 4. Anisotropic displacement parameters ($\text{\AA}^2 \times 10^3$) for C13H10BN6O4Ta. The anisotropic displacement factor exponent takes the form: $-2\pi^2 [h^2 a^{*2} U^{11} + \dots + 2 h k a^* b^* U^{12}]$

	U ¹¹	U ²²	U ³³	U ²³	U ¹³	U ¹²
Ta	22(1)	18(1)	16(1)	-1(1)	4(1)	0(1)
O(1)	150(20)	23(9)	55(14)	-7(8)	70(15)	-13(10)
O(2)	59(15)	55(12)	53(15)	-7(10)	-27(11)	-11(10)
O(3)	100(20)	150(30)	38(13)	37(14)	25(13)	101(18)
O(4)	87(15)	43(12)	37(12)	-21(9)	43(11)	-44(10)
N(1)	17(10)	-4(5)	42(12)	1(6)	15(9)	2(6)
N(2)	24(11)	16(8)	8(8)	-16(6)	-2(7)	-6(7)
N(3)	13(10)	35(10)	0(6)	-7(6)	-3(6)	-2(8)
N(4)	0(7)	19(8)	24(10)	-9(7)	7(7)	-3(6)
N(5)	15(4)	13(4)	26(4)	14(9)	-4(3)	-13(8)
C(3)	2(9)	34(11)	35(12)	17(9)	3(8)	21(7)
C(6)	46(13)	4(6)	26(10)	14(6)	25(9)	25(7)
C(9)	19(5)	16(4)	45(6)	10(13)	5(5)	22(9)
B(1)	21(6)	17(5)	19(5)	-26(9)	11(4)	-16(10)

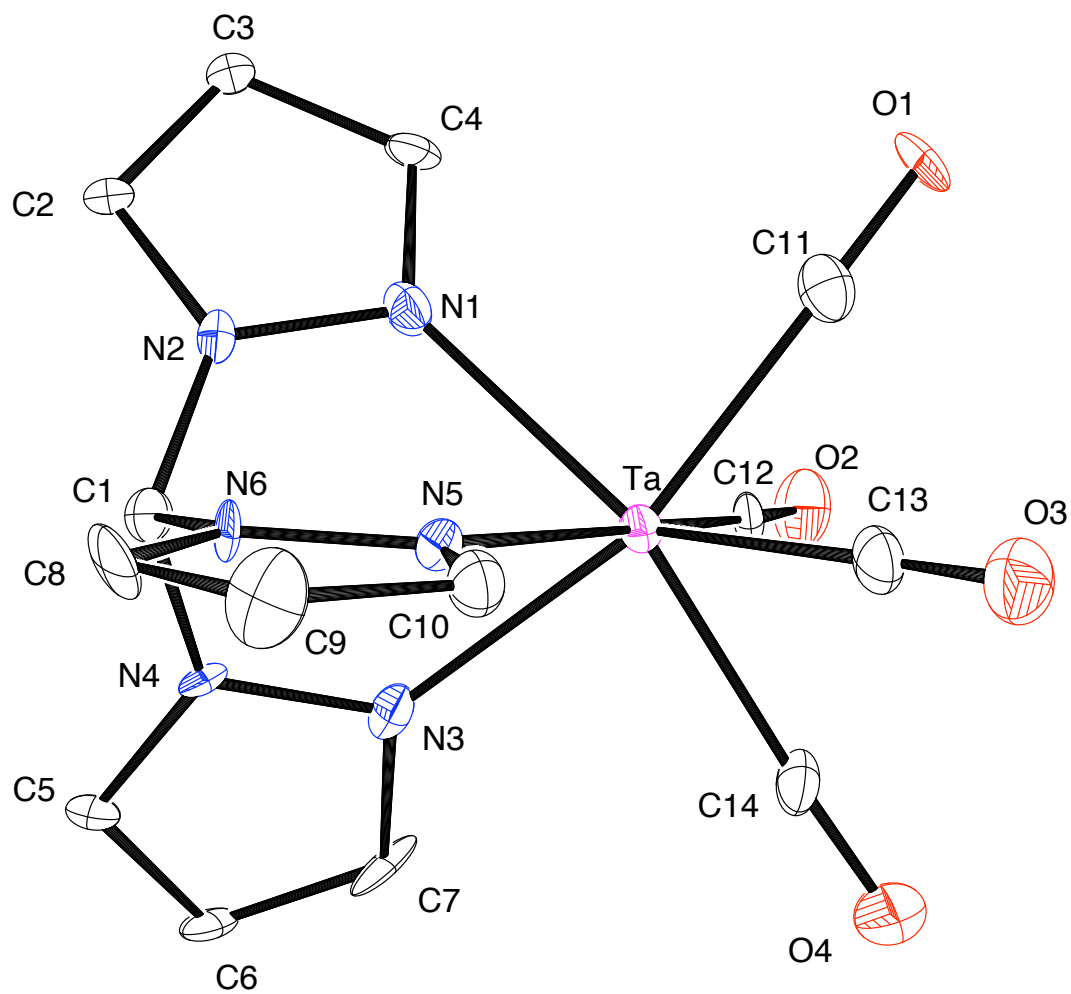
Crystallographic Data for [TaTpm(CO)₄]I (6)(I⁻ anion and CHCl₃ solvent molecule omitted from ORTEP drawing below)

Table 1. Crystal data and structure refinement for C₁₅H₁₁Cl₃IN₆O₄Ta.

Empirical formula	C ₁₅ H ₁₁ Cl ₃ I N ₆ O ₄ Ta	
Formula weight	753.50	
Temperature	153(2) K	
Wavelength	0.71073 Å	
Crystal system	Monoclinic	
Space group	C2/c	
Unit cell dimensions	a = 11.3370(8) Å	
	b = 14.724(1) Å	β = 100.991(2)°.
	c = 27.571(2) Å	
Volume	4517.7(6) Å ³	
Z	8	
Density (calculated)	2.216 Mg/m ³	
Absorption coefficient	6.621 mm ⁻¹	
F(000)	2816	
Crystal size	0.38 x 0.32 x 0.26 mm ³	
Theta range for data collection	1.50 to 32.40°.	
Index ranges	-15 ≤ h ≤ 14, -19 ≤ k ≤ 21, -39 ≤ l ≤ 40	
Reflections collected	19217	
Independent reflections	6737 [R(int) = 0.0409]	
Completeness to theta = 32.40°	95.3 %	
Absorption correction	Empirical	
Max. and min. transmission	0.2779 and 0.1875	
Refinement method	Full-matrix least-squares on F ²	
Data / restraints / parameters	6737 / 0 / 271	
Goodness-of-fit on F ²	2.237	
Final R indices [I > 2σ(I)]	R1 = 0.0991, wR2 = 0.2948	
R indices (all data)	R1 = 0.1082, wR2 = 0.2968	
Largest diff. peak and hole	3.227 and -3.053 e.Å ⁻³	

Table 2. Atomic coordinates ($\times 10^4$) and equivalent isotropic displacement parameters ($\text{\AA}^2 \times 10^3$) for C₁₅H₁₁Cl₃N₆O₄Ta. U(eq) is defined as one third of the trace of the orthogonalized U^{ij} tensor.

	x	y	z	U(eq)
Ta	650(1)	2671(1)	1305(1)	20(1)
I(1)	5235(1)	3206(1)	434(1)	22(1)
Cl(1)	6328(8)	2406(4)	1928(3)	79(3)
Cl(2)	6010(8)	614(5)	1512(3)	73(2)
Cl(3)	4065(6)	1498(8)	1845(2)	85(3)
O(1)	-1573(11)	3905(9)	1459(5)	37(3)
O(2)	163(15)	4221(9)	462(5)	46(3)
O(3)	1294(14)	3587(11)	2381(5)	47(3)
O(4)	3028(13)	3911(10)	1452(5)	45(3)
N(1)	-813(12)	1722(8)	923(4)	24(2)
N(2)	-617(11)	819(8)	866(4)	22(2)
N(3)	1665(12)	1750(8)	872(4)	24(2)
N(4)	1473(10)	833(8)	830(4)	19(2)
N(5)	951(11)	1373(8)	1779(4)	23(2)
N(6)	832(12)	527(7)	1584(4)	22(2)
C(1)	556(13)	430(9)	1058(4)	20(2)
C(2)	-1587(12)	397(10)	605(5)	22(2)
C(3)	-2468(14)	1031(11)	500(6)	29(3)
C(4)	-1926(14)	1858(11)	698(6)	30(3)
C(5)	2242(13)	436(11)	587(5)	26(3)
C(6)	2941(12)	1107(11)	447(5)	23(3)
C(7)	2596(15)	1885(12)	641(5)	32(4)
C(8)	1140(16)	-126(10)	1925(6)	33(3)
C(9)	1460(20)	284(13)	2372(6)	42(4)
C(10)	1332(14)	1221(10)	2270(5)	26(3)
C(11)	-795(16)	3468(11)	1424(5)	31(3)
C(12)	357(15)	3668(10)	763(6)	28(3)
C(13)	1057(16)	3268(10)	2002(6)	29(3)
C(14)	2209(16)	3449(10)	1400(5)	28(3)
C(15)	5301(18)	1663(13)	1588(7)	39(4)

Table 3. Bond lengths [\AA] and angles [$^\circ$] for $\text{C}_{15}\text{H}_{11}\text{Cl}_3\text{IN}_6\text{O}_4\text{Ta}$.

Ta-C(12)	2.076(16)
Ta-C(14)	2.081(16)
Ta-C(13)	2.084(15)
Ta-C(11)	2.091(17)
Ta-N(3)	2.262(13)
Ta-N(1)	2.268(13)
Ta-N(5)	2.302(12)
Cl(1)-C(15)	1.74(2)
Cl(2)-C(15)	1.77(2)
Cl(3)-C(15)	1.70(2)
O(1)-C(11)	1.11(2)
O(2)-C(12)	1.15(2)
O(3)-C(13)	1.13(2)
O(4)-C(14)	1.14(2)
N(1)-C(4)	1.31(2)
N(1)-N(2)	1.363(16)
N(2)-C(2)	1.346(17)
N(2)-C(1)	1.451(18)
N(3)-C(7)	1.346(18)
N(3)-N(4)	1.369(16)
N(4)-C(5)	1.332(17)
N(4)-C(1)	1.440(17)
N(5)-N(6)	1.352(15)
N(5)-C(10)	1.360(18)
N(6)-C(8)	1.344(18)
N(6)-C(1)	1.433(17)
C(2)-C(3)	1.36(2)
C(3)-C(4)	1.43(2)
C(5)-C(6)	1.37(2)
C(6)-C(7)	1.35(2)
C(8)-C(9)	1.36(3)
C(9)-C(10)	1.41(2)

C(12)-Ta-C(14)	73.5(6)
C(12)-Ta-C(13)	110.0(5)
C(14)-Ta-C(13)	67.5(6)
C(12)-Ta-C(11)	72.1(6)
C(14)-Ta-C(11)	110.1(7)
C(13)-Ta-C(11)	70.2(6)
C(12)-Ta-N(3)	94.1(5)
C(14)-Ta-N(3)	83.8(5)
C(13)-Ta-N(3)	134.0(6)
C(11)-Ta-N(3)	155.8(5)
C(12)-Ta-N(1)	95.7(5)
C(14)-Ta-N(1)	157.8(5)
C(13)-Ta-N(1)	134.6(6)
C(11)-Ta-N(1)	83.8(6)
N(3)-Ta-N(1)	77.7(4)
C(12)-Ta-N(5)	168.8(5)
C(14)-Ta-N(5)	110.8(5)
C(13)-Ta-N(5)	81.1(5)
C(11)-Ta-N(5)	114.4(5)
N(3)-Ta-N(5)	76.5(4)
N(1)-Ta-N(5)	76.6(4)
C(4)-N(1)-N(2)	104.9(13)
C(4)-N(1)-Ta	132.7(11)
N(2)-N(1)-Ta	122.3(9)
C(2)-N(2)-N(1)	112.2(12)
C(2)-N(2)-C(1)	127.7(12)
N(1)-N(2)-C(1)	120.0(12)
C(7)-N(3)-N(4)	103.5(12)
C(7)-N(3)-Ta	133.2(11)
N(4)-N(3)-Ta	123.1(9)
C(5)-N(4)-N(3)	111.4(12)
C(5)-N(4)-C(1)	129.4(13)
N(3)-N(4)-C(1)	119.1(11)
N(6)-N(5)-C(10)	103.4(11)
N(6)-N(5)-Ta	123.1(9)

C(10)-N(5)-Ta	133.4(10)
C(8)-N(6)-N(5)	112.9(12)
C(8)-N(6)-C(1)	127.9(11)
N(5)-N(6)-C(1)	118.7(11)
N(6)-C(1)-N(4)	111.3(11)
N(6)-C(1)-N(2)	109.8(11)
N(4)-C(1)-N(2)	111.5(10)
N(2)-C(2)-C(3)	106.9(13)
C(2)-C(3)-C(4)	105.1(13)
N(1)-C(4)-C(3)	110.9(14)
N(4)-C(5)-C(6)	107.2(13)
C(7)-C(6)-C(5)	105.8(12)
N(3)-C(7)-C(6)	111.9(13)
N(6)-C(8)-C(9)	107.8(14)
C(8)-C(9)-C(10)	104.8(14)
N(5)-C(10)-C(9)	111.2(14)
O(1)-C(11)-Ta	175.9(13)
O(2)-C(12)-Ta	178.2(15)
O(3)-C(13)-Ta	179.0(16)
O(4)-C(14)-Ta	176.7(15)
Cl(3)-C(15)-Cl(1)	112.6(12)
Cl(3)-C(15)-Cl(2)	110.7(12)
Cl(1)-C(15)-Cl(2)	109.9(11)

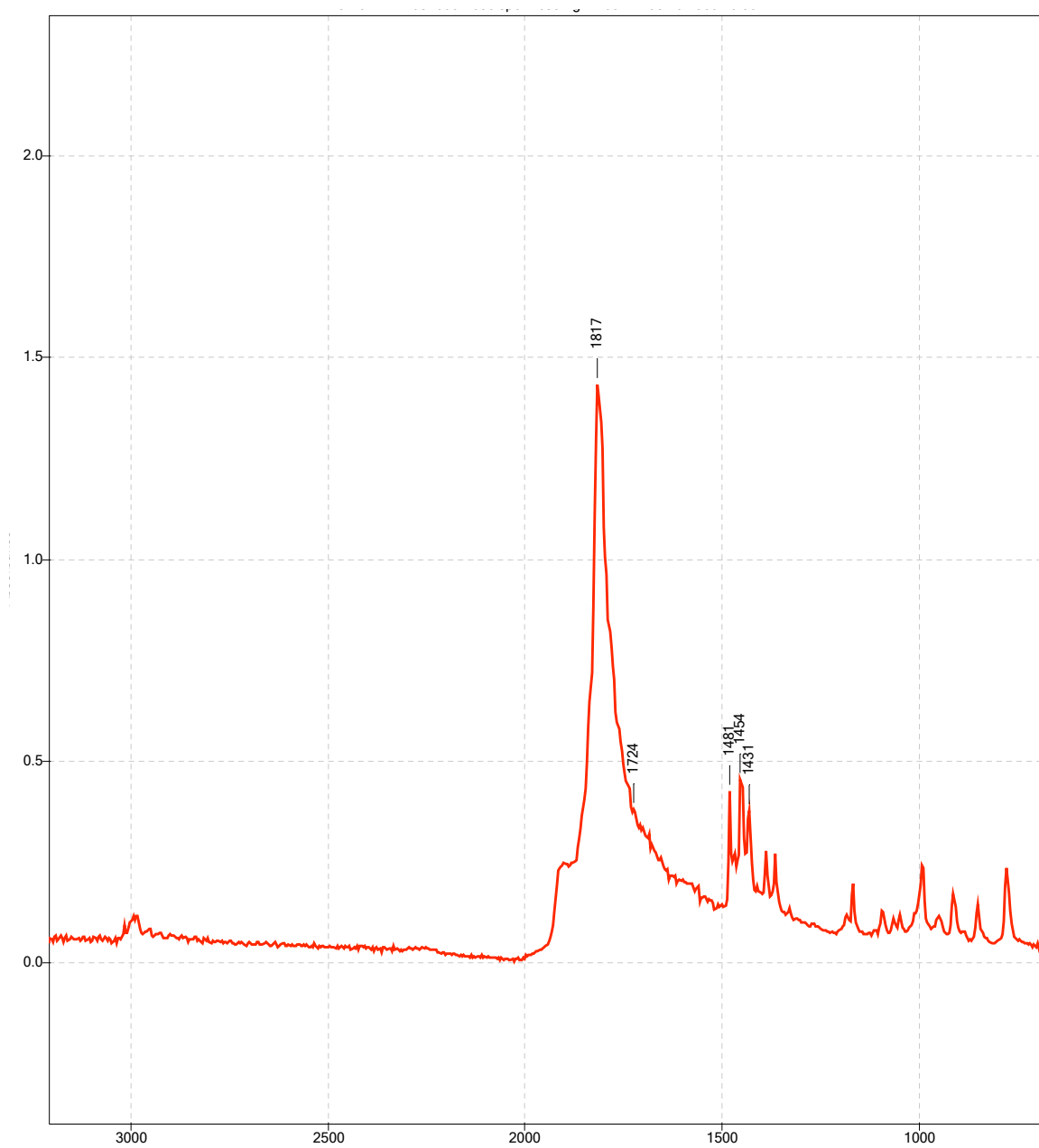
Symmetry transformations used to generate equivalent atoms:

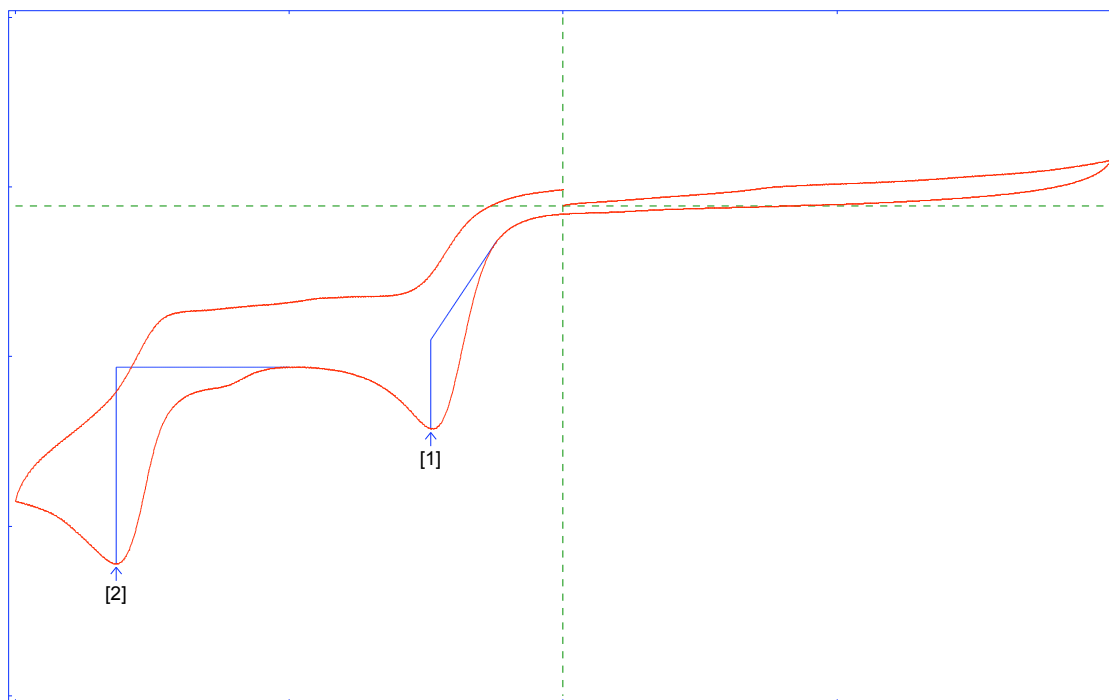
Table 4. Anisotropic displacement parameters ($\text{\AA}^2 \times 10^3$) for C15H11Cl3IN6O4Ta. The anisotropic displacement factor exponent takes the form: $-2\pi^2 [h^2 a^{*2} U^{11} + \dots + 2 h k a^* b^* U^{12}]$

	U ¹¹	U ²²	U ³³	U ²³	U ¹³	U ¹²
Ta	20(1)	16(1)	24(1)	-1(1)	6(1)	1(1)
I(1)	18(1)	17(1)	33(1)	1(1)	6(1)	0(1)
Cl(1)	98(6)	35(3)	82(4)	13(3)	-44(4)	-23(3)
Cl(2)	93(5)	49(3)	76(4)	-18(3)	14(3)	20(3)
Cl(3)	48(4)	159(9)	46(3)	6(4)	8(2)	17(4)
O(1)	29(6)	30(6)	55(7)	-11(5)	15(5)	17(5)
O(2)	66(10)	23(6)	49(7)	7(5)	11(6)	-3(6)
O(3)	50(9)	45(8)	43(7)	-13(6)	4(5)	0(7)
O(4)	33(7)	44(8)	58(8)	-3(6)	11(5)	-6(6)
N(1)	24(6)	20(6)	29(6)	-1(4)	3(4)	6(5)
N(2)	24(6)	13(5)	29(5)	-4(4)	4(4)	-1(4)
N(3)	27(6)	18(6)	27(5)	-2(4)	2(4)	-6(5)
N(4)	10(5)	20(5)	26(5)	-1(4)	3(4)	-7(4)
N(5)	21(6)	16(5)	33(6)	-2(4)	9(4)	-3(4)
N(6)	28(6)	4(4)	33(6)	-3(4)	7(4)	-2(4)
C(1)	24(7)	15(6)	23(6)	5(4)	4(4)	0(5)
C(2)	12(6)	23(6)	33(6)	-3(5)	7(4)	-3(5)
C(3)	14(7)	24(7)	48(8)	-9(6)	6(5)	-3(5)
C(4)	13(7)	24(7)	56(9)	2(6)	12(6)	6(5)
C(5)	12(6)	28(7)	41(7)	-6(6)	9(5)	1(5)
C(6)	10(6)	33(7)	27(6)	-2(5)	7(4)	-7(5)
C(7)	34(8)	46(9)	19(6)	-8(5)	11(5)	-34(7)
C(8)	36(9)	14(6)	49(9)	5(6)	9(6)	16(6)
C(9)	59(13)	32(9)	33(8)	15(7)	5(7)	-3(8)
C(10)	27(8)	20(6)	30(6)	-1(5)	2(5)	2(6)
C(11)	40(9)	25(7)	29(6)	2(5)	10(6)	4(7)
C(12)	30(8)	14(6)	43(8)	-13(5)	15(6)	-2(5)
C(13)	35(9)	17(6)	36(7)	-1(5)	9(6)	3(6)
C(14)	38(9)	17(6)	32(7)	-5(5)	11(6)	-5(6)
C(15)	37(10)	32(9)	47(9)	12(7)	1(7)	6(7)

Table 5. Hydrogen coordinates ($\times 10^4$) and isotropic displacement parameters ($\text{\AA}^2 \times 10^{-3}$) for C₁₅H₁₁Cl₃N₆O₄Ta.

	x	y	z	U(eq)
H(1GB)	521	-220	980	25
H(1)	-1643	-212	514	27
H(2)	-3255	944	334	35
H(3)	-2310	2419	671	37
H(5)	2294	-182	524	32
H(6)	3532	1043	257	28
H(7)	2958	2446	618	38
H(8)	1132	-748	1866	40
H(9)	1716	8	2677	50
H(10)	1487	1675	2508	31
H(15)	5033	1928	1260	47

Infrared Spectrum of **1** (HATR)

Cyclic Voltammogram of **1** in CH₃CN

High Resolution Mass Spectrometry Data for [TaTpm(CO)₃(PMe₃)⁺ (8)

Analysis Info

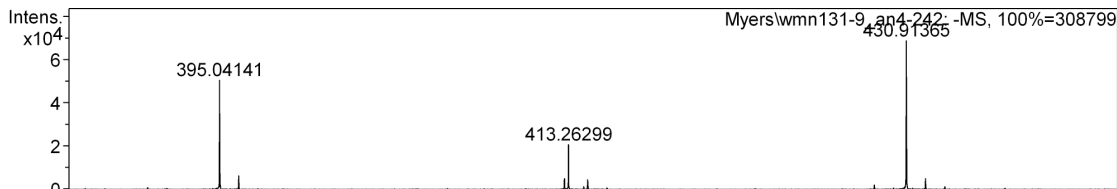
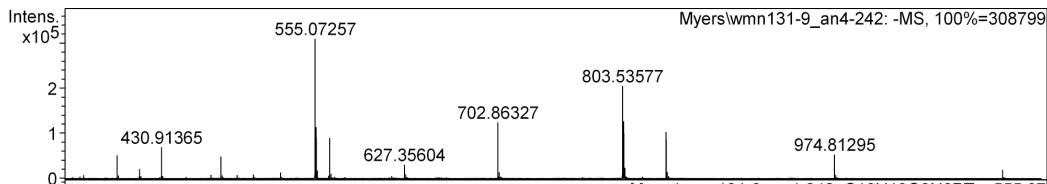
Analysis Name	Myers\wmn131-9_an4-242	Acquisition Date	6/23/2010 8:45:05 PM
Method	Linear	Operator	BioTOF
Sample Name		Instrument	BioTOF- NT

Acquisition Parameter

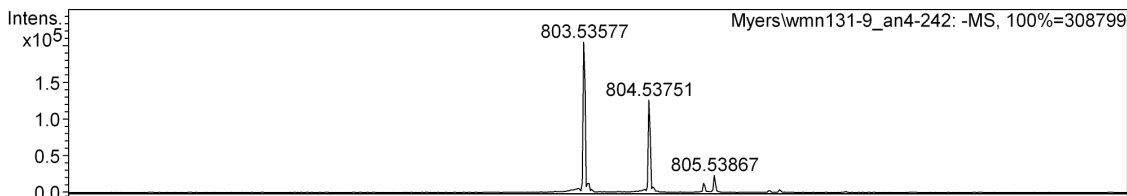
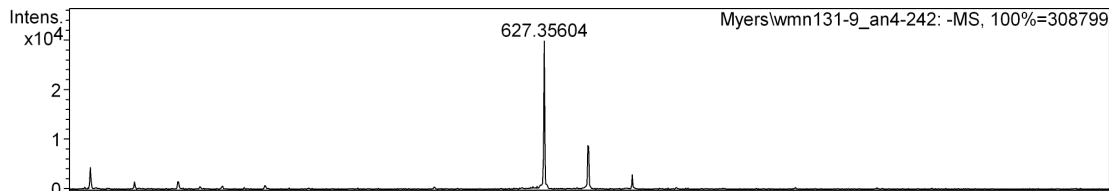
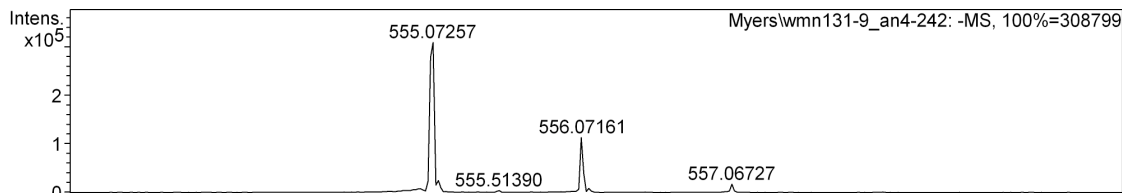
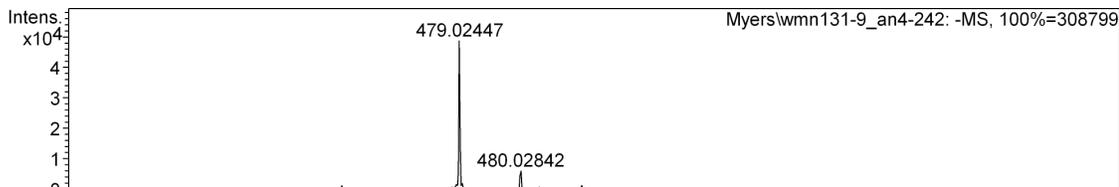
Source Type	n/a	Ion Polarity	n/a	Set Corrector Fill	n/a
Scan Range	n/a	Capillary Exit	n/a	Set Pulsar Pull	n/a
Scan Begin	n/a	Hexapole RF	n/a	Set Pulsar Push	n/a
Scan End	n/a	Skimmer 1	n/a	Set Reflector	n/a
		Hexapole 1	n/a	Set Flight Tube	n/a
				Set Detector TOF	n/a

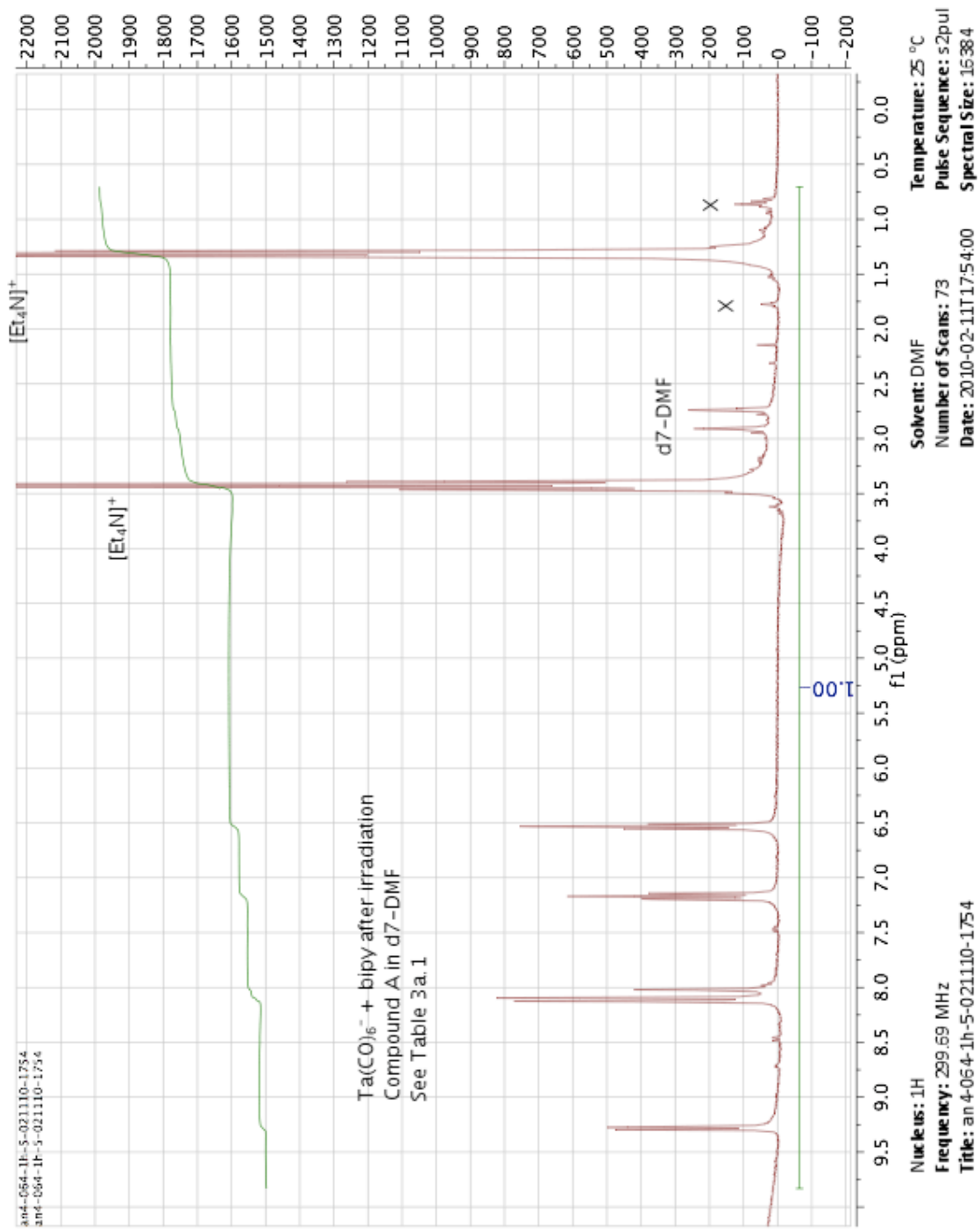
#	m/z	I	FWHM	Res.
1	368.03105	6705	0.01701	21636
2	395.04141	50496	0.01729	22851
3	396.04287	6303	0.01839	21535
4	413.26299	20676	0.01657	24947
5	430.91365	68718	0.02179	19780
6	470.91072	7545	0.02857	16485
7	479.02447	48684	0.01986	24121
8	480.02842	6102	0.03075	15611
9	492.05533	7113	0.03255	15116
10	505.29927	8310	0.02023	24978
11	527.07347	12504	0.02183	24147
12	555.07257	308799	0.03421	16224
13	556.07161	113247	0.02201	25266
14	557.06727	16932	0.02129	26160
15	566.05192	5490	0.02375	23832
16	566.88846	89784	0.02741	20682
17	567.89242	9498	0.02321	24469
18	627.35604	29811	0.02318	27066
19	628.35891	8757	0.03818	16457
20	702.86327	123804	0.02970	23665
21	703.86554	12915	0.02802	25124
22	803.53577	204762	0.03769	21317
23	804.53751	125874	0.03624	22200
24	805.37887	12645	0.03949	20395
25	805.53867	23067	0.03498	23029
26	838.83721	102069	0.03087	27176
27	839.83959	13935	0.03249	25851
28	974.81295	52671	0.03652	26695
29	975.81624	7341	0.04361	22376
30	1110.78804	18957	0.04417	25150
<hr/>				
#	m/z	I	FWHM	Res.
1	555.07307	2000	0.02000	27754
2	556.07576	397	0.02000	27804
3	557.07813	50	0.02000	27854

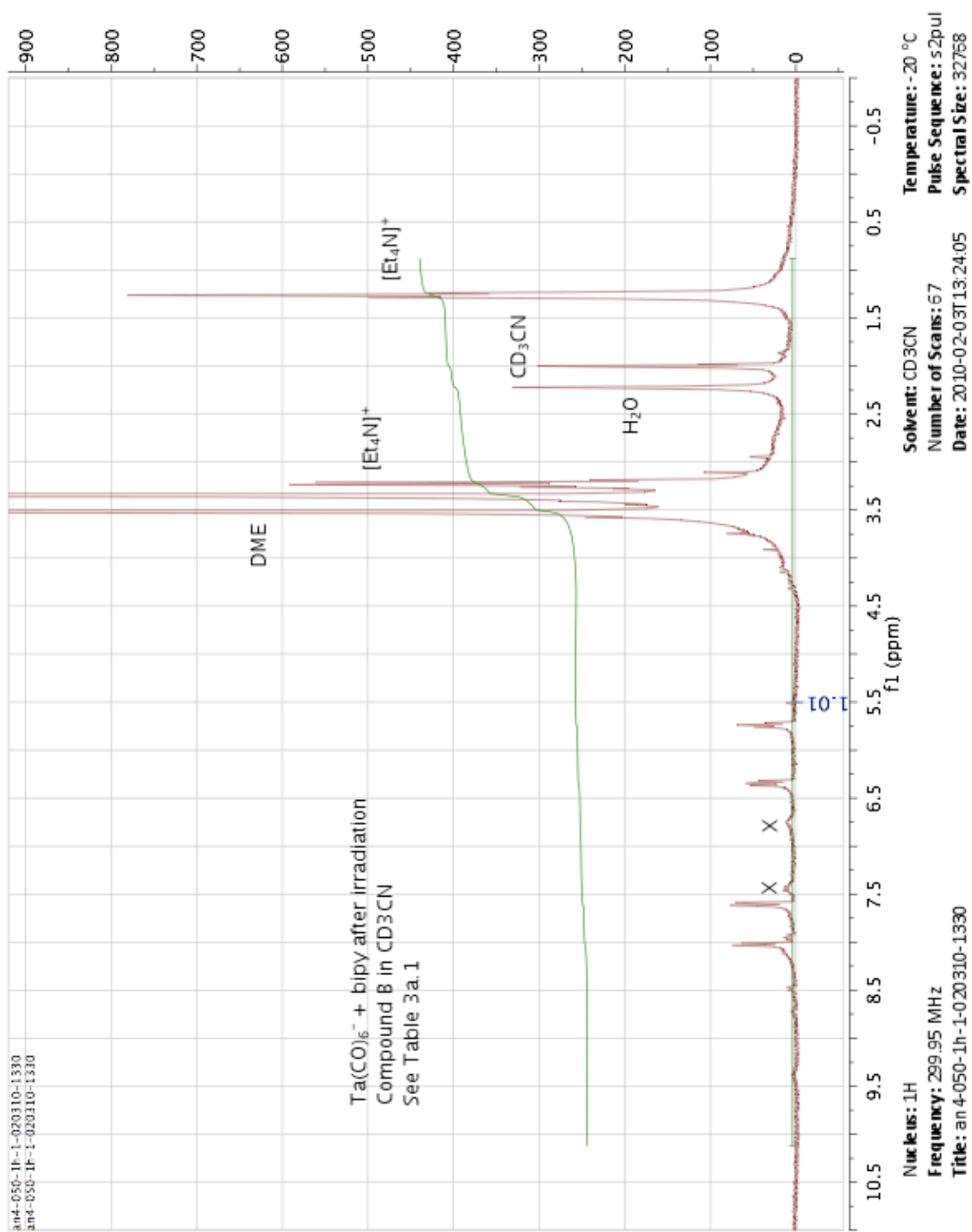
Mass Spectrum List Report

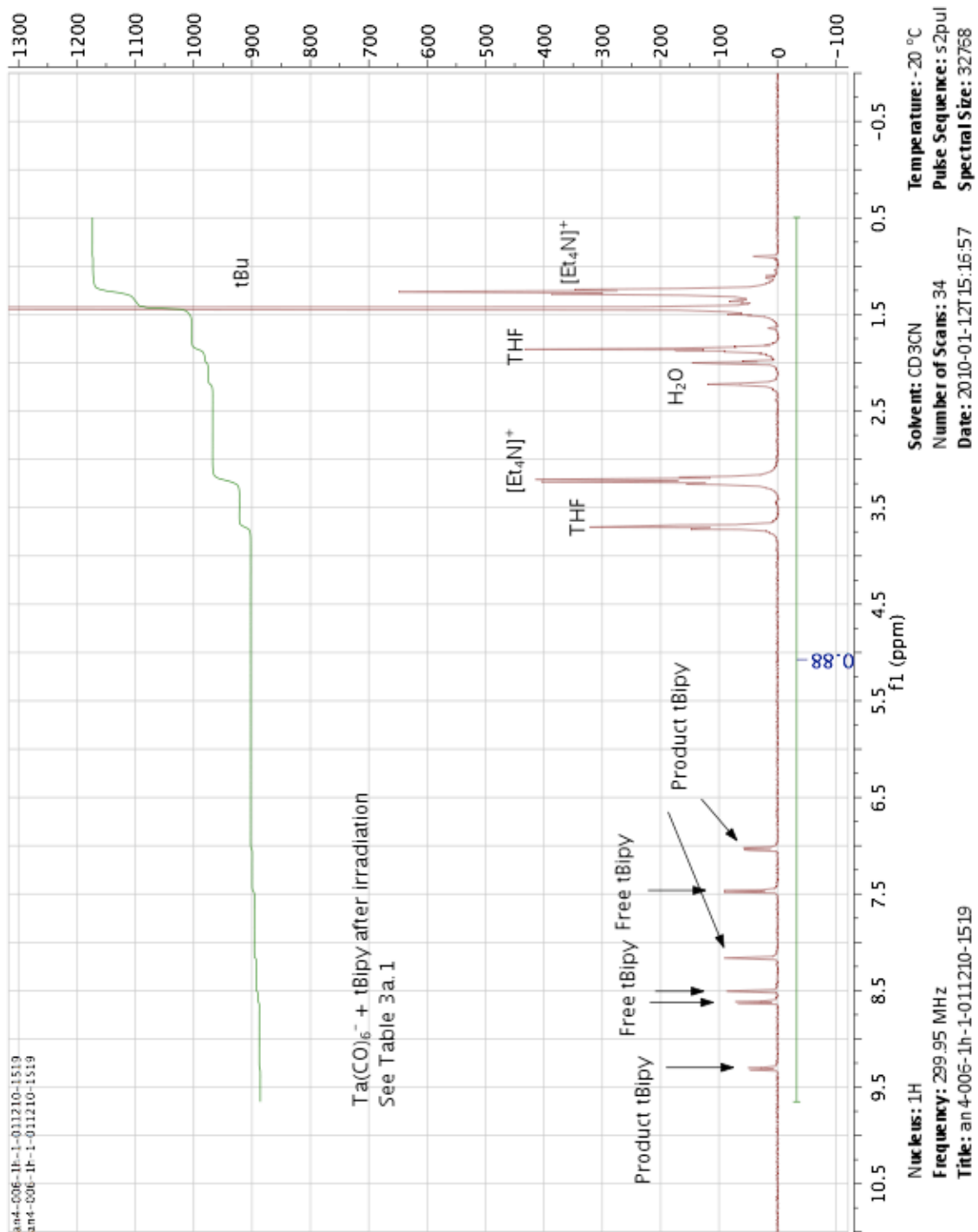


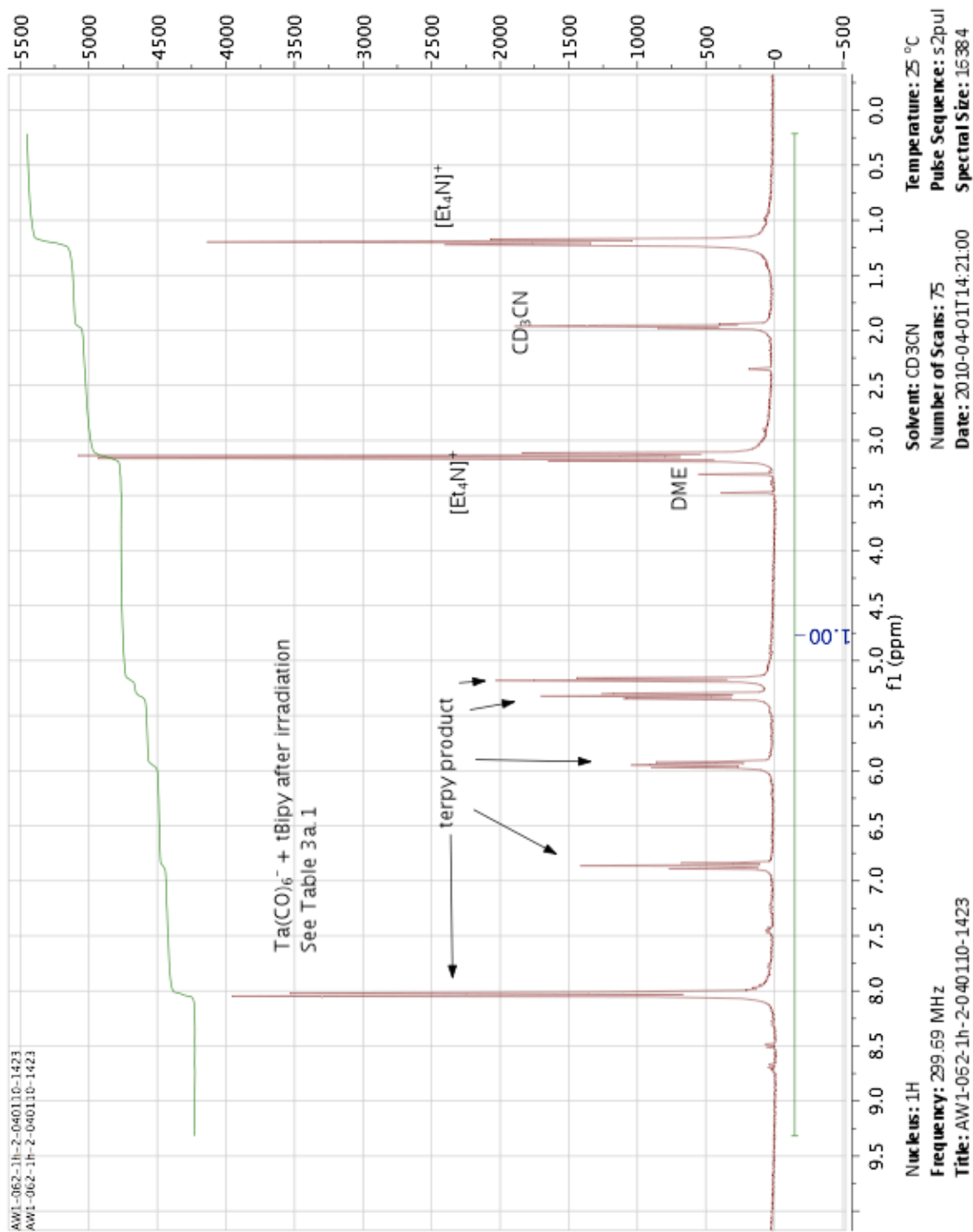
Note: Peak at 413.26299 present in background scan

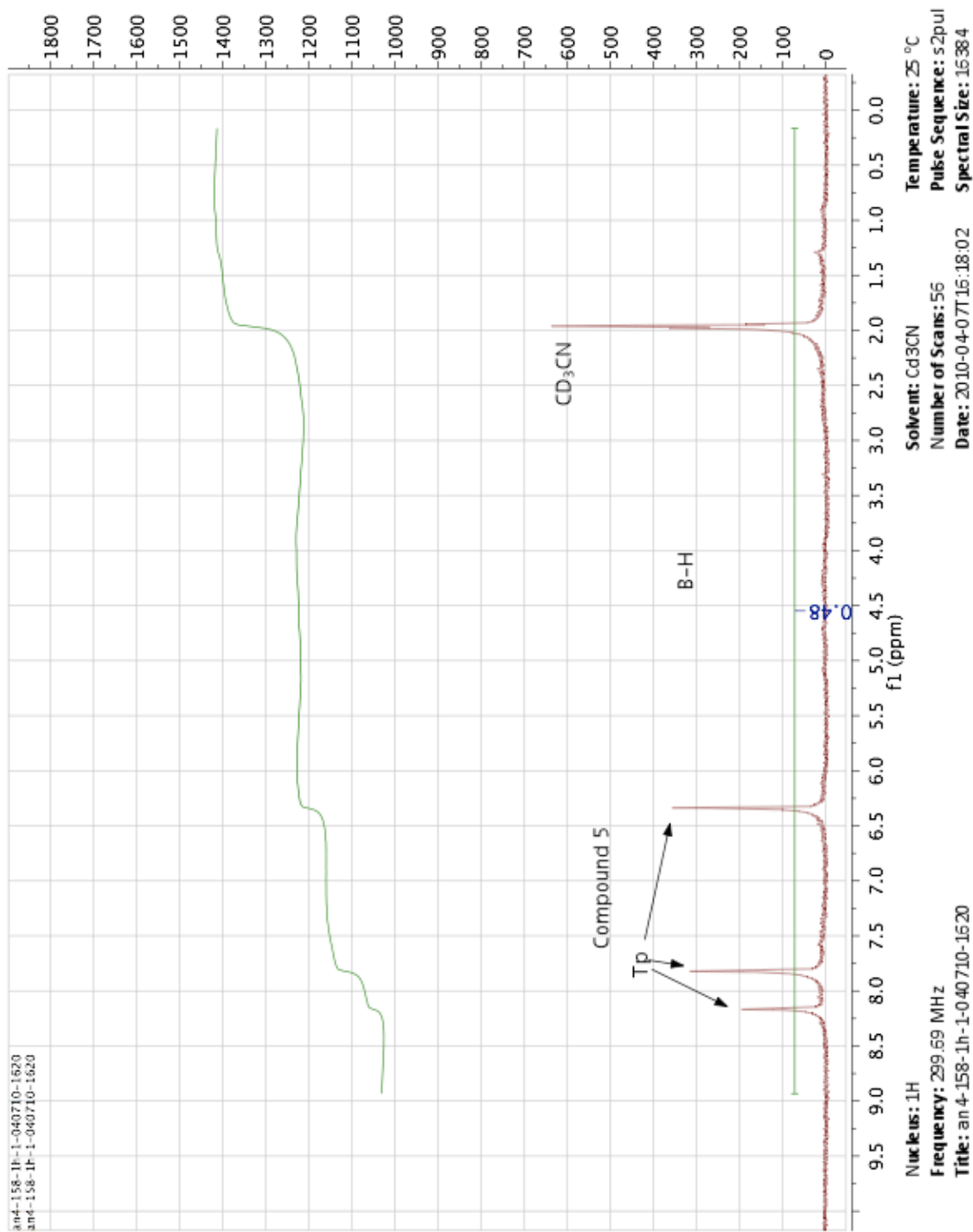


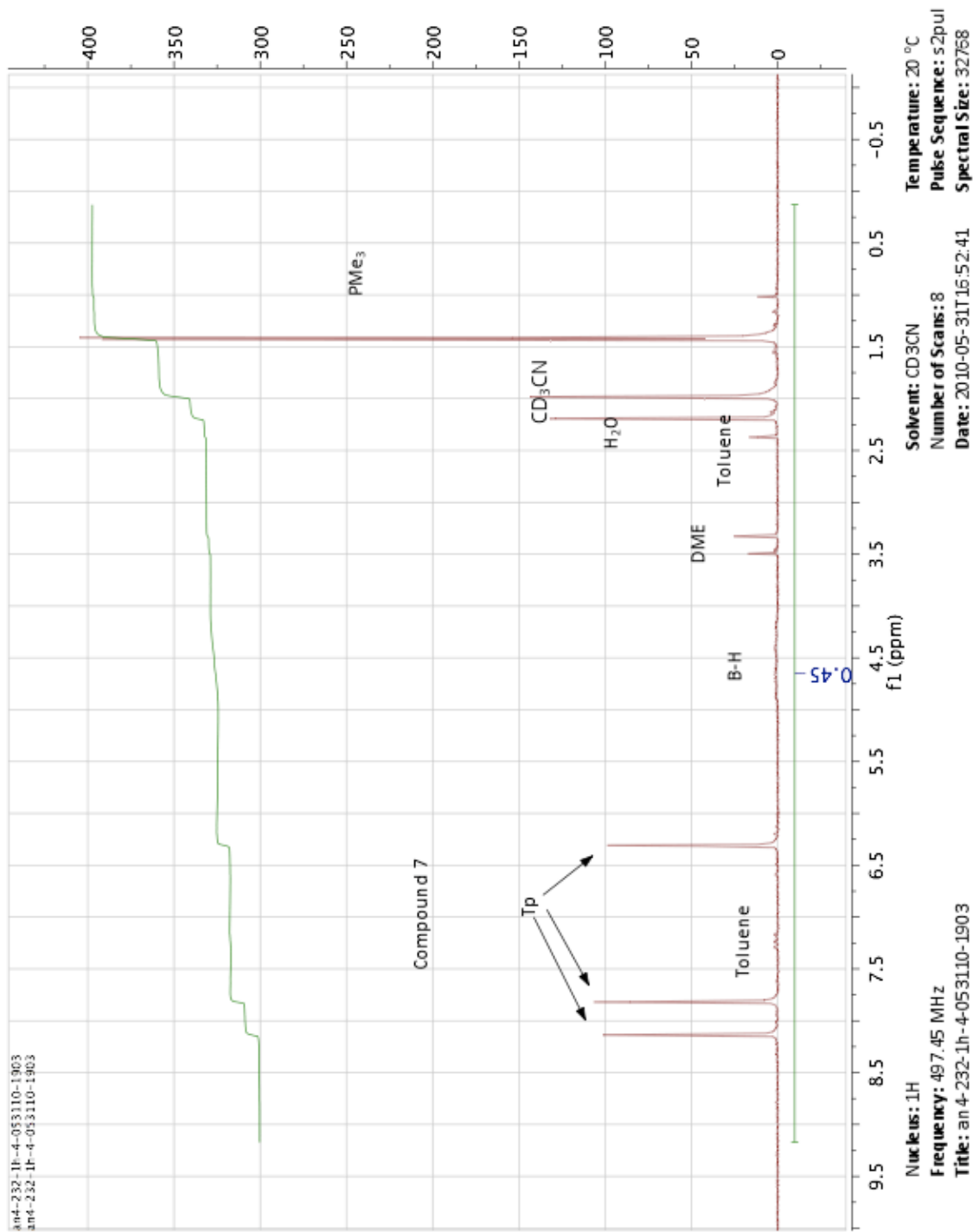


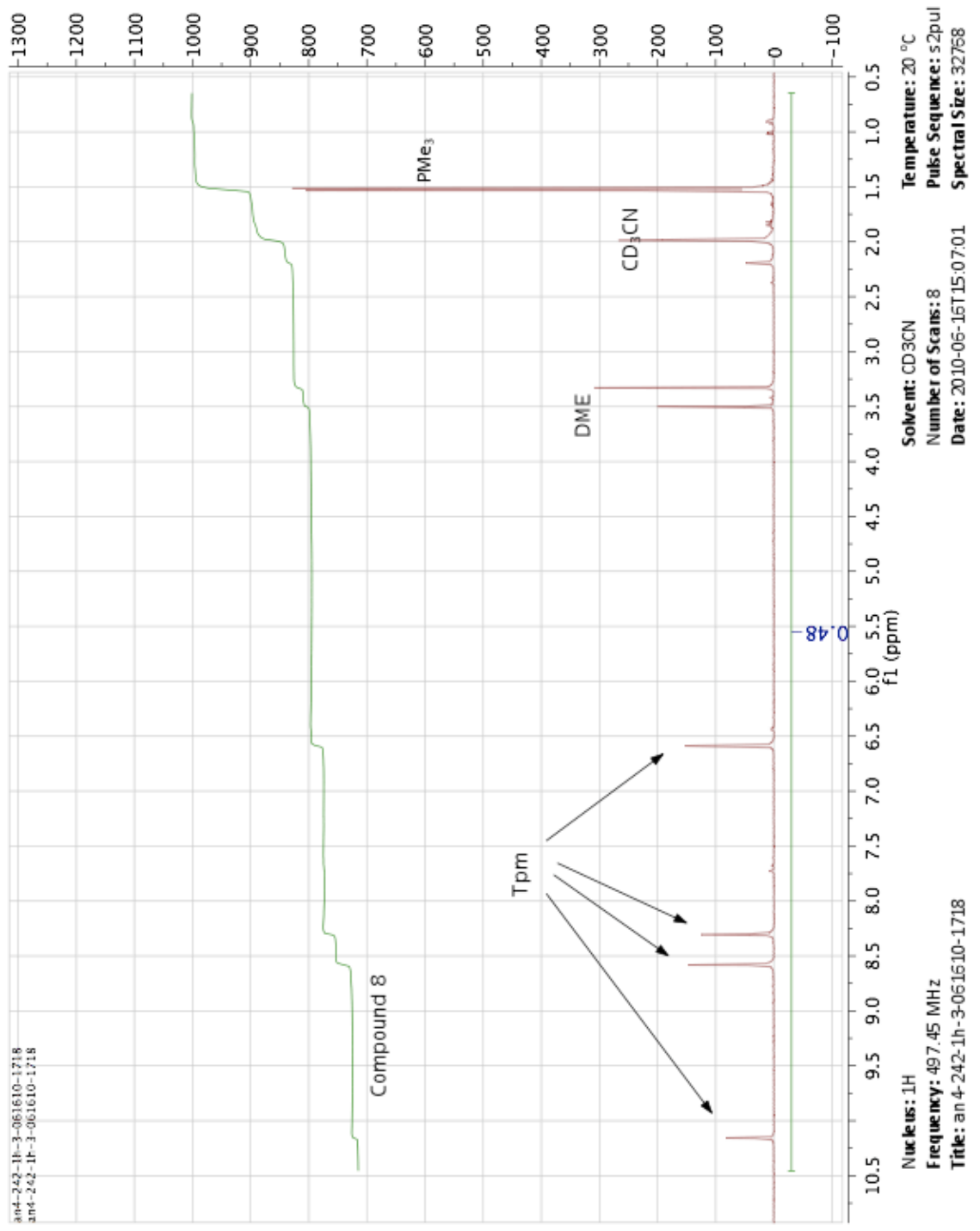








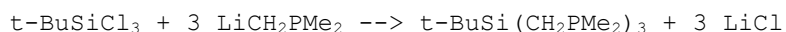
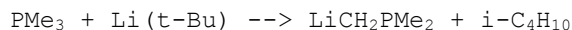




Unpublished Synthesis of *tert*-BuSi(CH₂PMe₂)₃ (trimpsi) from Dr. Greg Girolami

Gregory S. Girolami

tert-BUTYLTRIS[(DIMETHYLPHOSPHINO)METHYL]SILANE



General Procedure

All operations are carried out in vacuum or under purified argon using standard Schlenk techniques. Solvents are distilled from benzophenone under nitrogen immediately before use. *tert*-Butyllithium (Aldrich) is used as obtained, whereas *tert*-butyltrichlorosilane (Petrarch) is sublimed at 25°C/0.1 torr before use. Trimethylphosphine is prepared using a literature procedure.¹

A. (DIMETHYLPHOSPHINO)METHYLLITHIUM²

Procedure

A 2-L three-necked round-bottom flask is fitted with an argon inlet, a magnetic stirring bar, a 125-mL pressure-equalizing graduated dropping funnel (stoppered), and a stopper. The flask is flushed with argon, cooled to 0°C, and charged with trimethylphosphine (135 mL, 1.33 mol). *tert*-Butyllithium (800 mL of a 1.7 M solution in pentane, 1.36 mol) is added slowly, with stirring, via the dropping funnel in 125-mL portions over a total of three hours. After the addition is complete, the solution is allowed to warm to room temperature. The solution begins to develop a white precipitate within an hour, and is allowed to stir for a total of seven days, after which the

precipitate is collected by cannula filtration.³ The precipitate is washed with pentane until the washings are colorless (4 x 100 mL), and then is dried for about an hour under an argon flow. Yield: 105.0 g (96%).

(Dimethylphosphino)methyl lithium is a pyrophoric powder, very sensitive to air and moisture, and is used directly in the following procedure.

B. tert-BUTYLTRIS[(DIMETHYLPHOSPHINO)METHYL]SILANE⁴

Procedure

The (dimethylphosphino)methyl lithium (105.0 g, 1.28 mol) from step A is suspended in diethyl ether (375 mL) at 0°C. tert-Butyltrichlorosilane (72.26 g, 0.375 mol) is dissolved in diethyl ether (250 mL) and added dropwise with stirring over a period of two hours. The slurry is stirred for 24 hours at room temperature. The mixture is transferred via cannula into centrifuge bottles, and is centrifuged for 30 min. at 3000 rpm. The solution is decanted by cannula, and the solvent is removed under vacuum. Pentane is added to the remaining viscous yellow oil, and the solution is stored at -20°C overnight to precipitate residual (dimethylphosphino)methyl lithium.⁵ The solution is filtered, concentrated under vacuum, and transferred to a micro-scale distillation apparatus, whose head is wrapped with glass wool. After the remaining pentane is removed under vacuum, the product is distilled into a Schlenk tube which has been cooled to -78°C; b.p. 107-118°C at 0.1 torr. Care should be taken not to heat the oil bath higher than about 150°C, as substantial decom-

position of the pot contents will occur. Yield: 66.40 g (80 mL, 56%). Anal. Calcd. for $C_{13}H_{33}P_3Si$: C, 50.3; H, 10.72. Found: C, 49.3; H, 10.60.

Properties

tert-Butyltris[(dimethylphosphino)methyl]silane is a viscous, colorless liquid (est. density = 0.83 g cm^{-3}) with an acrid phosphine odor. It is moderately sensitive to air and moisture. The infrared spectrum shows the following absorptions: 2930(s), 2900(s), 2870(s), 2835(s), 2790(w), 1470(m), 1460(m), 1450(m), 1420(s), 1410(s), 1380(w), 1350(m), 1320(w), 1280(m), 1265(m), 1240(w), 1090(s, br), 1030(w), 1000(w), 930(s), 890(s), 860(s), 815(s), 765(s, br), 700(s, br), 670(s), and 500(s) cm^{-1} . The ^1H NMR spectrum in C_6D_6 shows signals at δ 0.72 (d, $J_{PH} = 0.90 \text{ Hz}$, 6H, $\text{SiCH}_2\text{PMe}_2$), 0.96 ("t", $^2J_{PH} + ^6J_{PH} = 2.40 \text{ Hz}$, 18H, PMe_2), and 1.06 (s, 9H, CMe_3). The $^{13}\text{C}\{^1\text{H}\}$ NMR spectrum in C_6D_6 shows signals at δ 16.1 (AB_2X pattern, $J_{AX} = 22.5 \text{ Hz}$, $J_{BX} = 4.1 \text{ Hz}$, $\text{SiCH}_2\text{PMe}_2$), 18.8 (AB_2X pattern, $J_{AX} = 13.5 \text{ Hz}$, $J_{BX} = 1.0 \text{ Hz}$, PMe_2), 27.2 (s, CMe_3), and 27.7 (q, $J_{PC} = 2.8 \text{ Hz}$, CMe_3). The $^{31}\text{P}\{^1\text{H}\}$ NMR spectrum in C_6D_6/C_6H_6 shows a singlet at δ -54.0. The electron impact mass spectrum shows a base peak at m/e 295 (P - CH_3).

References

- (1) M. L. Leutkens, W. L. Elcesser, J. C. Huffman, A. P. Sattelberger Inorg. Chem. **1984**, 23, 1718-1726.
- (2) H. H. Karsch and H. Schmidbaur Z. Naturforsch. **1977**, 32B, 762-767.
- (3) **CAUTION:** The filtration is done with a small piece of filter paper wired to the end of a cannula, which can be pulled off from the end of the cannula and left in the reaction flask prior to removing the cannula from the flask. If the filter stick is removed from the flask with residual (dimethylphosphino)methyl lithium on the tip, the residual pentane vapor in the flask will be ignited.
- (4) H. H. Karsch and A. Appelt Z. Naturforsch. **1983**, 38B, 1399-1405.
- (5) If residual (dimethylphosphino)methyl lithium or tert-butyl lithium remains in the crude reaction mixture during distillation, a side reaction occurs at distillation temperatures to give significant amounts of a byproduct, characterized as (t-Bu)Si(Me)(CH₂PMe₂)₂. B.p. 85-100°C at 0.1 torr. Anal. Calcd. for C₁₁H₂₈P₂Si: C, 52.8; H, 11.27. Found: C, 51.9; H, 11.10. ¹H NMR (C₆D₆): δ 0.11 (s, 3H, SiMe), 0.59 ("q", ²J_{PH} + ⁴J_{PH} = 37.3 Hz, 4H, SiCH₂PMe₂), 0.95 (s, 21H, PMe₂ and CMe₃). ¹³C{¹H} NMR (C₆D₆): δ -4.5 (t, J_{PC} = 13 Hz, SiMe), 16.0 ("dd", ¹J_{PC} = 32 Hz, ³J_{PC} = 7 Hz, SiCH₂PMe₂), 17.8 (s, CMe₃), 18.5 ("t", ¹J_{PC} + ⁵J_{PC} = 30 Hz, PMe₂), 27.0 (s, CMe₃). ³¹P{¹H} NMR (C₆D₆/C₆H₆): δ -53.6.